UCRL-ID-145181

# Determination of Reactive Surface Area of Melt Glass

*W. L. Bourcier, S. Roberts, D. K. Smith, S. Hulsey, L. Newton*
*A. Sawvel, C. Bruton, C. Papelis, W. Um, C. E. Russell,*
*J. Chapman*

**October 1, 2000**

***U.S. Department of Energy***

Lawrence
Livermore
National
Laboratory

## DISCLAIMER



This work was performed under the auspices of the U. S. Department of Energy by the University of California, Lawrence Livermore National Laboratory under Contract No. W-7405-Eng-48.

**UCRL-ID 145181**

# Determination of Reactive Surface Area of Melt Glass

William L. Bourcier, Sarah Roberts, David K. Smith, Suzanne Hulsey, Leon Newton, April Sawvel, and Carol Bruton

Lawrence Livermore National Laboratory

Livermore, California

Charalambos Papelis, Wooyong Um, Charles E. Russell and Jenny Chapman

Desert Research Institute

University and Community College System of Nevada

Las Vegas, Nevada

Prepared for the Underground Test Area Project

U. S. Department of Energy

National Nuclear Security Administration

Nevada Operations Office

Final Report

October 2000

**TABLE OF CONTENTS**

## EXECUTIVE SUMMARY

A comprehensive investigation of natural and manmade silicate glasses, and nuclear melt glass was undertaken in order to derive an estimate of glass reactive surface area. Reactive surface area is needed to model release rates of radionuclides from nuclear melt glass in the subsurface. Because of the limited availability of nuclear melt glasses, natural volcanic glass samples were collected which had similar textures and compositions as those of melt glass. A flow-through reactor was used to measure the reactive surface area of the analog glasses in the presence of simplified NTS site ground waters. A measure of the physical surface area of these glasses was obtained using the BET gas-adsorption method. The studies on analog glasses were supplemented by measurement of the surface areas of pieces of actual melt glass using the BET method. The variability of the results reflect the sample preparation and measurement techniques used, as well as textural heterogeneity inherent to these samples. Based on measurements of analog and actual samples, it is recommended that the hydraulic source term calculations employ a range of 0.001 to 0.01 $m^2/g$ for the reactive surface area of nuclear melt glass.

## PART 1. INTRODUCTION

Melt glass produced from an underground nuclear test contains the majority of the long-lived and high health-risk radionuclides. The release of these radionuclides to the environment is directly related to the surface area of melt glass that is accessible to groundwater because glass dissolves when in contact with water. This "reactive surface area" of the glass, therefore, is a crucial parameter controlling the rate of radionuclide release following a nuclear test. An accurate estimate of reactive surface area must be included in the near-field reactive transport model to predict release rates of radionuclides from the melt glass. Release rates of radionuclides from glass are highly dependent on glass surface area in the rate law used to predict radionuclide releases (Tompson et al., 1999; Pohll et al., 1998).

In previous studies, the Desert Research Institute (DRI) and Lawrence Livermore National Laboratory (LLNL) used widely varying values for melt glass surface areas in their calculations of release rates of radionuclides from the melt glass that will be made available for hydrologic transport (Pohll et al., 1998; Tompson et al., 1999). The surface areas were estimated using different techniques, reflecting the controversy that exists on the appropriate measure of melt glass surface area. Hydrologic source term calculations for the SHOAL test employed a glass surface area of 500 $cm^2/g$, which is three orders of magnitude larger than the surface area of 0.5 $cm^2/g$ estimated for CAMBRIC melt glass by Tompson et al. (1999). The SHOAL surface area is based on BET[1] surface area measurements of crushed particulate material from the RAINIER melt glass reported by Essington and Sharp (1968). The CAMBRIC value is an estimate based on analogy with a measured reactive surface area for a fractured high-level waste glass.

The difference in the estimated glass surface areas used in the SHOAL and the CAMBRIC studies arises from our poor knowledge of the morphologies and textures of melt glasses, the lack of knowledge of the relationships of these textures to their reactive surface areas, the lack of actual measurements of reactive surface areas of melt glasses, and ambiguities regarding the use of laboratory-derived rate constants and surface areas to describe processes in the field, as discussed below.

To provide a technical basis for the selection of melt glass surface areas, DRI and LLNL have collaborated to better determine the relationship between melt glass textures and surface area, and to carry out surface area measurements and flow-through glass dissolution experiments on melt glasses and natural analog glasses.

This report summarizes FY1999 and FY2000 work at LLNL and DRI that was directed towards estimating reactive surface area of the melt glasses. Our goal is to provide a probable range of reactive surface area of melt glasses to be used in calculation of the hydrologic source term. This report is a compilation of four separate parts. Part 2 is an LLNL-EES report on flow-through tests of natural analog rhyolite glass cores. Part 3 is a DRI report on gas adsorption (BET)

[1] BET refers to the Brunauer, Emmett and Teller (1938) method of determining surface area of solids by measuring the volume of a monolayer of adsorbed gas.

measurements of crushed portions of these same cores and other glasses similar in composition to the melt glasses. Part 4 is an LLNL-C&MS report on BET surface area measurements of melt glass samples from the Nevada Test Site. Part 5 is co-authored by both laboratories and recommends reactive surface area to be used for hydrologic source term modeling. This report builds upon an earlier LLNL report summarizing our knowledge of the physical characteristics of melt glass (Kersting and Smith, 1999).

**Statement of problem**

Calculation of the hydrologic source term requires a measure of the reactive surface area of melt glass as it exists underground. Reactive surface area can be thought of as the glass surface area that contacts the moving groundwater as it flows through the melt glass. Internal surface area, such as the surfaces of closed pores, is not part of the reactive surface area. Very restricted internal surface area, such as the surfaces of pores with narrow throats, may contribute negligibly to reactive surface area because transport of radionuclides from these pores to the moving fluid is restricted.

The reactive surface area of the melt glass is expected to vary according to the texture and other physical characteristics of the melt glass on a variety of spatial scales. The textures associated with the melt glasses are complicated by some of the phenomena associated with the formation of glass. Of most importance are the following:

(1) When glasses cool from the outside, thermal gradients normal to the cooling surface cause differential thermal contraction that causes cracking. Even slowly cooled meter-sized glass masses can end up as composites of fist-sized glass pieces along with finer material in a 3-D mosaic of cracks. A similar cracking process probably takes place as the melt glass cools.

(2) Volatiles included in the cooling silicate liquid will tend to exsolve during cooling and result in high porosity zones of bubbles, analogous to pumice in natural glasses. These zones will have higher porosities than massive (non-vesicular) glass. However, it is unknown whether the high porosity will translate into a zone of high permeability and high reactive surface area.

(3) Reactions between the melt glass and water during cooling of the glass and in the ambient environment will give rise to hydrous alteration products. This reaction has a positive molar volume change and will therefore have a tendency to decrease the permeability in the zones that contain the hydrous phases. Decreased permeability leads to decreased contact between fluid and glass and thus reduced reactive surface area.

All three aspects are difficult to quantify without detailed field examination of the actual melt glass in the subsurface.

The problem is further complicated by the high degree of heterogeneity of the melt glass itself. An underground nuclear explosion results in the formation of a cavity followed by its collapse and in-fall of a rubble chimney. Glass is produced

from the condensation of high temperature plasma created at the time of explosion, shock melting associated with the force of the explosion, and melting of wall rock along the edge of the cavity (Borg et al., 1976). Photos taken from exploratory post-shot drifts show that the melt zone is a breccia of rhyolite blocks, introduced during cavity collapse, incorporated into a puddle glass horizon which is variably cracked and vesicular (Fig. 1). The relative proportions of massive to fractured and vesicular or pumicious glass is unknown, and their distributions in space are probably chaotic.


**Figure 1-1.** Photo taken from the exploratory drifts drilled into the RAINIER underground nuclear test, RAINIER Mesa, NTS (Wadman and Richards, 1961). Light buff colored material is tuffaceous host rock; dark material is melt glass; white rims around tuff are vesicular (bubble-rich) glass. The melt glass is clearly very heterogeneous. In addition, upper zones tend to be vesicular due to escape of buoyant gases from melt.

Useful data on reactive surface area could be obtained from tests of relatively large (meters in length) masses of the intact interstitial glass, but such samples are not available. Drilling into melt glasses to obtain smaller samples is costly to carry out, and even the physical process of drilling is believed to damage brittle glass. Even if pristine samples were available, they still do not provide any measure of reactive surface area along fractures, which may be the dominant flow paths given the extremely low permeability of unfractured glass. Flow may also take place preferentially through vesicular zones, the gas-rich zones that

have a highly porous texture similar to pumice. The high porosity of these zones may translate into high permeability and therefore dominant flow paths. Radionuclides that enter the fluid as a result of dissolution of glass along the fractured zones and the vesicular zones probably dominate the radionuclide flux from the melt glass. Therefore we need an estimate of melt glass reactive surface areas for a variety of textures in order to predict radionuclide release rates.

The problem of determining a reactive melt glass surface area is complicated by the known difference between physical surface areas measured using the BET method and reactive surface areas estimated in field studies. Many studies have shown that reactive surface areas of rocks and soils in the field (based on analysis of entire watersheds) are 1 to 2 orders of magnitude smaller than the BET surface areas of crushed samples of the same materials measured in the laboratory (e.g. White and Peterson, 1990; White and Brantley, 1995). The BET surface areas of minerals, in turn, tend to be about an order of magnitude greater than the geometric surface areas of similarly sized mineral grains (White and Peterson, 1990).

Various explanations have been proposed to explain the apparent discrepancy between chemically reactive surface areas in the field and BET measurements in the laboratory (e.g. Blum and Stillings, 1995). For example, hydrologic heterogeneity and preferential flow on scales that traditional macroscopic hydrologic modeling can not address, may result in contact of only a fraction of the surface of minerals by moving fluid. In such a case, much of the available surface area is isolated from fluid flow, and elemental fluxes to and from these surfaces are diffusion-limited. In addition, relatively slow flow allows species dissolved from glass and minerals to build up in solution and slow down the rates of dissolution due to saturation effects. These areas are also more likely to host alteration minerals associated with glass dissolution, and therefore further reduce permeability. Both of these processes may contribute to the low reactive surface areas measured in the field. The discrepancies between chemically reactive surface area and BET-measured surface area must be reconciled in our modeling.

**Technical approach**

An accurate measure of reactive surface area would best be obtained from the results of leach tests of large volumes of the melt glass breccia, either *in situ*, or extracted as monoliths. The volumes should be large enough to be representative of the entire melt glass. Because no such samples exist, some compromise must be made based on analog samples, and the Hunt sidewall samples[2] of the melt glass zone that are available for tests. Given this situation, the approach for providing defensible estimates of reactive surface areas for the melt glass is as follows.

1. Natural volcanic glass samples were collected from the Obsidian Dome area of Eastern California that have similar compositions and a similar range of

[2] "Hunt sidewall samples" are rock samples taken downhole by injecting a coring device laterally into the wall and removing the materialse loosened in this process.

textures to those observed for melt glasses (Figure 1-3; also compare Figures 1-1, 1-2, and photos in Appendix 1-2 and Appendix 1-3). Because melt glasses are dominantly melted rhyolitic tuffs (with addition of small concentrations of radionuclides and other elements from the test components), they are very close in composition to natural volcanic rhyolites and obsidians (Schwartz et al., 1984; Smith, 1995). The samples are large enough (up to two feet in diameter) to capture some of the heterogeneity of texture observed for the melt glass, including fracturing.

**Table 1-1.** Natural glass samples used in tests. All descriptive information is based on qualitative field observations of the samples. "Massive" refers to dense glass with no obvious porosity.

| Sample | Location | Description |
|---|---|---|
| 1 | Obsidian Dome | massive flow banded obsidian. |
| 2 | Obsidian Dome | massive flow-banded obsidian with pumice layers |
| 3 | Obsidian Dome | textures similar to 1 but less dense |
| 4 | Obsidian Dome | texture similar to 1 but much larger sample |
| 5 | Obsidian Dome | slightly vesicular sample, less dense than 1 |
| 6 | Obsidian Dome | pumiceous sample light in color, faint banding |
| 7 | Pumice Mine Rd.* | large banded pumice lump, less dense than samples 1-6 |
| 8 | Pumice Mine Rd. | banded pumice slightly more dense than 7 |
| 9 | Pumice Mine Rd. | banded pumice slightly more dense than 8 |
| 10 | Pumice Mine Rd. | volcanic breccia; clasts of rhyolite in glassy matrix |
| 11 | Pumice Mine Rd. | very low density homogeneous pumice chunk |

*The Pumice Mine Road location is a few miles northeast of Obsidian Dome.

Although volcanic glasses and melt glasses are generated under very different circumstances, there is no reason to question that their dissolution behavior will be similar provided they have similar compositions. Silicate melts retain no history of the thermal event that produced them (see Chapter 7 in Doremus 1994). Once cooled below the glass transition temperature (the temperature below which liquid structure is frozen into the glass), glasses retain characteristics that are functions primarily of only composition and cooling rate. In fact, dissolution tests of crushed melt glasses provide dissolution rates almost identical to rates measured for natural glasses of similar composition (see Chapter 6 in Tompson et al., 1999). Because melt glasses cooled adjacent to relatively cool country rock and therefore cooled fairly rapidly, their best analog among available igneous rocks is a volcanic rock which cooled near the earth's surface surrounded by cool country rock.

**Figure 1-2**. Volcanic glass samples from Obsidian Dome near Mammoth Lake, California. Bottom close-up photo shows variety of textures exhibited by these samples and similarities to textures of melt glass shown in Figure 1-1.

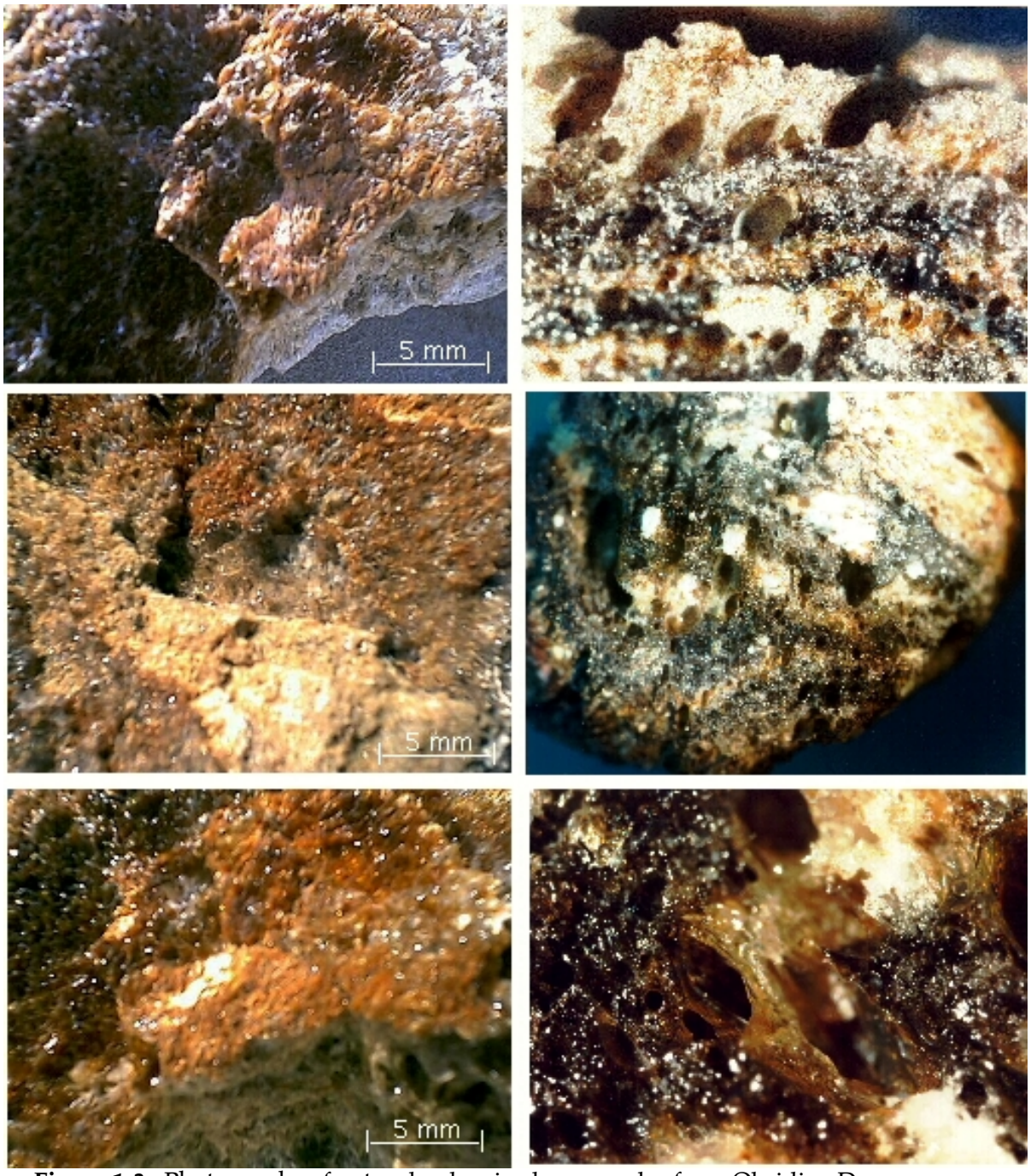


**Figure 1-3**. Photographs of natural volcanic glass samples from Obsidian Dome near Mammoth Lake, California on left side of diagram, compared with photographs of archived melt glasses from unknown shots. Scales for melt glasses are unknown but believed to be roughly similar to scales shown for natural glasses based on vesicle sizes.

2. Reactive surface areas of cores obtained from the natural glasses were calculated from measured silicon release rates using a flow-through reactor (see Part 2). Hydraulic conductivities were calculated from measured flow rates and pressure gradients. The cores were drilled at various orientations to the flow textures in order to measure the directional variability of hydraulic conductivity and reactive surface area. Although we were primarily interested in the reactive surface area, the hydraulic conductivity could be conveniently derived by measuring the pressure gradient across the core. The hydraulic conductivity of the melt glass is also used as input to source term calculations.

3. BET surface area measurements of the same suite of samples were carried out using a surface area analyzer specially designed for samples having relatively low surface area. Various size fractions of crushed materials were used. BET measurements were also made on additional samples of *in situ* vitrified glasses and tektite glasses as described in Part 3.

4. BET surface area measurements were made on pieces of sidewall core samples of nuclear melt glasses from the RAINIER and ROQUEFORT tests as reported in Part

**Limitations of the technical approaches**

Surface areas were estimated in this study using two methods. The first method involved pumping fluids through intact cores of natural glass samples that have textures and compositions similar to those observed for melt glasses. The analyzed composition of the fluid leaving the glass core was used to calculate the surface area of the glass core based on previous knowledge of the intrinsic rate of glass dissolution (see discussion in Part 2). The surface area determined with this method is a *reactive* surface area because it is a measure of the amount of glass that has contacted and reacted with water. The method involving flow-tests of cores is limited by the following factors.

(1) The flow rates in the tests are higher than those that are present in the subsurface.

The calculated fluid flow velocities (Darcy velocities) of the core tests varied between about 8 and 400 m/year. For comparison, calculated fluid flow velocities through the melt glass for the CHESHIRE test vary between 1 and 15 m/year, with the faster rates corresponding to higher temperatures/earlier times (Maxwell and Carle, 2000, pers. comm.). Our experimental flow rates are therefore generally higher than the predicted field rates but include the upper range for this test. Further work is required to define the relationship between flow rate and reactive surface area needed for any correction that should be made to account for generally slower flow rates in the field.

A related concern is that the degree of core saturation (hydrologic) may be different in the cores used in the flow test experiments and the nuclear melt glass. The cores were in contact with water on time scales of a few days to

several weeks. Longer contact times may lead to a greater degree of hydrologic saturation. A higher degree of saturation means that a larger fraction of the surface area is in contact with water, leading to a greater amount of dissolution and higher estimated reactive surface areas. In addition, these experiments could be sensitive to the geometry of the experiment.

(2) The cores are not large enough to capture all scales of heterogeneity of the subsurface.

Based on underground photographs of the RAINIER test, the scale of heterogeneity of the melt glass is on the order of meters. In order to capture this, experiments would have to be performed on samples several meters in dimension. What we provide with tests of smaller samples is a measure of reactive surface area on a smaller scale that does not account for the impact of large through-going fractures. Our tests of fractured samples show that fractures tend to decrease the reactive surface area (a six-inch diameter core that had a prominent fracture parallel to flow had one of the lowest measured reactive surface areas; test 2/4). Because of this, it is likely that our measured reactive surface areas of samples that do not contain fractures are probably higher than what would be measured for an identical sample that does contain fractures.

The scale of heterogeneity is not the only aspect of the flow experiments dependent on geometry; anisotropy plays a critical role in regard to the orientation of heterogeneity relative to the flow direction. Though the in situ anisotropy and heterogeneity are fully unknown for a nuclear cavity, the experiments described here included varying sample orientation relative to flow direction to address this issue. In addition, in general, we do not know the extent of fracturing in the melt glass, nor the continuity of these fractures.

(3) The cores are analog samples and not actual melt glass.

The effect of this factor is difficult to estimate, although textures in both types of glasses are similar (see Figure 1-3) and the same physical mechanisms (rapid cooling with de-gassing) are operating in the formation of the glasses in both cases. In addition, the compositions of these silicate glasses are similar and resulting dissolution mechanisms and rates should be comparable (Schwartz et al., 1984; Tompson et al., 1999).

The second method to estimate reactive surface area was to determine physical surface areas of crushed melt glasses and analog glasses by the gas absorption (BET) method. The BET method is limited by the following factors.

(1) The method includes in its results a contribution from glass surface area opened up during sample preparation (crushing and grinding) that would not be present in the subsurface, and therefore should not be included in the surface area parameter.

The BET technique cannot be used on large intact samples. It is limited to fragments with physical dimensions less than about one centimeter. Therefore

the samples must be crushed or fragmented before BET analysis. This will result in contributions to surface area that are artifacts of sample preparation, including in particular the opening up of closed porosity, and the exposure of new surface area along fractures generated during crushing. The presence of such contributions can only be estimated based on careful measurements of specific surface area as a function of particle size, as was performed for this study.

(2) The BET method is very sensitive to small amounts of clay alteration on the glass.

Clays are common alteration products of silicate glasses during weathering and have a very large surface area. Even very small amounts of clay could make a significant contribution to the measured BET surface area (see discussion in Part 3). Exact quantification of the contribution of clays to the total surface is not trivial, however, and was not conducted in this study.

(3) BET is a measure of total physical surface area, not reactive surface area.

Physical surface area is not the same as reactive surface area. A fluid packet traveling through the glass will not react with glass surface area that it does not contact. BET surface area measurements of crushed samples include contributions from closed pores, dead-end pores, and restricted flow paths that will see little or no fluid contact. BET measurements of *physical* surface area are therefore conservative maximum values of *reactive* surface area.

As mentioned above, many studies have shown that reactive surface areas of minerals in the field are 1 to 2 orders of magnitude smaller than the BET surface areas of the minerals measured in the laboratory (e.g. White and Brantley, 1995; White and Peterson, 1990). This is in the same range as the differences between many of our BET measurements and our reactive surface area measurements from the flow-through tests discussed below.

Our results from both the flow-through tests of glass cores and BET measurements of glasses have been used to provide a basis to estimate the melt glass reactive surface area used to define the hydrologic source term. We summarize the test results and recommend a range of probable values for reactive surface area in Part 5.

**References**

Blum, A. E. and L. L. Stillings (1995) Feldspar dissolution kinetics. in *Chemical Weathering Rates of Silicate Minerals*. A. F. White and S. L. Brantley eds., Mineralogical Society of America, Reviews in Mineralogy, Volume 31, p. 291-351.

Borg, I.Y., R. Stone, H.B. Levy, L.D. Ramspott (1976) Information pertinent to the migration of radionuclides in ground water at the Nevada Test Site, Part I:

Review and analysis of existing information. Lawrence Livermore National Laboratory, UCRL-52078.

Bourcier, W. L. and S. Roberts (1999) Experimental determination of melt glass surface area. Unpublished interim report for UGTA project, 19 p.

Brunauer, S., P. H. Emmett, and E. Teller (1938) Adsorption of gases in multimolecular layers. J. Am. Chem. Soc. 60:309-319.

Doremus, R. H. (1994) *Glass Science*. New York, John Wiley & Sons.

Eaton, G. F. and D. K. Smith (2000) Aged nuclear explosion melt glass: Radiography and scanning electron microscope analyses documenting radionuclide distribution and glass alteration. Livermore Lawrence Livermore National Laboratory Report, UCRL-JC-136658, 10 pages.

Essington, E. H. and J. V. A. Sharp (1968) Some aspects of ground water solution chemistry, underground nuclear explosion zones, Nevada Test Site. *Geological Society of America Memoir 110: The Nevada Test Site*., E. B. Eckel, ed., p. 263-273.

Kersting, A.B. and D.K. Smith (1999) Observations of Nuclear Explosive Melt Glass Textures and Surface Areas, Lawrence Livermore National Laboratory, unpublished report prepared for the Underground Test Area of the U.S. Department of Energy, Nevada Operations Office, 8p. with illustrations.

Pohll, G., J. Chapman, A. Hassan, L. Papelis, R. Andricevic, and C. Shirley (1998) Evaluation of groundwater flow and transport at the SHOAL underground Nuclear Test: An interim report. Las Vegas, Desert Research Institute. Report DOE/NV/11508-35.

Schwartz, L., A. Piwinskii, F. Ryerson, H. Tewes, and W. Beiriger (1984) Glass produced by underground nuclear explosions. in *Natural Glasses*. L.D. Pye, J.A. O'Keefe, and V.D. Fréchette eds., North-Holland, p. 559-591.

Smith, D.K. (1995) Characterization of nuclear explosive melt debris. Radiochimica Acta, 69:157-167.

Tompson A. F. B., Bruton C. J., and Pawloski G. A. eds. (1999) Evaluation of the hydrologic source term from underground nuclear tests in Frenchman Flat at the Nevada Test Site: The CAMBRIC Test, Lawrence Livermore National Laboratory, Report Number UCRL-ID-132300; March 1999, 319 p.

Wadman R. E. and Richards W. D., (1961) Post-shot geologic studies of excavations below RAINIER ground zero, Lawrence Radiation Laboratory, Report Number UCRL- 6586, 27 p.

White A. F. and Brantley S. L. (1995) Chemical weathering rates of silicate minerals: an overview. In *Chemical Weathering Rates of Silicate Minerals*., Vol.

31, A. F. White and S. L. Brantley, eds., pp. 1-21. Mineralogical Society of America.

White, A. F. and M. L. Peterson (1990) Role of reactive surface area characterization in geochemical kinetic models. *Chemical Modeling in Aqueous Systems II.* D. Melchoir and. R. Bassett, eds. American Chemical Society Symposium 416, p. 461-475.

## PART 2. DETERMINATION OF REACTIVE SURFACE AREAS FROM FLOW-THROUGH TESTS OF NATURAL ANALOG GLASS SAMPLES

*William L. Bourcier, Sarah Roberts, Leon Newton, April Sawvel, and Carol Bruton*
*Lawrence Livermore National Laboratory*

### Introduction

Our method for measuring reactive surface area of glass cores[3] can be described as follows. If we pump a fluid of known composition through a glass core, and measure the total amount of glass that dissolves into the fluid in the process, we obtain a measure of the integrated amount of glass dissolution. The total amount of glass dissolved can be obtained from a chemical analysis of the reacted fluid. If, in addition, we know the reaction rate of the glass per unit area for a given solution composition from previous measurements, we can directly compute the surface area for the glass core. All this is done under assumed steady-state conditions where the rate of glass dissolution is not changing.

To calculate the surface area from the test data we start with the rate equation commonly used to describe silicate glass dissolution that has the form (Tompson et al., 1999, p 33-39):

$$rate = Aka_{H+}^{p}\left(\frac{c_{sat} - c}{c_{sat}}\right) \qquad (2\text{-}1)$$

where *rate* is the dissolution rate in units of grams glass dissolved per unit time, $A$ is the reactive surface area, $k$ is the rate coefficient, $a_{H+}{}^{p}$ provides for the pH dependence of the dissolution rate where p is a real exponent, $c_{sat}$ is the silica saturation value for the glass, and $c$ is the silica concentration in the fluid. The tests are designed such that the fluid remains far from silica saturation, so that c is small relative to $c_{sat}$ and therefore the last term is approximately equal to one. Because the rate coefficient and pH dependence are already known as a function of temperature from previous experiments (Tompson et al. 1999), the reactive surface area is the only unknown in the equation. Therefore we can simplify and rearrange equation 2-1 to obtain:

$$Area = \frac{rate}{k'} \qquad (2\text{-}2)$$

where k' is the product of the rate coefficient times the $a_{H+}$ term.

The silica concentration under steady state conditions was used as the rate indicator because it is the most abundant element in the glass. Previous work on the dissolution of silicate glass has shown that dissolution is nearly

[3] Splits from these same cores were used in the surface area measurements reported in part 3 of this report.

stoichiometric far from saturation (Knauss et al., 1990). Thus the rate of silica release is proportional to the rate of glass dissolution. The dissolution rate is simply the rate of silica release divided by the fraction of silica in the glass. The glasses we used were approximately 32—36 wt. % Si (see Table 2-2). For example, for sample #3/7-N-8 (see data in Appendix 2-1), the measured rate of Si release is the concentration of silicon times the flow rate in mL/day (0.24 $\mu$g/mL*57.75 mL/day = 13.85 $\mu$g/day). The overall glass dissolution rate is that value divided by the weight fraction of Si in the glass (13.85 $\mu$g/day / 0.35 = 40 $\mu$g glass/day), where 0.35 is the weight fraction of Si in core #7.

As an example, we use the experimental data for sample #3/7-N-8 from Appendix 2-1 to compute the reactive surface area of the glass as follows. From the known temperature and pH of the experiment, the rate coefficient ($k'$ in equation 2-2) is computed from the data in Table 10 of Tompson et al. (1999) (and reproduced here in Table 2-1) and the Arrhenius equation

$$k = A_p e^{-E_a / RT} \qquad (2\text{-}3)$$

that is used to compute the effect of temperature on rate coefficient. We arbitrarily assume that one mole of glass is equal to 100 grams. The resulting rate coefficient is calculated to be $9.2\text{x}10^{-5}$ g/m$^2$/day. The rate of glass dissolution, calculated above, is 40 $\mu$g glass/day, or $4.0\text{x}10^{-5}$ g glass/day. By inserting these two values into equation (2-2) we can calculate the reactive surface area as:

$$4.0\text{x}10^{-5} \ / \ 9.2\text{x}10^{-5} = 0.43 \text{ m}^2$$

The core weighs 509.7 grams so the specific reactive surface area is

$$0.43/509.7 = 0.000844 \text{ m}^2/\text{g}$$

or 8.4 cm$^2$/g.

**Table 2-1.** Parameters used with equations (2-1) and (2-3) to compute rate coefficient.

| Factor | Symbol | Value | Units |
|---|---|---|---|
| Arrhenius Pre-Exponential factor | $A_p$ | $9.94\text{x}10^{-6}$ | moles/cm$^2$-sec |
| Activation energy | $E_a$ | 83,680 | Joules/mole |
| Exponent for $H^+$ dependence | p | -0.33 | |
| Temperature | T | 298.15 | Kelvins |
| Gas constant | R | 8.31 | Joules/mole-deg |

Note that the reactive surface areas measured with this technique correspond to an integrated surface area that implicitly reflects the wide variety of flow environments likely to be present in the sample. These include internal porosity that is not accessible to fluids, zones of restricted fluid contact in which diffusional mass transport dominates, and fast flow through fractures. It is the integrated sum of reactive transport in all these types of zones that we try to measure in the experiment. For this reason, we expect these measured surface

areas to be much smaller than measurements of physical (e.g. BET) surface area made on crushed glass samples. The purpose of using intact core is to preserve as much of the textural heterogeneity of the sample as possible. Such heterogeneity, and its impact on fluid flow, is lost when the sample is crushed.

The sample hydraulic conductivity (K) was determined from the measured flow rate and the differential pressure across the length of the sample core. The expression used to calculate K is a simplified form of Darcy's Law:

$$Q = \frac{KA\Delta P}{L} \qquad (2\text{-}4)$$

where Q is the flux of fluid through the sample, K is the hydraulic conductivity, ΔP is the pressure gradient across the core, and A and L are the area of the core face and core length, respectively. Rearranging Darcy's Law for K we obtain:

$$K = \frac{Q\,L}{A\,\Delta P} \qquad (2\text{-}5)$$

which is the expression used to calculate the hydraulic conductivities for our experiments listed in Appendix 2-1.

**Selection and preparation of glass cores**

The natural glass samples we collected ranged in size from about 6 inches to two feet in average dimension. They were selected to include textures that match the variability of textures found in melt glasses. These include homogeneous vesicular glass (pumice), breccias (larger angular pieces in a fine-grained matrix), specimens containing massive glass mixed with vesicular glass, and mixtures of all three textures. Some samples were selected because they had prominent fractures (see photograph of sample 2/4 in Appendix 2-2) so that we could investigate the effects of fractures on reactive surface area. Samples were cored either parallel or perpendicular to the flow banding of the natural glass. Three sizes of cores ( 1.75", 2.75", and 6" in diameter) were prepared with a water cooled coring device. Different diameter cores were used to better capture the scales of heterogeneity and their effect on reactive surface area. The ends of the cores were ground with a precision grinding machine to the size designated for each of the three flow-through reactors. After grinding, the core sample was placed in an ultrasonic bath with deionized water for 15 minutes to remove fines generated from grinding. After rinsing, the cores were placed in a 100°C oven until dry. When cool, the samples were weighed and photographed, and the core dimensions were recorded.

Porosity was calculated from core weights and volumes. Core volumes were calculated from the measured core dimensions. The density of massive rhyolite glass was measured by wet immersion to be 2.5 $g/cm^3$. Porosities calculated in this manner are labeled "Porosity-dry" in Appendix 2-1. We also calculated the porosities of the cores after soaking them overnight or longer in water and then weighing them wet. These porosities provide an indication of how much of the total porosity is accessible to water. These porosities, labeled "Porosity-wet" in

Appendix 2-1, are generally much smaller than the dry porosities, indicating that water does not fill the majority of the pore space under these experimental conditions.

We determined the composition of some of the pumice cores used in the experiments. Because of the similarities of compositions of the samples, the known lack of sensitivity of reaction rate to the small compositional range of the samples, and the large expense for analysis of rock samples, we only analyzed 4 of the 12 samples tested. The data are shown in Table 2-2. For these analyses, the sample was first fused in lithium metaborate at 500°C, quenched, dissolved in dilute nitric acid, and then analyzed using ICP-AES. The compositions do not sum to 100 because we have not analyzed for several minor and trace components.

**Table 2-2.** Chemical composition of natural glass samples used in flow-through reactor tests from locations listed in Table 1-1. Row labelled "*Si*" is weight % Si that is used to compute reactive surface area from Si concentrations in solution.

| Oxide | Wt % Oxide sample 2 | Wt % Oxide sample 6 | Wt % Oxide sample 10 | Wt % Oxide sample 11 |
|---|---|---|---|---|
| **$Al_2O_3$** | 13.77 | 13.87 | 12.47 | 12.47 |
| **CaO** | 0.78 | 0.76 | 0.56 | 0.56 |
| **FeO** | 1.52 | 1.52 | 0.98 | 1.00 |
| **$K_2O$** | 4.77 | 4.84 | 4.45 | 4.54 |
| **MgO** | 0.10 | 0.12 | 0.03 | 0.05 |
| **$Na_2O$** | 4.26 | 4.19 | 3.95 | 3.98 |
| **$SiO_2$** | 71.03 | 69.74 | 75.54 | 76.16 |
| ***Si*** | *33.2* | *32.6* | *35.3* | *32.6* |
| **Total** | 96.2 | 95.0 | 97.9 | 98.8 |

**Flow-through apparatus**

Three flow-through reactors were designed and built to perform these tests. Each reactor holds a core of solid material up to 6 inches in diameter and 8 inches in length. A schematic of the apparatus is shown in Figure 2-1, and a photograph of the 1.75" core apparatus is shown in Figure 2-2. The core is sealed on the outside with flexible tubular membranes. The entire core is subjected to external pressure to squeeze the membrane against the outside of the core to prevent fluid flow along the core wall. All fluid flow is therefore confined to the inside of the core. Gas was used as the confining pressure medium for very permeable samples, which could be tested at fairly low pressures. For safety reasons, at higher confining pressures (and less permeable samples) we used liquid water as a pressure medium.

In order to pressurize with water, we constructed a bladder reservoir which contained nitrogen pressurized water. A line connected the bottom of the bladder (below liquid/vapor contact) to the pressure chamber surrounding the

core. The confining pressure was varied by varying the nitrogen pressure in the bladder. For reasons of operator safety, we constructed safety shields

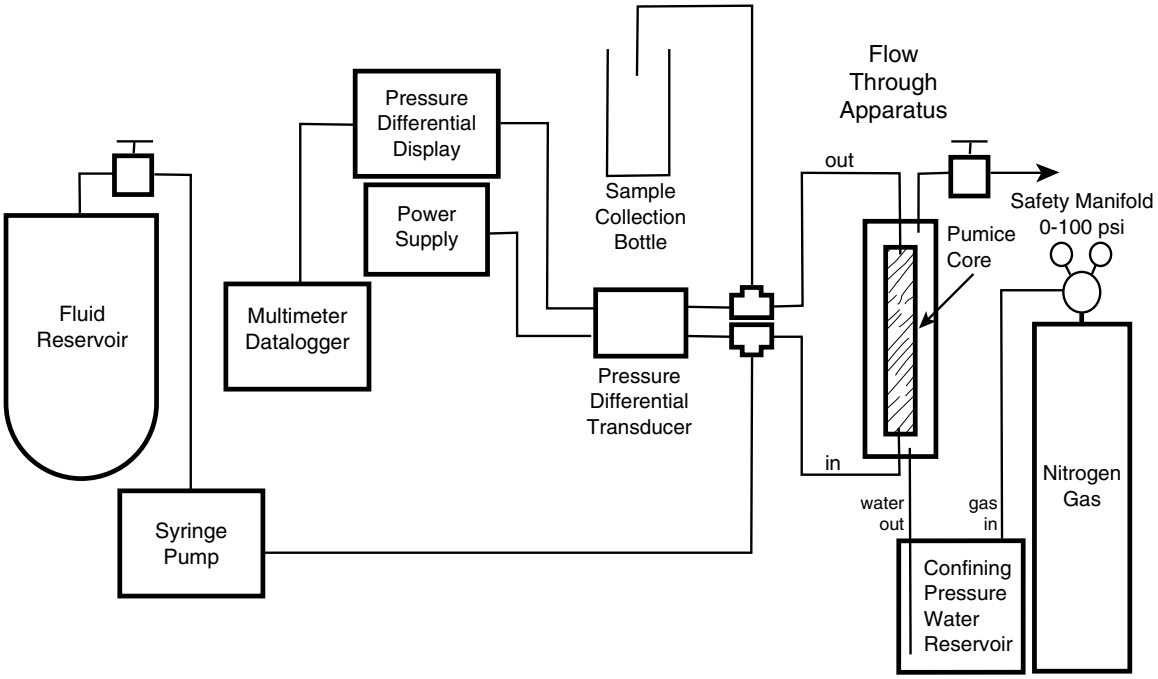


**Figure 2-1**. Schematic diagram of flow-through experiment.

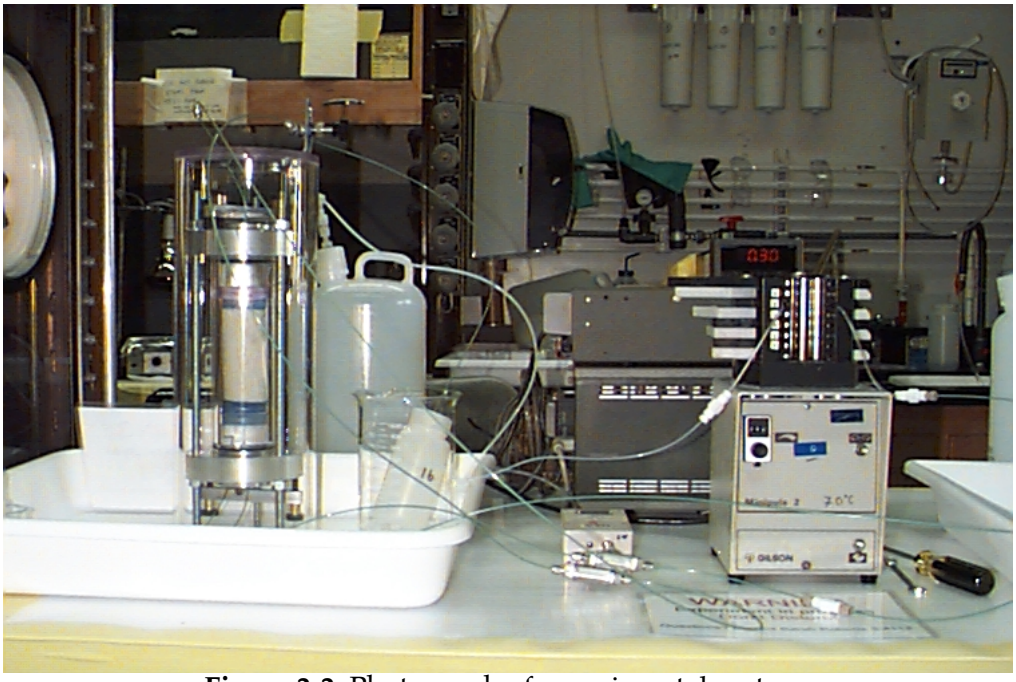

**Figure 2-2**. Photograph of experimental system.

around the entire apparatus. The pressure gradient across the core was measured by a pressure transducer placed between the top and bottom of the core. Pressure gradient data were collected during each sampling event (except for samples 2/7 and 3/7 which were so permeable that the pressure drop was below detection) and used to compute the hydraulic conductivity of the core.

**Experimental procedure**

Fluids of known composition were pumped vertically upwards through the cores. The fluid was a 5 millimolal sodium bicarbonate solution with a pH of 8.5. This solution has the same ionic strength, pH, and pH buffer capacity as typical groundwaters from the NTS. But because it has no dissolved rock constituents, it makes it more convenient and accurate to measure dissolution rates from the concentrations of species dissolved from the glass. The composition of the leachate fluids are given in Appendix 2-1.

A peristaltic pump was used initially to pump fluid through the cores. Problems arose when flow rates became unstable, so a pulse pump was used to try to provide more stable flow rates. Flow rates continued to be unstable for some of the cores using the pulse pump, so we switched to a syringe pump. The syringe pump performed well for all samples.

Once the flow stabilized at the desired rate and several pore volumes had been pumped through the sample, samples were collected periodically for analysis. Note that it is possible that not all the pores were filled with water under these conditions. However, these conditions are not unlike those that will exist underground, where the glass may also have zones where water does not penetrate. The samples were taken in polyethylene containers and then filtered with 0.2 μm Nucleopore filters, and acidified. Filtration excluded particulate or colloidal material which is not believed to result from dissolution of the glass. Because we use dissolved silica to determine the glass reaction rate, we are interested only in dissolved elements that are present in solution as a result of dissolution from the glass surface. Samples were analyzed by inductively coupled plasma atomic emission spectroscopy (ICP-AES).

Although we routinely measure dissolved cations using ICP-AES, for these experiments we needed a rapid turnaround time so that we could be sure we were using the right flow rate. Too high a flow rate would produce cation concentrations too low to measure. Too low a flow rate would generate high cation concentrations where saturation effects would slow reaction rates and complicate data interpretation. For this reason, and because the glass samples are primarily made up of silica, we used silica as an indicator of reaction rate. The molybdenum blue method for silica analysis (Iler, 1979, p. 98-100) was used. It is designed to measure silica concentrations in the range of 0.1 - 1 ppm. In this way we could get feedback on our experimental conditions within a few hours of sampling. All samples were eventually analyzed using ICP-AES. The ICP-AES data set is reported in Appendix 2-1.

**Experimental results**

The experimental data from the flow-through reactor experiments for the twelve cores that were tested are listed in Appendix 2-1. We selected cores based on a desire to perform tests on as wide a variety of textures as possible. We also cored the glass specimens both parallel and perpendicular to flow-banding, in order to evaluate the magnitude of any anisotropy in reactive surface area.

The experimental conditions of the tests are designed to avoid saturation effects. This means that there should be a simple relationship between flow rate and silica concentration: if the fluid flows twice as fast, the silica concentration should be half as large. If saturation effects were present, this would not be true. We therefore plot the product of silica concentration times flow rate. If this value is approximately constant then we confirm we are at steady state and there are no significant saturation effects. We need to avoid saturation effects because they cannot be quantitatively accounted for in the analysis of the data.

A typical plot of silica concentration times flow rate for experiment #3/7 is shown in Fig. 2-3. (For each sample label, the first number (3) identifies the number of the core drilled into the rock, and the second number (7) corresponds to the rock sample listed in Table 1-1). The dissolution rate starts out relatively high, probably due to dissolution of fine grained material, and also preferential dissolution of sharp fractured and stressed surfaces that are generated during sample preparation. Solids having a high curvature, such as sharp edged cracks, are known to have preferentially high dissolution rates and solubilities owing to higher surface free energies (Blum and Stillings, 1995; p.304-305). After a few

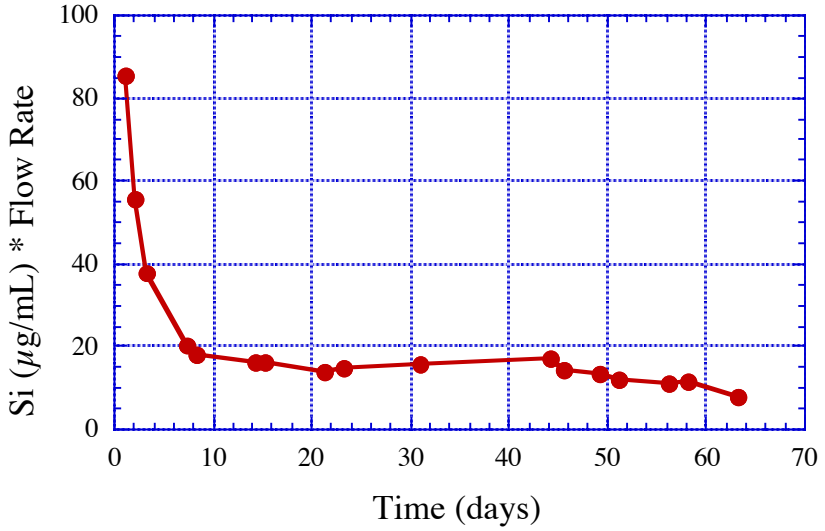


**Figure 2-3**. Silicon concentration times flow rate vs. time for test 3/7 showing evidence for steady state dissolution after about 10 days.

days, the rates tend to stabilize at nearly constant values. We assume this is the steady state reaction rate. The fact that it is relatively constant over flow rates

that vary in this experiment from 60 to 120 ml/day also suggests that saturation effects are negligible.

**Table 2-3.** Density, porosity, hydraulic conductivity, and reactive surface area for all cores tested.

| Sample ID[1] - Core Orientation[2] | Core Texture | Density ($g/cm^3$) | Porosity Wet (%) | Porosity Dry (%) | Hydraulic Conductivity (m/day) | Reactive Surface Area ($cm^2/g$) |
|---|---|---|---|---|---|---|
| 1/1 (perp.) | Massive flow banded obsidian | 2.01 | 4 | 19 | 1.5E-3 | 38 |
| 1/2 (par.) | Massive obsidian with pumice layers | 1.66 | 5 | 34 | 1.3E-3 | 16 |
| 1/4 | Massive flow banded obsidian with pumice layers | 1.25 | 18 | 50 | 2.1E-2 | 13 |
| 2/4 | Fractured obsidian breccia | 1.24 | 22 | 50 | 3.2E-3 | 3 |
| 3/4 | Massive flow banded obsidian | 2.21 | 3 | 12 | 7.8E-3 | 36 |
| 1/7 (par.) | Medium density pumice | 1.17 | 13 | 53 | 3.8E-3 | 24 |
| 2/7 (par.) | Medium density pumice | 1.14 | 9 | 55 | - | 2 |
| 3/7 (perp.) | Medium density pumice | 1.11 | 12 | 56 | - | 8 |
| 1/8 (perp.) | Dense banded pumice | 1.44 | 5 | 42 | 1.4E-4 | 47 |
| 1/10 | Breccia | 1.44 | 17 | 42 | 9.5E-4 | 65 |
| 2/11 (par.) | Very low density pumice | 0.55 | 24 | 78 | 7.3E-3 | 34 |
| 3/11 (par.) | Very low density pumice | 0.47 | 26 | 81 | 2.9E-1 | 26 |

1 Number after the slash corresponds to sample numbers of cores listed in Table 2-3.
2 "perp" indicates core cut perpendicular to flow banding, "par" indicates core cut parallel to flow banding

**Discussion of experimental results**

The values for reactive surface area and hydraulic conductivity obtained from the data are listed in Table 2-3.

*Reactive Surface Area*

Reactive surface areas varied from 2 to 65 $cm^2/g$ with an average of 26 $cm^2/g$. Many of values clustered between 10 and 38 $cm^2/g$. Based on Figure 2-4a and b, there appears to be a weak correlation of surface area with sample porosity. In addition, cores cut parallel to flow banding tended to have the lower measured reactive surface areas (sample 2/7, 1/2, and 1/7; see photos in Appendix 2-2). Another sample without obvious flow banding but with a prominent fracture running through it parallel to the flow direction (sample 2/4) also had a very low reactive surface area. The data are consistent with most of the fluid being channeled through the fracture in that sample and very little fluid moving through the matrix. One would expect highly fractured zones to have the lowest reactive surface areas because fluid packets move quickly through fractures and therefore have effectively lower surface area to volume ratios than fluid packets which move slowly through the matrix and react over a longer time period. Two of the three samples cut perpendicular to flow banding had very high surface areas. In these samples, it may be that fluids are forced to have more intimate contact with the rock matrix because there is no available high permeability fast path through the rock.

It is useful to compare our measured reactive surface areas with estimated surface areas based on sample textures. It was not known prior to our experiments whether the vesicles in pumice are interconnected or isolated from fluid flow. If connected, a simple estimate of surface area is simply that of the surface of the interior walls of the individual bubbles times a surface roughness factor (typically in the range of 3-20 with an average value of 7, see White and Peterson, 1990). For a fairly homogeneous pumice sample such as core 11 (see test 3/11 and photograph in Appendix 2-3), the observed vesicle size is about 1-3 mm with an additional population of smaller vesicles. The calculated physical surface area of this sample is at minimum about 70 $cm^2/g$ based on a surface roughness factor of 7 and excluding the smaller vesicles. Including the smaller vesicles would increase the calculated surface area by a factor of 10 or more. Our measured reactive surface area is about 25 $cm^2/g$, much lower than the estimated physical surface area. This suggests that the fluid does not contact all the surface area available in the sample, probably due to a lack of interconnectedness of some of the vesicles.

*Hydraulic Conductivity*

The measured hydraulic conductivity generally tended to increase with porosity (see Figure 2-4 a and b). Based on our limited data, the samples cut perpendicular to flow banding had lower conductivities than the samples cut parallel to flow banding. The sample with the lowest hydraulic conductivity

(sample 1/8) was a relatively dense pumice with fluid flow direction perpendicular to flow banding. The low measured reactive surface area of sample 2/7, whose flow banding was oriented parallel to flow, also suggests there are favored high permeability paths through pumice layers. This is consistent with the hydraulic conductivity of this sample being too high to measure (the pressure gradient across the sample, as well as sample 3/7, was below detection).

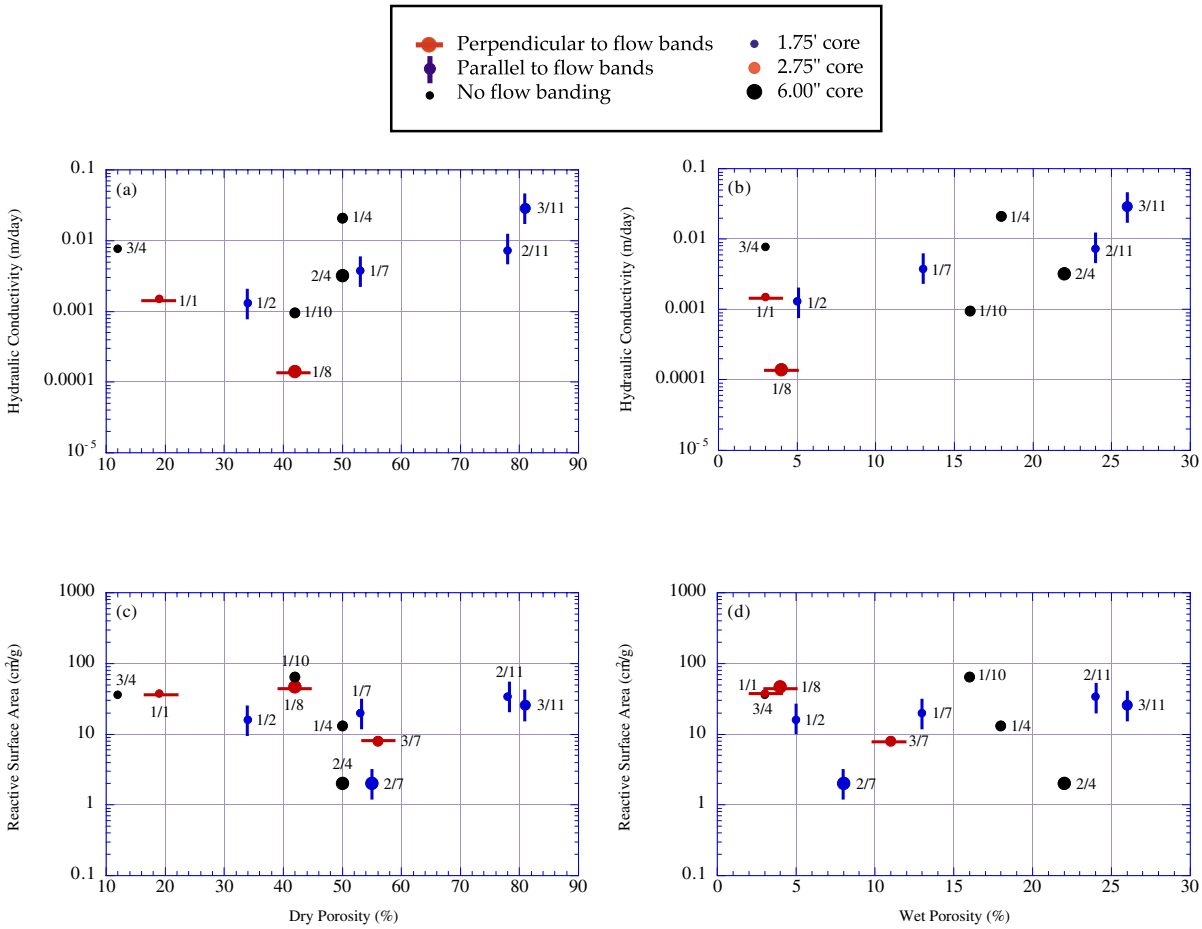


**Figure 2-4**. Hydraulic conductivity and reactive surface area vs. sample dry porosity (a,c) and wet porosity (b,d). Large circles correspond to the 6" diameter cores, medium circles correspond to 2.75" cores, and small circles correspond to 1.75" cores. Blue sample points with vertical lines correspond to samples cored parallel to flow texture. Red sample points with horizontal lines correspond to cores cut perpendicular to flow texture. Black circles indicate samples with no flow banding. Sample labels refer to data points discussed in text.

The plot of hydraulic conductivity vs. reactive surface area shown in Figure 2-5 is complex, as might be expected based on the variety of textures and orientations of samples tested. The two samples cut perpendicular to flow banding had among the highest reactive surface areas and lowest hydraulic conductivities measured. Note that sample 3/7 does not follow this pattern. This suggests that

in general fluids driven upwards thermally through the melt glass may react more substantially with the glass due to the higher reactive surface areas of their flow paths. Fluids that are allowed to flow through high permeability zones such as fractures and banding features will leach less material because of the lower reactive surface areas of their flow paths. Although the magnitude of the effect is not large, it may be important to consider the heterogeneous nature of the melt glass in order to correctly predict radionuclide mobilization.

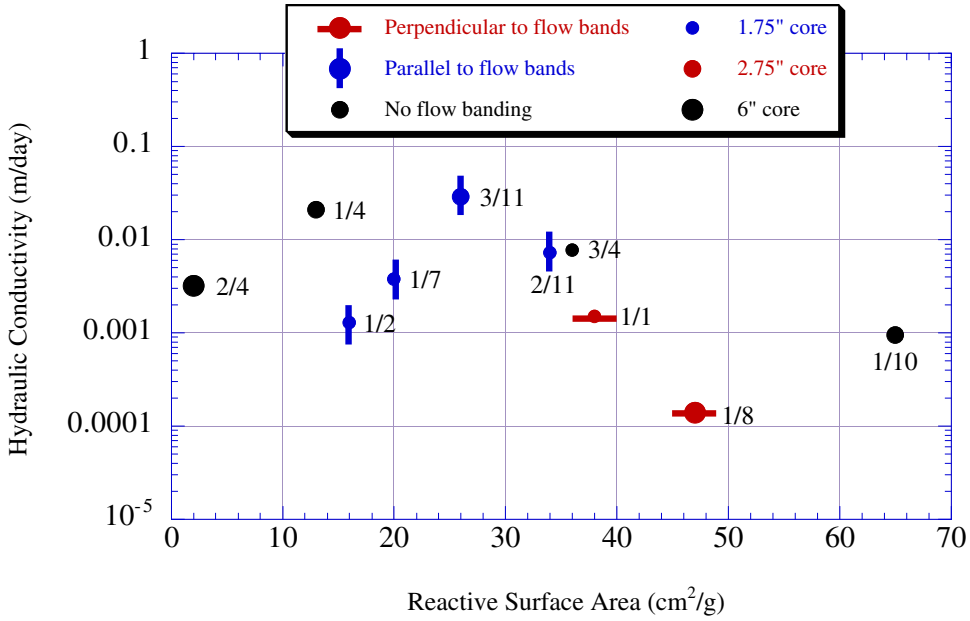


**Figure 1-5**. Hydraulic conductivity vs. reactive surface area for glass core experiments. Large circles correspond to the 6" diameter cores, medium circles correspond to 2.75" cores, and small circles correspond to 1.75" cores. Blue sample points with parallel lines correspond to samples cored parallel to flow texture. Red sample points with horizontal lines correspond to cores cut perpendicular to flow texture. Black circles indicate samples with no flow banding. Sample labels refer to data points discussed in text.

## Tracer experiment

A tracer test was performed on core 1/7 in order to determine whether there are fluid "fast paths" through this core. We assume that fractures provide a fast path through the system, but we were uncertain about the hydrologic properties of vesicular zones. Core 1/7 appears to be a nearly homogeneous pumice sample. Therefore we were interested in knowing how the measured tracer breakthrough time compares with the breakthrough time calculated assuming ideal plug flow behavior.

In the tracer test, the leachate solution is doped with a low concentration of a non-reactive component. The time it takes for the component, called the tracer, to break-through the sample, and the shape of the breakthough curve provide

information on the nature of its flow path. In ideal plug flow, the tracer would arrive at the distal end of the pumice core after one residence time. The residence time is the total pore volume of the sample divided by the fluid flux. If the tracer flows through the sample along a fast path, analogous to that provided by a fracture, the tracer would arrive in less than the residence time. As discussed below, the pumice did provide a fast flow path based on a breakthrough that was about four times faster than predicted assuming ideal plug flow behavior.

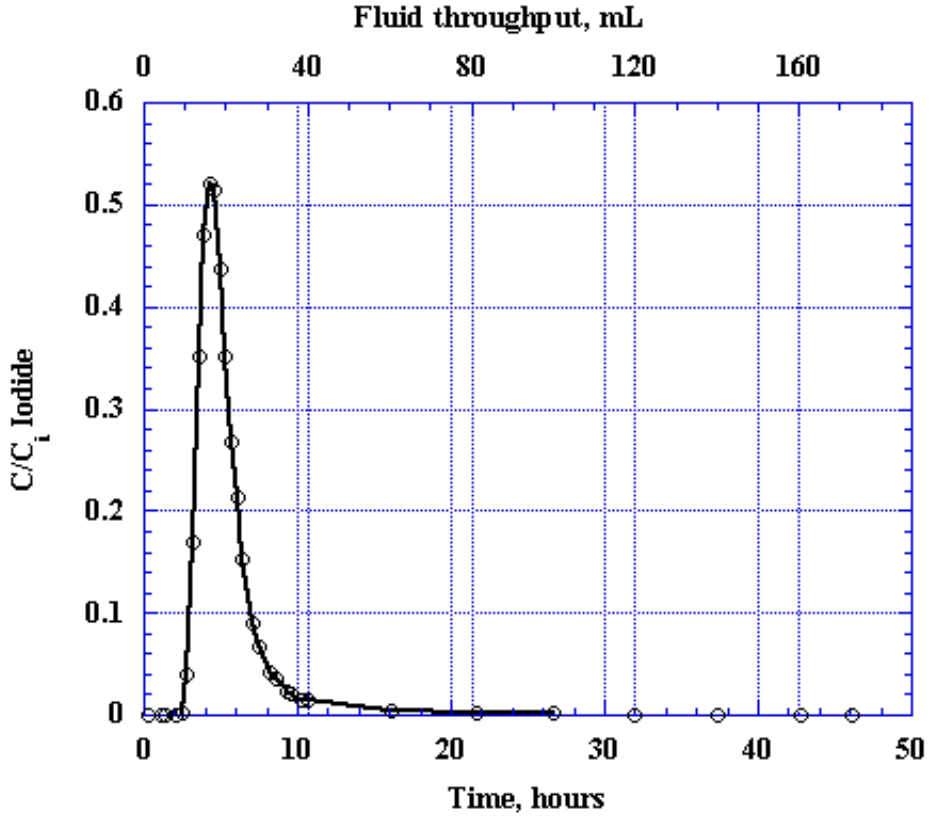


**Figure 2-6**. Normalized iodide concentration ($C/C_I$) versus elapsed time (bottom axis) and fluid flux (top axis). One pore volume equals approximately 84 mL using dry porosity and 21 mL using wet porosity.

We used iodide as our tracer. Five milliliters of a 2 mmol LiI (plus 3 mmol $NaHCO_3$ solution to maintain a constant ionic strength) was injected and pumped through the sample at a constant flow rate of about 90 mL/day. The outflow solution was then monitored for iodide (see data in Table 2-4). The breakthrough curve is shown in Figure 2-6. After about 20 mL of fluid had passed through the core (which corresponds to a time of (20 mL /90 mL/day) or 5.3 hours), iodide could be detected in the outflow. Ideal plug flow behavior predicts breakthrough after one pore volume of flow through the sample. The pore volume is equal to the sample volume times the porosity. If we use the dry porosity to calculate the breakthrough time, we get 158.84*0.53 = 84.2 mL (see data in Appendix 2-1). The breakthrough time is therefore 84.2mL/90mL/day =0.94 days or 22.5 hours. The iodide traveled through the core about 5 times faster than predicted based on ideal plug flow behavior. Alternatively, if we use

the wet porosity, which includes only the pores that are filled when the sample is soaked in water, the breakthrough time is calculated to be 5.5 hours (158.84*0.13 = 20.65 mL; 20.65mL /90 mL/day = 0.23 days; 5.5 hours), very close to the measured breakthrough time. Apparently the wet porosity provides a more accurate measure of the volume of interconnected pores. A simple interpretation of this result is that only about 20% of the vesicles in this sample are interconnected, provide a continuous flow path for water, and therefore allow ideal plug flow behavior.

**Table 2-4**. Concentration data from the tracer test on core 1/7. Total volume corresponds to the accumulated volume since tracer injection. $C/C_i$ is the ratio of measured iodide concentration to iodide concentration in the injected leachate.

| $C/C_I$ Iodide | Total volume (mL) | Time elapsed (hrs) |
|---|---|---|
| 6.17E-05 | 1.33 | 0.35 |
| 5.29E-05 | 3.99 | 1.07 |
| 3.30E-05 | 5.31 | 1.42 |
| 4.44E-05 | 7.97 | 2.13 |
| 1.56E-03 | 9.30 | 2.48 |
| 4.02E-02 | 10.62 | 2.83 |
| 1.70E-01 | 11.98 | 3.19 |
| 3.52E-01 | 13.32 | 3.55 |
| 4.70E-01 | 14.66 | 3.91 |
| 5.20E-01 | 16.01 | 4.27 |
| 5.15E-01 | 17.32 | 4.62 |
| 4.37E-01 | 18.68 | 4.98 |
| 3.52E-01 | 20.04 | 5.34 |
| 2.67E-01 | 21.39 | 5.70 |
| 2.13E-01 | 22.72 | 6.06 |
| 1.53E-01 | 24.01 | 6.40 |
| 8.95E-02 | 26.73 | 7.13 |
| 6.73E-02 | 28.07 | 7.49 |
| 4.20E-02 | 30.75 | 8.20 |
| 3.49E-02 | 32.12 | 8.57 |
| 2.40E-02 | 34.79 | 9.28 |
| 2.03E-02 | 36.09 | 9.62 |
| 1.57E-02 | 38.79 | 10.34 |
| 1.43E-02 | 40.12 | 10.70 |
| 3.54E-03 | 60.47 | 16.13 |
| 1.99E-03 | 81.18 | 21.65 |
| 1.67E-03 | 99.90 | 26.64 |
| 9.85E-04 | 119.88 | 31.97 |
| 9.03E-04 | 140.23 | 37.39 |
| 8.21E-04 | 160.66 | 42.84 |
| 7.09E-04 | 172.93 | 46.11 |

The tracer results help to explain the observed differences between reactive surface area measured in the flow-through core tests, and BET-measured surface areas as discussed in Parts 3 and 4. Apparently the fluids contact mainly glass surfaces along the flow paths that probably correlate with the "wet porosity" volume. Some of the glass surface area that is seen by the sorbing gas and is therefore included in the BET measurement, is in low-permeability restricted zones that do not communicate with the bulk of the fluid passing through the sample. These restricted zones therefore do not provide a radionuclide source term that is proportional to their total surface area.

**Summary and conclusions**

Our method for determining reactive surface provides values for reactive surface areas of materials similar in texture and composition to materials present in the melt glasses. The reactive surface areas for the twelve samples tested range from 2 to 65 $cm^2/g$ (0.0002-.0065$m^2/g$), with most of the values centered around an average value of 26 $cm^2/g$ (.0026 $m^2/g$). Hydraulic conductivities were in the range of 0.0001-0.29 m/day with most of the values between 0.01 and 0.001 m/day.

The range in both parameters is surprisingly small given the wide range of sample textures and orientations used. This would seem to simplify future process-based hydrologic source term modeling (e.g. Tompson et al., 1999) because detailed descriptions of glass morphology and the chaotic distribution of textures in the cavity are not necessary to describe melt glass dissolution. In addition, the hydraulic conductivity values obtained in this study are similar to those that have been used in modeling thermal-induced flow at CHESHIRE (Maxwell and Carle, 2000, pers. comm.). A comparison of these reactive surface areas with physical surface areas of the same glasses measured by BET is given in Part 5.

The tracer flow-through test revealed that fluid flowed through only about 20 vol% of the total porosity in an apparently homogeneous sample that was only 1.75 inches in diameter. This test demonstrates the existence of flow heterogeneity on a small scale. Questions remain, however, about the dependence of the effective porosity on flow rate. Effective porosity is defined here as the portion of the total porosity that serves as a flow path. If effective porosity increases, the surface area availability for reaction increases.

The potential for the reactive surface area of glass to decrease significantly with time owing to precipitation of protective coatings of secondary minerals should also be considered. Secondary mineral formation is favored by the high temperatures and enhanced glass-fluid reaction rates following the test. The flow-through experiments described in this paper were conducted in the absence of secondary mineral precipitation. In real puddle glasses that contain alteration minerals, these minerals are relatively stable in the groundwaters and they may contain some of the released radionuclides. For these reasons, our reactive surface areas determined from the tests described in this report should be considered conservative upper bounds when used to derive a source term

derived from glass reaction with groundwaters. The existence of alteration minerals and their effects on radionuclide retardation are accounted for in modeling of radionuclide release and transport as separate processes and not included as a part of the reactive surface area term (Tompson et al., 1999).

**References**


Blum A. E. and Stillings L. L. (1995) Feldspar dissolution kinetics. In *Chemical Weathering Rates of Silicate Minerals*, Mineralogical Society of America reviews in Mineralogy Vol. 31, A. F. White and S. L. Brantley, eds., pp. 291-351.

Doremus, R. H. (1994) *Glass Science*. New York, John Wiley & Sons.

Iler R. K. (1979) *The Chemistry of Silica*. John Wiley and Sons. 866 p.

Kersting A. B. and Smith D. K. (1999) Observations of nuclear explosive melt glass textures and surface areas. Lawrence Livermore National Laboratory, Draft Report, September, 1999, 18 p.

Knauss, K. G., W. L. Bourcier, K.D. McKeegan, C.I. Merzbacher, S.N. Nguyen, F.J. Ryerson, D. K. Smith, H.C. Weed, L. Newton (1990) Dissolution kinetics of a simple nuclear waste glass as a function of pH, time, and temperature. Materials Research Society Symposium Proceedings 176: 371-381.

Tompson A. F. B., Bruton C. J., and Pawloski G. A. eds. (1999) Evaluation of the hydrologic source term from underground nuclear tests in Frenchman Flat at the Nevada Test Site: The CAMBRIC Test, Lawrence Livermore National Laboratory, Report Number UCRL-ID-132300; March 1999, 319 p.

The following tables list all measured and derived data from the flow-through dissolution tests of the pumice and rhyolite glass cores. The following notes identify and clarify various table entries.

The solution used in the experiments is indicated by an *'N'* in the sample identifier. N refers to a 0.005 molal sodium bicarbonate solution. The bicarbonate solution has roughly the same ionic strength, pH, and pH-buffering capacity as typical NTS groundwaters.

If the sample exhibited flow banding, the core was oriented either *perpendicular* or *parallel* to the flow banding, as indicated for each core. Samples exhibiting no flow banding are also noted.

The sample *porosity-dry* was calculated from the measured weight and volume of the dry core using a density of 2.5 g/cm$^3$ for massive rhyolite glass. To measure the wet weight, the cores were submerged in water overnight, removed from the water and the wet weight recorded. The sample *porosity-wet* was calculated similarly as the dry porosity using the wet core weight. These are therefore bulk porosities as compared to effective porosities determined using tracers.

The difference between *Mass 0* and *Mass 1* is the mass of fluid sample collected over the *Collection Time*. *Time Elapsed* refers to the elapsed time since the start of the experiment.

*Confining pressure* refers to the pressure on the flexible jacket surrounding the core. The jacket prevented fluids from passing around the outside of the core rather than passing through the core. psi $D_o$ refers to the differential pressure in psi across the core that drove fluid flow. This value was used to calculate the hydraulic conductivity of the sample.

*Si* is the measured silicon concentration in solution in $\mu$g/mL (ppm). *Si*FlowRate* should be constant for steady state conditions.

*Dissolution rate* in grams per day is a calculated rate (Eq. 2-1) based on the measured Si concentration, flow rate, and Si content of the glass.

*Reaction rate* coefficient is calculated from a glass dissolution rate model according to Eq. 2-3 and Table 2-2 (Chapter 6 of Tompson et al., 1999).

*Reactive surface area* (the quotient of glass dissolution rate/rate coefficient, Eq. 2-2) is given as a raw value ($m^2$), and as bulk volume ($m^2/m^3$) and mass normalized ($m^2/g$) values.

*Hydraulic conductivity* is computed from sample geometry, differential pressure, and Darcy's Law (Eq. 2-4).

The *affinity term* (1-Q/K) is calculated using the solubility product of amorphous silica for K and the measured silica concentration for Q.

The *residence time* is computed from the bulk porosity and flow rate for both the dry and wet cores.

Entries in italic are estimated values based on like data. Commonly we did not have differential pressure data for every sample measurement, but the values were nearly constant in time. For these samples, the differential pressure was estimated from related data. These data are therefore more uncertain.

**Core # 1/1 cored perpendicular to flow banding**

| Length (in) | Length (cm) | Diameter (in) | Diameter (cm) | Weight-dry (g) | Weight-wet (g) | Volume ($cm^3$) | Porosity-dry (%) | Porosity-wet (%) | Density ($g/cm^3$) |
|---|---|---|---|---|---|---|---|---|---|
| 4.05 | 10.29 | 1.75 | 4.44 | 320.16 | 326.13 | 159.03 | 19 | 4 | 2.01 |

| Sample ID | Mass 0 (g) | Mass 1 (g) | Collection Time (hrs) | Solution Mass (g) | Time Elapsed (days) | Flow Rate (mL/day) | pH Measured | Confining Pres. (psi) | psi $D_o$ | Si ($\mu$g/mL) | Si*Flow Rate ($\mu$g/day) |
|---|---|---|---|---|---|---|---|---|---|---|---|
| 1/1-N-1 | 24.10 | 94.37 | 28.38 | 70.26 | 10.11 | 59.41 | 8.78 | <8 | 3.60 | 0.84 | 49.84 |
| 1/1-N-2 | 24.37 | 77.19 | 21.23 | 52.82 | 12.56 | 59.70 | 8.11 | <8 | 3.85 | 0.80 | 47.67 |

| Sample ID | Glass Dissolution (g/day) | Reaction Rate (g/ $m^2$/day) | Reactive Surface Area ($m^2$) | Reactive Surface Area ($m^2/m^3$) | Reactive Surface Area ($cm^2/g$) | Hydraulic Conductivity (mD) | Hydraulic Conductivity (m/day) | Affinity Term (1-Q/K) | Residence Time-dry (hours) | Residence Time-wet (hours) | Fluid Velocity (m/year) |
|---|---|---|---|---|---|---|---|---|---|---|---|
| 1/1-N-1 | 1.42E-04 | 1.60E-04 | 8.88E-01 | 5.58E+03 | 27.74 | 1.8 | 1.56E-03 | 0.98 | 12.51 | 2.42 | 373.16 |
| 1/1-N-2 | 1.36E-04 | 8.75E-05 | 1.56E+00 | 9.79E+03 | 48.63 | 1.7 | 1.47E-03 | 0.99 | 12.45 | 2.40 | 374.94 |

**Core # 1/2 cored parallel to flow banding**

| Length (in) | Length (cm) | Diameter (in) | Diameter (cm) | Weight-dry (g) | Weight-wet (g) | Volume ($cm^3$) | Porosity-dry (%) | Porosity-wet (%) | Density ($g/cm^3$) |
|---|---|---|---|---|---|---|---|---|---|
| 4.01 | 10.19 | 1.74 | 4.42 | 259.32 | 267.34 | 156.51 | 34 | 5 | 1.66 |

| Sample ID | Mass 0 (g) | Mass 1 (g) | Collection Time (hrs) | Solution Mass (g) | Time Elapsed (days) | Flow Rate (mL/day) | pH Measured | Confining Pres. (psi) | psi $D_o$ | Si ($\mu$g/mL) | Si*Flow Rate ($\mu$g/day) |
|---|---|---|---|---|---|---|---|---|---|---|---|
| 1/2-N-7 | 24.09 | 74.36 | 18.78 | 50.26 | 15.10 | 64.22 | 8.29 | 20 | *4.15* | 0.34 | 21.54 |
| 1/2-N-8 | 24.20 | 64.00 | 17.93 | 39.80 | 17.07 | 53.26 | 8.22 | 20 | *4.15* | 0.29 | 15.67 |

| Sample ID | Glass Dissolution (g/day) | Reaction Rate (g/ $m^2$/day) | Reactive Surface Area ($m^2$) | Reactive Surface Area ($m^2/m^3$) | Reactive Surface Area ($cm^2/g$) | Hydraulic Conductivity (mD) | Hydraulic Conductivity (m/day) | Affinity Term (1-Q/K) | Residence Time-dry (hours) | Residence Time-wet (hours) | Fluid Velocity (m/year) |
|---|---|---|---|---|---|---|---|---|---|---|---|
| 1/2-N-7 | 6.49E-05 | 1.42E-04 | 4.56E-01 | 2914.89 | 17.59 | *1.7* | *1.46E-03* | 0.99 | 19.73 | 2.99 | 298.10 |
| 1/2-N-8 | 4.72E-05 | 1.34E-04 | 3.52E-01 | 2.25E+03 | 13.57 | *1.4* | *1.21E-03* | 0.99 | 23.78 | 3.61 | 247.23 |

**Core # 1/4** **no flow orientation**

| Length (in) | Length (cm) | Diameter (in) | Diameter (cm) | Weight-dry (g) | Weight-wet (g) | Volume ($cm^3$) | Porosity-dry (%) | Porosity-wet (%) | Density (g/ $cm^3$) |
|---|---|---|---|---|---|---|---|---|---|
| 4.30 | 10.92 | 2.80 | 7.10 | 542.02 | 620.51 | 432.34 | 50 | 18 | 1.25 |

| Sample ID | Mass 0 (g) | Mass 1 (g) | Collection Time (hrs) | Solution Mass (g) | Time Elapsed (days) | Flow Rate (mL/day) | pH Measured | Confining Pres. (psi) | psi $D_o$ | Si ($\mu$g/mL) | Si*Flow Rate ($\mu$g/day) |
|---|---|---|---|---|---|---|---|---|---|---|---|
| 1/4-N-2 | 24.23 | 70.77 | 18.92 | 46.54 | 8.06 | 59.05 | 8.30 | <8 | 0.11 | 0.51 | 29.90 |
| 1/4-N-3 | 24.29 | 61.28 | 14.83 | 36.99 | 11.01 | 59.85 | 8.82 | <8 | 0.11 | 0.57 | 33.92 |

| Sample ID | Glass Dissolution (g/day) | Reaction Rate (g/ $m^2$/day) | Reactive Surface Area ($m^2$) | Reactive Surface Area ($m^2/m^3$) | Reactive Surface Area ($cm^2$/g) | Hydraulic Conductivity (mD) | Hydraulic Conductivity (m/day) | Affinity Term (1-Q/K) | Residence Time-dry (hours) | Residence Time-wet (hours) | Fluid Velocity (m/year) |
|---|---|---|---|---|---|---|---|---|---|---|---|
| 1/4-N-2 | 8.54E-05 | 1.03E-04 | 8.30E-01 | 1.92E+03 | 15.32 | 24.4 | 2.11E-02 | 0.99 | 87.60 | 31.89 | 30.00 |
| 1/4-N-3 | 9.69E-05 | 1.68E-04 | 5.77E-01 | 1.33E+03 | 10.65 | 24.7 | 2.14E-02 | 0.99 | 86.42 | 31.46 | 30.41 |

**Core # 2/4** **no flow orientation**

| Length (in) | Length (cm) | Diameter (in) | Diameter (cm) | Weight-dry (g) | Weight-wet (g) | Volume ($cm^3$) | Porosity-dry (%) | Porosity-wet (%) | Density (g/ $cm^3$) |
|---|---|---|---|---|---|---|---|---|---|
| 5.31 | 13.48 | 5.96 | 15.13 | 3011.10 | 3546.2 | 2424.15 | 50 | 22 | 1.24 |

| Sample ID | Mass 0 (g) | Mass 1 (g) | Collection Time (hrs) | Solution Mass (g) | Time Elapsed (days) | Flow Rate (mL/day) | pH Measured | Confining Pres. (psi) | psi $D_o$ | Si ($\mu$g/mL) | Si*Flow Rate ($\mu$g/day) |
|---|---|---|---|---|---|---|---|---|---|---|---|
| 2/4-N-12 | 24.27 | 46.25 | 6.22 | 21.98 | 124.12 | 84.84 | 8.85 | 12 | 0.30 | 0.33 | 27.93 |
| 2/4-N-13 | 24.32 | 70.66 | 11.65 | 46.34 | 125.47 | 95.46 | 8.33 | 12 | 0.30 | 0.36 | 34.62 |

| Sample ID | Glass Dissolution (g/day) | Reaction Rate (g/ $m^2$/day) | Reactive Surface Area ($m^2$) | Reactive Surface Area ($m^2/m^3$) | Reactive Surface Area ($cm^2$/g) | Hydraulic Conductivity (mD) | Hydraulic Conductivity (m/day) | Affinity Term (1-Q/K) | Residence Time-dry (hours) | Residence Time-wet (hours) | Fluid Velocity (m/year) |
|---|---|---|---|---|---|---|---|---|---|---|---|
| 2/4-N-12 | 7.98E-05 | 1.74E-04 | 4.58E-01 | 1.89E+02 | 1.52 | 3.5 | 3.01E-03 | 1.00 | 345.05 | 151.35 | 7.80 |
| 2/4-N-13 | 9.89E-05 | 1.06E-04 | 9.32E-01 | 3.85E+02 | 3.10 | 3.9 | 3.39E-03 | 1.00 | 306.65 | 134.51 | 8.78 |

**Core # 3/4 no flow orientation**

| Length (in) | Length (cm) | Diameter (in) | Diameter (cm) | Weight-dry (g) | Weight-wet (g) | Volume ($cm^3$) | Porosity-dry (%) | Porosity-wet (%) | Density (g/ $cm^3$) |
|---|---|---|---|---|---|---|---|---|---|
| 4.10 | 10.41 | 1.74 | 4.43 | 354.19 | 359.72 | 160.42 | 12 | 3 | 2.21 |

| Sample ID | Mass 0 (g) | Mass 1 (g) | Collection Time (hrs) | Solution Mass (g) | Time Elapsed (days) | Flow Rate (mL/day) | pH Measured | Confining Pres. (psi) | psi $D_o$ | Si ($\mu$g/mL) | Si*Flow Rate ($\mu$g/day) |
|---|---|---|---|---|---|---|---|---|---|---|---|
| 3/4-N-1 | 24.25 | 84.04 | 24.12 | 59.78 | 2.69 | 59.50 | 8.40 | 12 | 0.66 | 0.85 | 50.39 |
| 3/4-N-2 | 20.49 | 63.15 | 17.20 | 42.66 | 4.45 | 59.52 | 8.00 | 12 | 0.81 | 0.60 | 35.84 |

| Sample ID | Glass Dissolution (g/day) | Reaction Rate (g/ $m^2$/day) | Reactive Surface Area ($m^2$) | Reactive Surface Area ($m^2/m^3$) | Reactive Surface Area ($cm^2$/g) | Hydraulic Conductivity (mD) | Hydraulic Conductivity (m/day) | Affinity Term (1-Q/K) | Residence Time-dry (hours) | Residence Time-wet (hours) | Fluid Velocity (m/year) |
|---|---|---|---|---|---|---|---|---|---|---|---|
| 3/4-N-1 | 1.44E-04 | 1.12E-04 | 1.29E+00 | 8.04E+03 | 36.41 | 10.0 | 8.60E-03 | 0.98 | 7.56 | 2.23 | 408.42 |
| 3/4-N-2 | 1.02E-04 | 8.06E-05 | 1.27E+00 | 7.92E+03 | 35.87 | 8.1 | 7.02E-03 | 0.99 | 7.56 | 2.23 | 408.60 |

**Core # 1/7 cored parallel to flow banding**

| Length (in) | Length (cm) | Diameter (in) | Diameter (cm) | Weight-dry (g) | Weight-wet (g) | Volume ($cm^3$) | Porosity-dry (%) | Porosity-wet (%) | Density (g/ $cm^3$) |
|---|---|---|---|---|---|---|---|---|---|
| 4.03 | 10.24 | 1.75 | 4.45 | 186.60 | 207.62 | 158.84 | 53 | 13 | 1.17 |

| Sample ID | Mass 0 (g) | Mass 1 (g) | Collection Time (hrs) | Solution Mass (g) | Time Elapsed (days) | Flow Rate (mL/day) | pH Measured | Confining Pres. (psi) | psi $D_o$ | Si ($\mu$g/mL) | Si*Flow Rate ($\mu$g/day) |
|---|---|---|---|---|---|---|---|---|---|---|---|
| 1/7-N-21 | 24.31 | 38.90 | 11.18 | 14.60 | 120.85 | 31.32 | 8.56 | 12 | 0.80 | 0.46 | 14.40 |
| 1/7-N-22 | 24.21 | 34.66 | 7.63 | 10.45 | 121.62 | 32.86 | 8.43 | 12 | 0.80 | 0.53 | 17.49 |

| Sample ID | Glass Dissolution (g/day) | Reaction Rate (g/ $m^2$/day) | Reactive Surface Area ($m^2$) | Reactive Surface Area ($m^2/m^3$) | Reactive Surface Area ($cm^2$/g) | Hydraulic Conductivity (mD) | Hydraulic Conductivity (m/day) | Affinity Term (1-Q/K) | Residence Time-dry (hours) | Residence Time-wet (hours) | Fluid Velocity (m/year) |
|---|---|---|---|---|---|---|---|---|---|---|---|
| 1/7-N-21 | 4.11E-05 | 1.31E-04 | 3.13E-01 | 1.97E+03 | 16.80 | 4.3 | 3.67E-03 | 1.00 | 64.52 | 16.10 | 55.69 |
| 1/7-N-22 | 5.00E-05 | 1.16E-04 | 4.29E-01 | 2.70E+03 | 23.00 | 4.5 | 3.85E-03 | 1.00 | 61.50 | 15.35 | 58.42 |

**Core # 2/7 cored parallel to flow banding**

| Length (in) | Length (cm) | Diameter (in) | Diameter (cm) | Weight-dry (g) | Weight-wet (g) | Volume ($cm^3$) | Porosity-dry (%) | Porosity-wet (%) | Density (g/ $cm^3$) |
|---|---|---|---|---|---|---|---|---|---|
| 6.15 | 15.62 | 5.99 | 15.21 | 3226.40 | 3477.50 | 2840.02 | 55 | 9 | 1.14 |

| Sample ID | Mass 0 (g) | Mass 1 (g) | Collection Time (hrs) | Solution Mass (g) | Time Elapsed (days) | Flow Rate (mL/day) | pH Measured | Confining Pres. (psi) | psi $D_o$ | Si ($\mu$g/mL) | Si*Flow Rate ($\mu$g/day) |
|---|---|---|---|---|---|---|---|---|---|---|---|
| 2/7-N-9 | 32.41 | 74.53 | 24.52 | 42.11 | 16.44 | 41.23 | 8.56 | 5 | - | 0.66 | 27.03 |
| 2/7-N-10 | 20.92 | 65.92 | 24.25 | 45.00 | 17.46 | 44.53 | 8.29 | 5 | - | 0.56 | 24.74 |

| Sample ID | Glass Dissolution (g/day) | Reaction Rate (g/ $m^2$/day) | Reactive Surface Area ($m^2$) | Reactive Surface Area ($m^2/m^3$) | Reactive Surface Area ($cm^2$/g) | Affinity Term (1-Q/K) | Residence Time-dry (hours) | Residence Time-wet (hours) | Fluid Velocity (m/year) |
|---|---|---|---|---|---|---|---|---|---|
| 2/7-N-9 | 7.72E-05 | 1.30E-04 | 5.95E-01 | 2.09E+02 | 1.84 | 0.99 | 902.01 | 146.15 | 9.36 |
| 2/7-N-10 | 7.07E-05 | 1.02E-04 | 6.94E-01 | 2.44E+02 | 2.15 | 0.99 | 835.07 | 135.31 | 10.11 |

**Core # 3/7 cored perpendicular to flow banding**

| Length (in) | Length (cm) | Diameter (in) | Diameter (cm) | Weight-dry (g) | Weight-wet (g) | Volume ($cm^3$) | Porosity-dry (%) | Porosity-wet (%) | Density (g/ $cm^3$) |
|---|---|---|---|---|---|---|---|---|---|
| 4.58 | 11.63 | 2.79 | 7.09 | 509.70 | 564.03 | 459.83 | 56 | 12 | 1.11 |

| Sample ID | Mass 0 (g) | Mass 1 (g) | Collection Time (hrs) | Solution Mass (g) | Time Elapsed (days) | Flow Rate (mL/day) | pH Measured | Confining Pres. (psi) | psi $D_o$ | Si ($\mu$g/mL) | Si*Flow Rate ($\mu$g/day) |
|---|---|---|---|---|---|---|---|---|---|---|---|
| 3/7-N-8 | 24.14 | 83.89 | 24.83 | 59.75 | 21.41 | 57.75 | 8.16 | 7 | - | 0.24 | 13.85 |
| 3/7-N-9 | 24.15 | 81.70 | 23.87 | 57.55 | 23.36 | 57.87 | 8.23 | 7 | - | 0.25 | 14.50 |

| Sample ID | Glass Dissolution (g/day) | Reaction Rate (g/ $m^2$/day) | Reactive Surface Area ($m^2$) | Reactive Surface Area ($m^2/m^3$) | Reactive Surface Area ($cm^2$/g) | Affinity Term (1-Q/K) | Residence Time-dry (hours) | Residence Time-wet (hours) | Fluid Velocity (m/year) |
|---|---|---|---|---|---|---|---|---|---|
| 3/7-N-8 | 3.96E-05 | 9.20E-05 | 4.30E-01 | 9.35E+02 | 8.44 | 1.00 | 106.37 | 22.57 | 45.15 |
| 3/7-N-9 | 4.14E-05 | 9.74E-05 | 4.25E-01 | 9.25E+02 | 8.35 | 0.99 | 106.14 | 22.52 | 45.25 |

**Core # 1/8** **cored perpendicular to flow banding**

| Length (in) | Length (cm) | Diameter (in) | Diameter (cm) | Weight-dry (g) | Weight-wet (g) | Volume ($cm^3$) | Porosity-dry (%) | Porosity-wet (%) | Density (g/ $cm^3$) |
|---|---|---|---|---|---|---|---|---|---|
| 4.99 | 12.66 | 6.00 | 15.23 | 3324.50 | 3431.30 | 2305.87 | 42 | 5 | 1.44 |

| Sample ID | Mass 0 (g) | Mass 1 (g) | Collection Time (hrs) | Solution Mass (g) | Time Elapsed (days) | Flow Rate (mL/day) | pH Measured | Confining Pres. (psi) | psi $D_o$ | Si ($\mu$g/mL) | Si*Flow Rate ($\mu$g/day) |
|---|---|---|---|---|---|---|---|---|---|---|---|
| 1/8-N-12 | 31.77 | 118.47 | 16.10 | 86.70 | 59.04 | 129.24 | 7.61 | 20 | 8.90 | 2.49 | 316.53 |
| 1/8-N-13 | 32.42 | 112.56 | 15.38 | 80.14 | 60.04 | 125.02 | 7.44 | 20 | 9.27 | 2.45 | 299.40 |

| Sample ID | Glass Dissolution (g/day) | Reaction Rate (g/ $m^2$/day) | Reactive Surface Area ($m^2$) | Reactive Surface Area ($m^2/m^3$) | Reactive Surface Area ($cm^2$/g) | Hydraulic Conductivity (mD) | Hydraulic Conductivity (m/day) | Affinity Term (1-Q/K) | Residence Time-dry (hours) | Residence Time-wet (hours) | Fluid Velocity (m/year) |
|---|---|---|---|---|---|---|---|---|---|---|---|
| 1/8-N-12 | 1.00E-03 | 5.34E-05 | 1.87E+01 | 8.13E+03 | 56.38 | 0.2 | 1.44E-04 | 0.96 | 181.26 | 19.83 | 55.95 |
| 1/8-N-13 | 9.04E-04 | 5.96E-05 | 1.52E+01 | 6.58E+03 | 45.65 | 0.2 | 1.33E-04 | 0.96 | 187.37 | 20.49 | 54.12 |

**Core # 1/10** **breccia sample**

| Length (in) | Length (cm) | Diameter (in) | Diameter (cm) | Weight-dry (g) | Weight-wet (g) | Volume ($cm^3$) | Porosity-dry (%) | Porosity-wet (%) | Density (g/ $cm^3$) |
|---|---|---|---|---|---|---|---|---|---|
| 4.43 | 11.26 | 2.79 | 7.07 | 638.69 | 713.64 | 442.43 | 42 | 17 | 1.44 |

| Sample ID | Mass 0 (g) | Mass 1 (g) | Collection Time (hrs) | Solution Mass (g) | Time Elapsed (days) | Flow Rate (mL/day) | pH Measured | Confining Pres. (psi) | psi $D_o$ | Si ($\mu$g/mL) | Si*Flow Rate ($\mu$g/day) |
|---|---|---|---|---|---|---|---|---|---|---|---|
| 1/10-N-4 | 35.70 | 90.60 | 21.05 | 54.90 | 9.33 | 62.60 | 8.09 | 20 | - | 2.20 | 137.72 |
| 1/10-N-5 | 24.11 | 81.89 | 23.82 | 57.79 | 12.22 | 58.23 | 8.17 | 20 | 3.34 | 1.80 | 104.69 |

| Sample ID | Glass Dissolution (g/day) | Reaction Rate (g/ $m^2$/day) | Reactive Surface Area ($m^2$) | Reactive Surface Area ($m^2/m^3$) | Reactive Surface Area ($cm^2$/g) | Hydraulic Conductivity (mD) | Hydraulic Conductivity (m/day) | Affinity Term (1-Q/K) | Residence Time-dry (hours) | Residence Time-wet (hours) | Fluid Velocity (m/year) |
|---|---|---|---|---|---|---|---|---|---|---|---|
| 1/10-N-5 | 3.90E-04 | 8.05E-05 | 4.85E+00 | 1.10E+04 | 75.86 | - | - | 0.96 | 71.68 | 28.73 | 34.32 |
| 1/10-N-5 | 2.96E-04 | 8.63E-05 | 3.44E+00 | 7.76E+03 | 53.79 | 0.8 | 7.10E-04 | 0.97 | 77.05 | 30.89 | 31.93 |

**Core # 2/11 cored parallel to flow banding**

| Length (in) | Length (cm) | Diameter (in) | Diameter (cm) | Weight-dry (g) | Weight-wet (g) | Volume ($cm^3$) | Porosity-dry (%) | Porosity-wet (%) | Density (g/ $cm^3$) |
|---|---|---|---|---|---|---|---|---|---|
| 4.05 | 10.29 | 1.75 | 4.43 | 87.17 | 125.44 | 158.72 | 66 | 24 | 0.55 |

| Sample ID | Mass 0 (g) | Mass 1 (g) | Collection Time (hrs) | Solution Mass (g) | Time Elapsed (days) | Flow Rate (mL/day) | pH Measured | Confining Pres. (psi) | psi $D_o$ | Si ($\mu$g/mL) | Si*Flow Rate ($\mu$g/day) |
|---|---|---|---|---|---|---|---|---|---|---|---|
| 2/11-N-22 | 20.49 | 71.35 | 17.62 | 50.86 | 36.23 | 69.29 | 8.68 | 5 | 1.46 | 0.19 | 13.36 |
| 2/11-N-23 | 24.26 | 99.18 | 26.48 | 74.92 | 41.59 | 67.90 | 8.82 | 5 | 0.63 | 0.26 | 17.40 |

| Sample ID | Glass Dissolution (g/day) | Reaction Rate (g/ $m^2$/day) | Reactive Surface Area ($m^2$) | Reactive Surface Area ($m^2/m^3$) | Reactive Surface Area ($cm^2$/g) | Hydraulic Conductivity (mD) | Hydraulic Conductivity (m/day) | Affinity Term (1-Q/K) | Residence Time-dry (hours) | Residence Time-wet (hours) | Fluid Velocity (m/year) |
|---|---|---|---|---|---|---|---|---|---|---|---|
| 2/11-N-22 | 3.75E-05 | 1.33E-04 | 2.82E-01 | 1.77E+03 | 32.32 | 5.2 | 4.49E-03 | 0.99 | 36.25 | 13.26 | 67.98 |
| 2/11-N-23 | 4.89E-05 | 1.54E-04 | 3.18E-01 | 2.01E+03 | 36.53 | 11.7 | 1.01E-02 | 1.00 | 36.99 | 13.53 | 66.62 |

**Core # 3/11 cored parallel to flow banding**

| Length (in) | Length (cm) | Diameter (in) | Diameter (cm) | Weight-dry (g) | Weight-wet (g) | Volume ($cm^3$) | Porosity-dry (%) | Porosity-wet (%) | Density (g/ $cm^3$) |
|---|---|---|---|---|---|---|---|---|---|
| 4.45 | 11.29 | 2.79 | 7.07 | 209.95 | 327.01 | 443.73 | 81 | 26 | 0.47 |

| Sample ID | Mass 0 (g) | Mass 1 (g) | Collection Time (hrs) | Solution Mass (g) | Time Elapsed (days) | Flow Rate (mL/day) | pH Measured | Confining Pres. (psi) | psi $D_o$ | Si ($\mu$g/mL) | Si*Flow Rate ($\mu$g/day) |
|---|---|---|---|---|---|---|---|---|---|---|---|
| 3/11-N-12 | 20.48 | 81.59 | 24.83 | 61.11 | 15.22 | 59.06 | 8.27 | 5 | *0.08* | 0.33 | 19.46 |
| 3/11-N-13 | 24.13 | 78.04 | 23.23 | 53.91 | 16.16 | 55.69 | 8.41 | 5 | *0.08* | 0.34 | 18.96 |

| Sample ID | Glass Dissolution (g/day) | Reaction Rate (g/ $m^2$/day) | Reactive Surface Area ($m^2$) | Reactive Surface Area ($m^2/m^3$) | Reactive Surface Area ($cm^2$/g) | Hydraulic Conductivity (mD) | Hydraulic Conductivity (m/day) | Affinity Term (1-Q/K) | Residence Time-dry (hours) | Residence Time-wet (hours) | Fluid Velocity (m/year) |
|---|---|---|---|---|---|---|---|---|---|---|---|
| 3/11-N-12 | 5.47E-05 | 9.15E-05 | 5.97E-01 | 1.35E+03 | 28.44 | *34.8* | *3.01E-02* | 0.99 | 146.19 | 47.57 | 20.79 |
| 3/11-N-13 | 5.32E-05 | 1.03E-04 | 5.15E-01 | 1.16E+03 | 24.52 | *32.8* | *2.83E-02* | 1.00 | 155.04 | 50.45 | 19.61 |

**Appendix 2-2. Photographs of cores tested.**

**Core #1/1, cored perpendicular to flow banding**
1.75” diameter, 4.05” length
porosity-wet = 4%, porosity-dry = 19%
hydraulic conductivity = 1.5E-3 m/day
reactive surface area = 38 $cm^2/g$

**Appendix 2-2. Photographs of cores tested.**

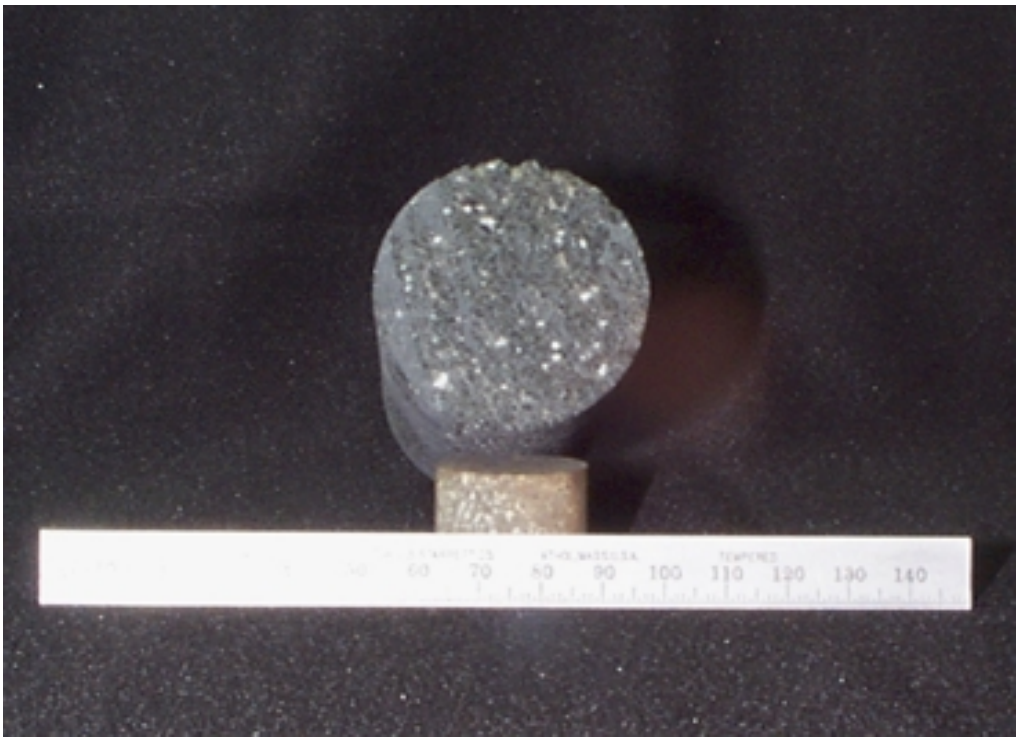

**Core #1/2, cored parallel to flow banding**
1.74” diameter, 4.01” length
porosity-wet = 5%, porosity-dry = 34%
hydraulic conductivity = 1.3E-3 m/day
reactive surface area = 16 $cm^2/g$

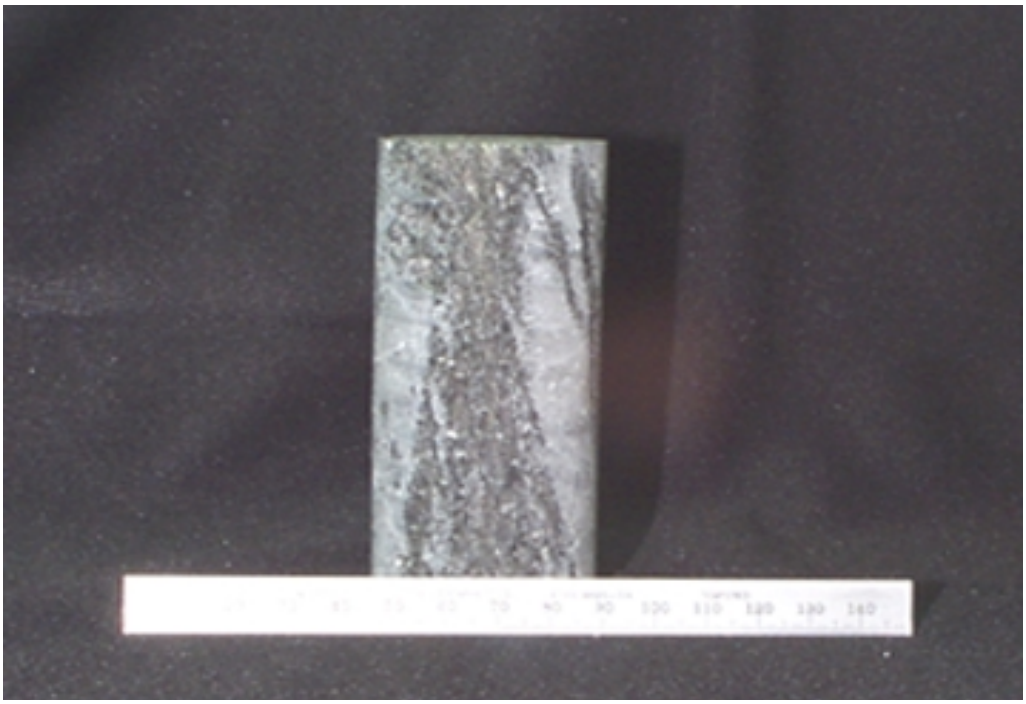

**Appendix 2-2. Photographs of cores tested.**

**Core #1/4, no flow orientation**
2.80” diameter, 4.30” length
porosity-wet = 18%, porosity-dry = 50%
hydraulic conductivity = 2.1E-2 m/day
reactive surface area = 13 $cm^2/g$

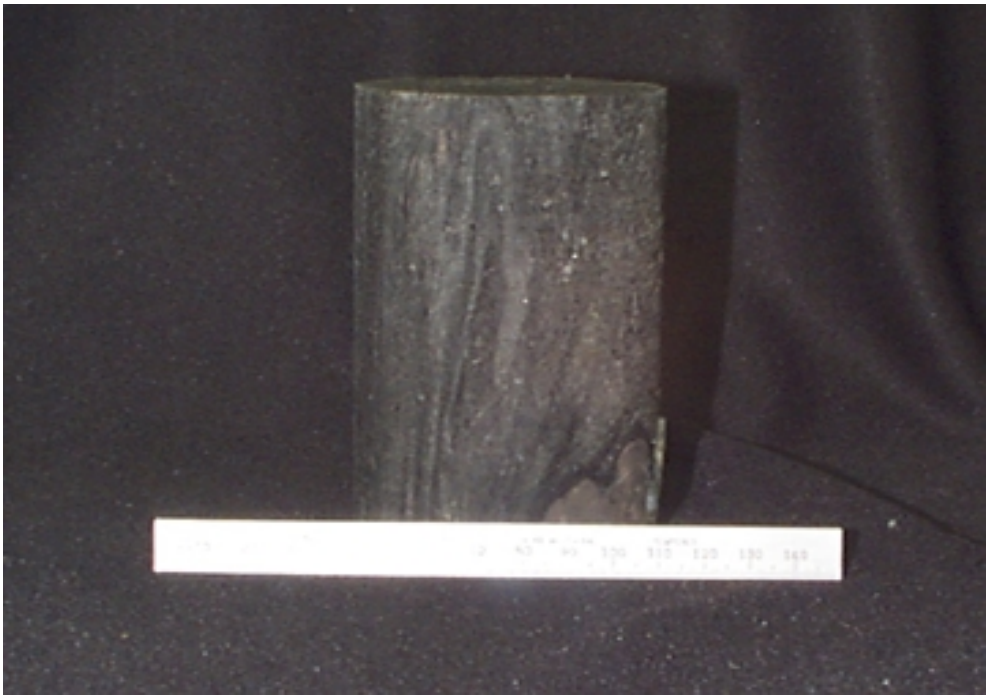

**Appendix 2-2. Photographs of cores tested.**

**Core #2/4, no flow orientation**
5.96” diameter, 5.31” length
porosity-wet = 22%, porosity-dry = 50%
hydraulic conductivity = 3.2E-3 m/day
reactive surface area = 2 $cm^2/g$

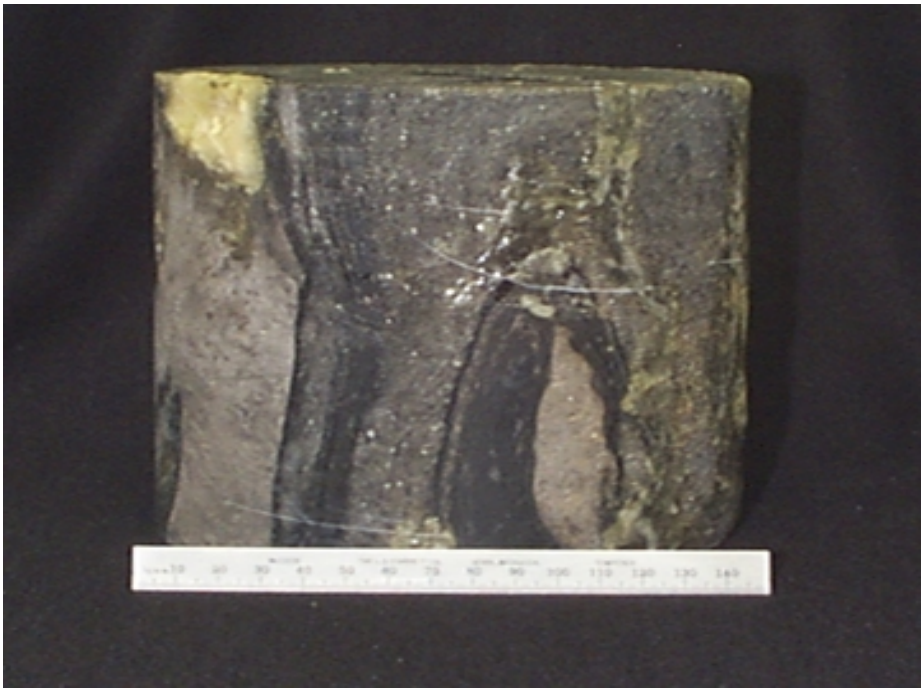

**Appendix 2-2. Photographs of cores tested.**

**Core #3/4, no flow orientation**
1.74" diameter, 4.10" length
porosity-wet = 3%, porosity-dry = 12%
hydraulic conductivity = 7.8E-3 m/day
reactive surface area = 36 $cm^2/g$

**Appendix 2-2. Photographs of cores tested.**

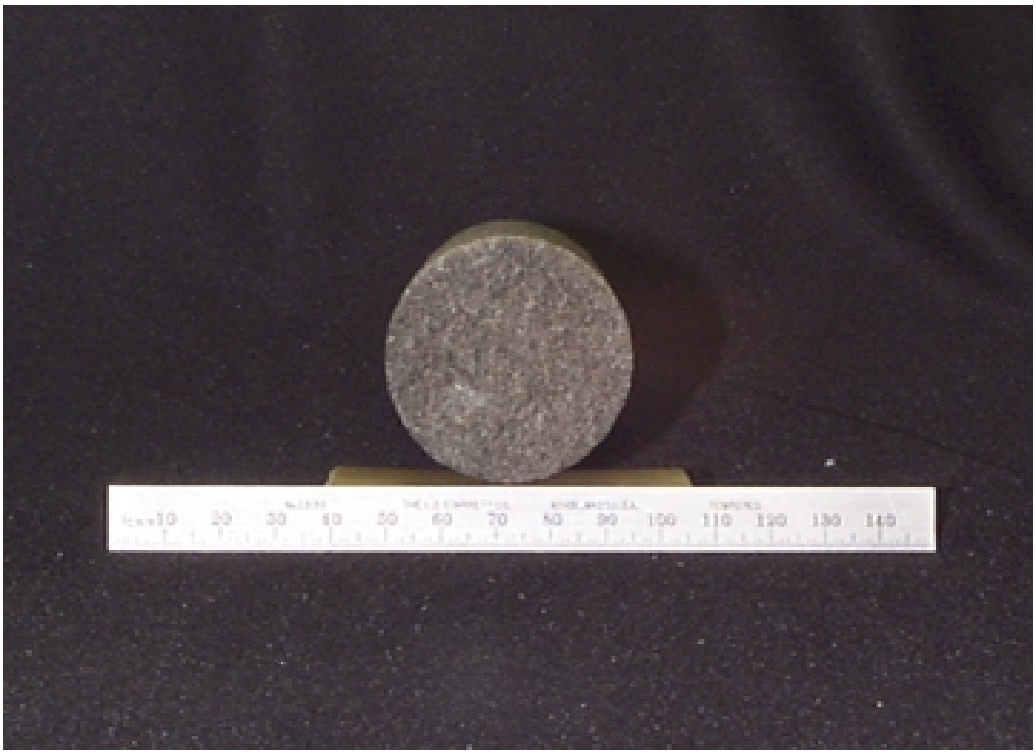

**Core #1/7, cored parallel to flow banding**
1.75” diameter, 4.03” length
porosity-wet = 13%, porosity-dry = 53%
hydraulic conductivity = 3.8E-3 m/day
reactive surface area = 20 $cm^2/g$

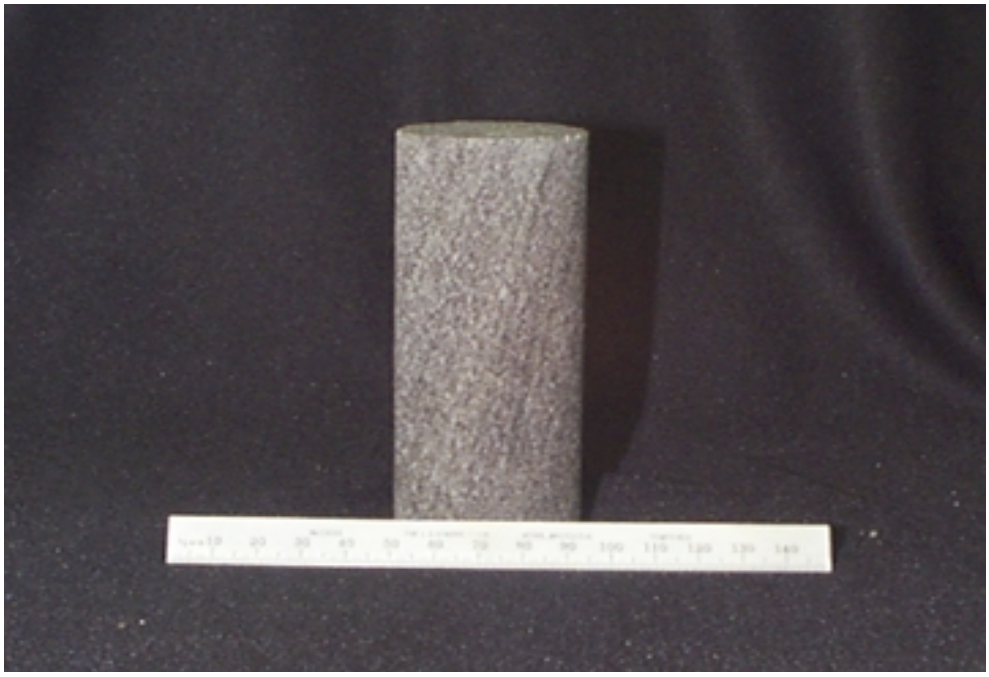

**Appendix 2-2. Photographs of cores tested.**

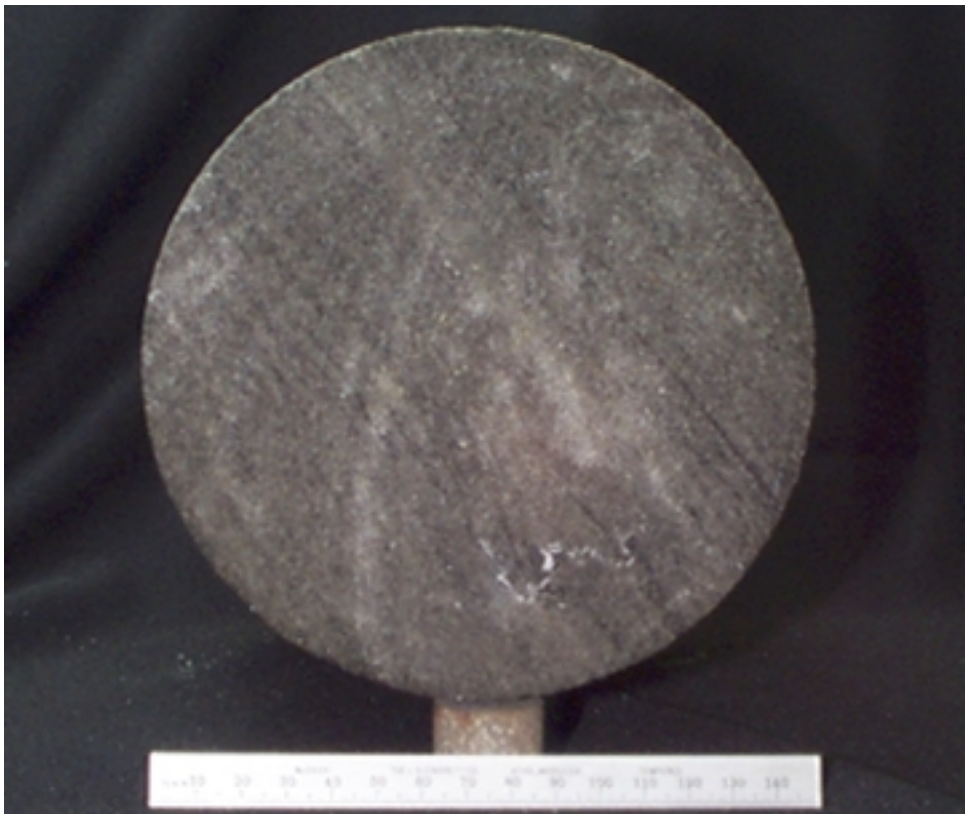

**Core #2/7, cored parallel to flow banding**
5.99” diameter, 6.15” length
porosity-wet = 9%, porosity-dry = 55%
reactive surface area = 2 $cm^2/g$

**Appendix 2-2. Photographs of cores tested.**

**Core #3/7, cored perpendicular to flow banding**
2.79” diameter, 4.58” length
porosity-wet = 12%, porosity-dry = 56%
reactive surface area = 8 $cm^2/g$

**Appendix 2-2. Photographs of cores tested.**

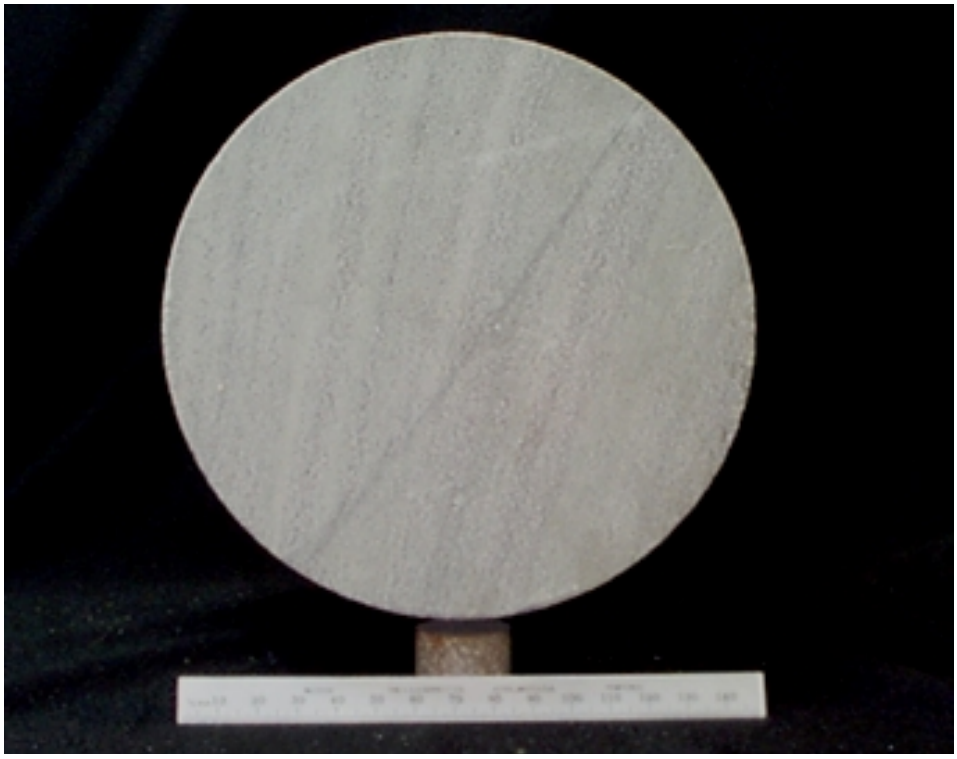

**Core #1/8, cored perpendicular to flow banding**
6.00” diameter, 4.98” length
porosity-wet = 5%, porosity-dry = 42%
hydraulic conductivity = 1.4E-4 m/day
reactive surface area = 47 $cm^2/g$

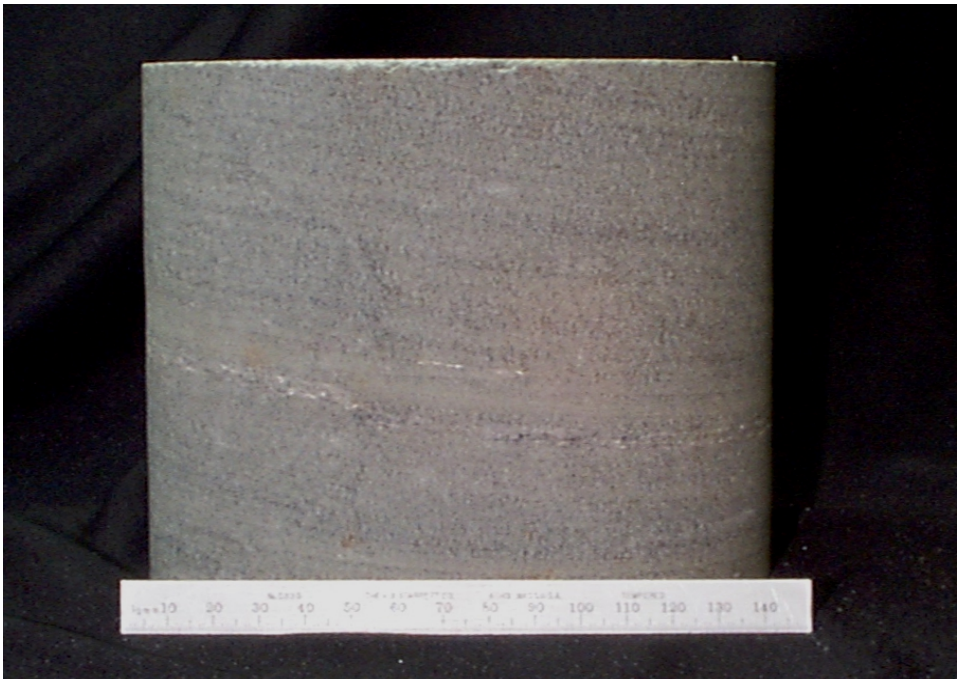

**Appendix 2-2. Photographs of cores tested.**

**Core #1/10, no flow orientation**
2.79" diameter, 4.43" length
porosity-wet = 17%, porosity-dry = 42%
hydraulic conductivity = 9.5E-4 m/day
reactive surface area = 65 $cm^2/g$

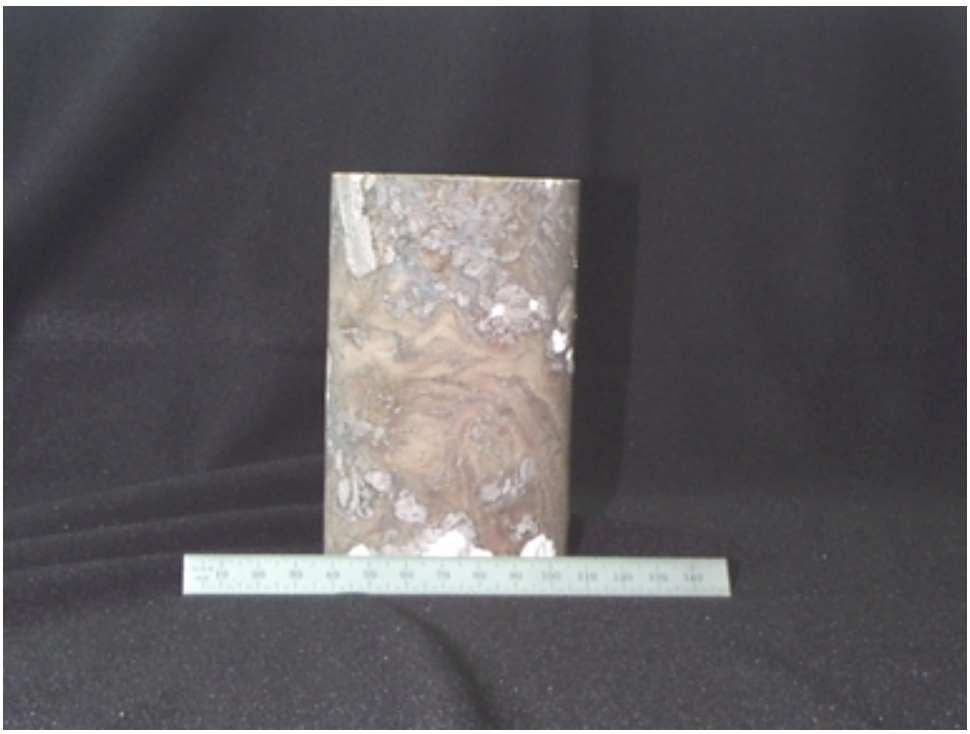

**Appendix 2-2. Photographs of cores tested.**

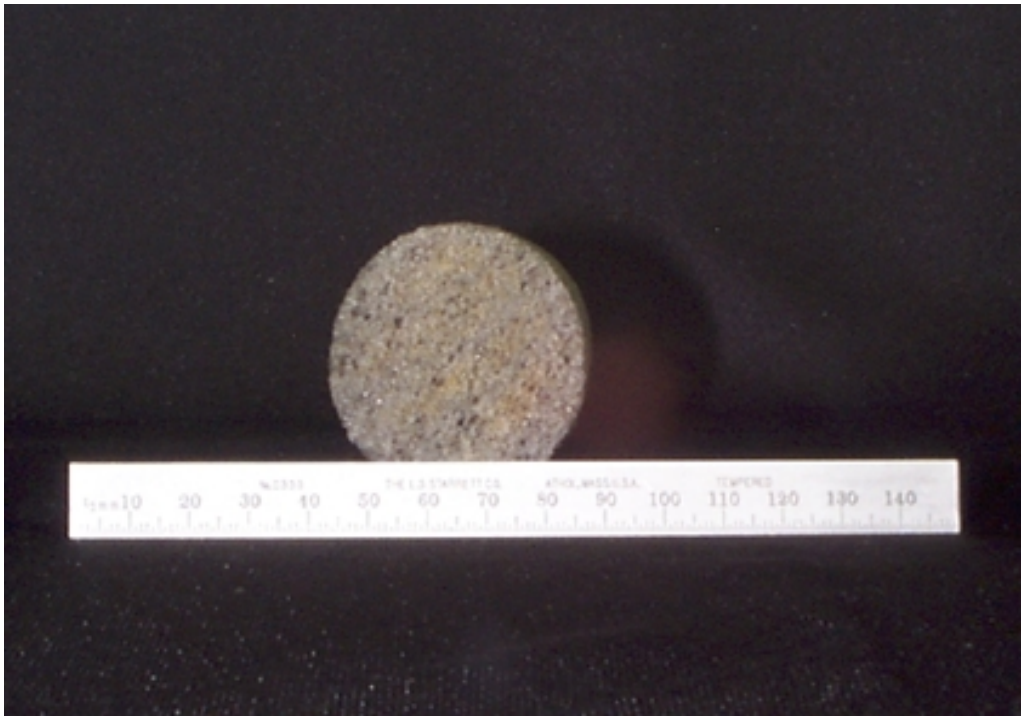

**Core #2/11, cored parallel to flow banding**
1.75” diameter, 4.05” length
porosity-wet = 24%, porosity-dry = 78%
hydraulic conductivity = 7.3E-3 m/day
reactive surface area = 34 $cm^2/g$

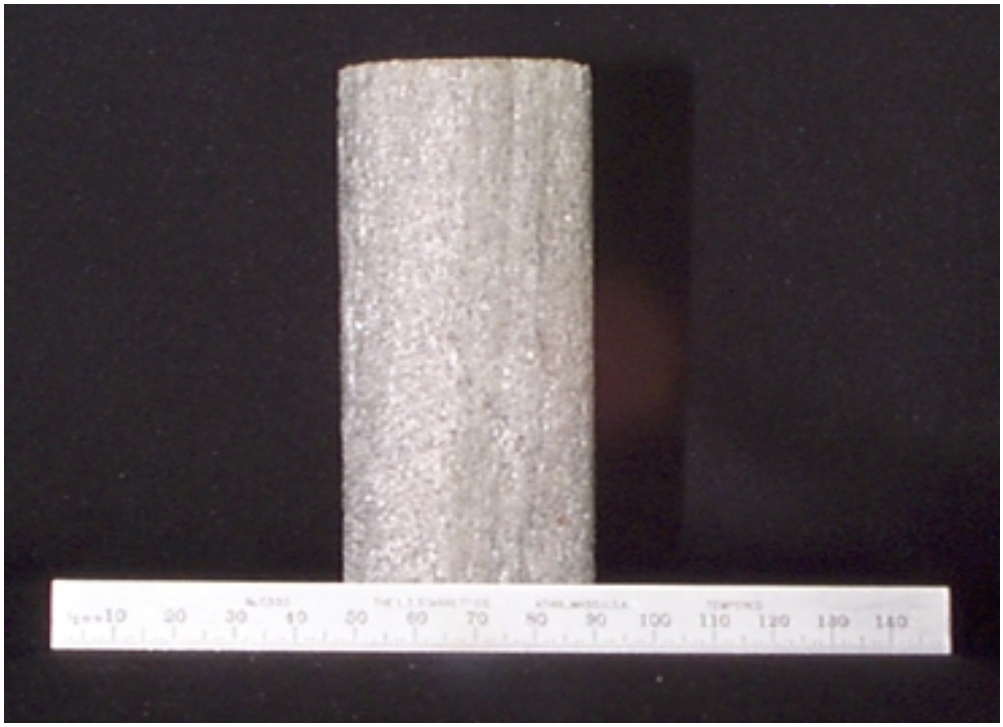

**Appendix 2-2. Photographs of cores tested.**

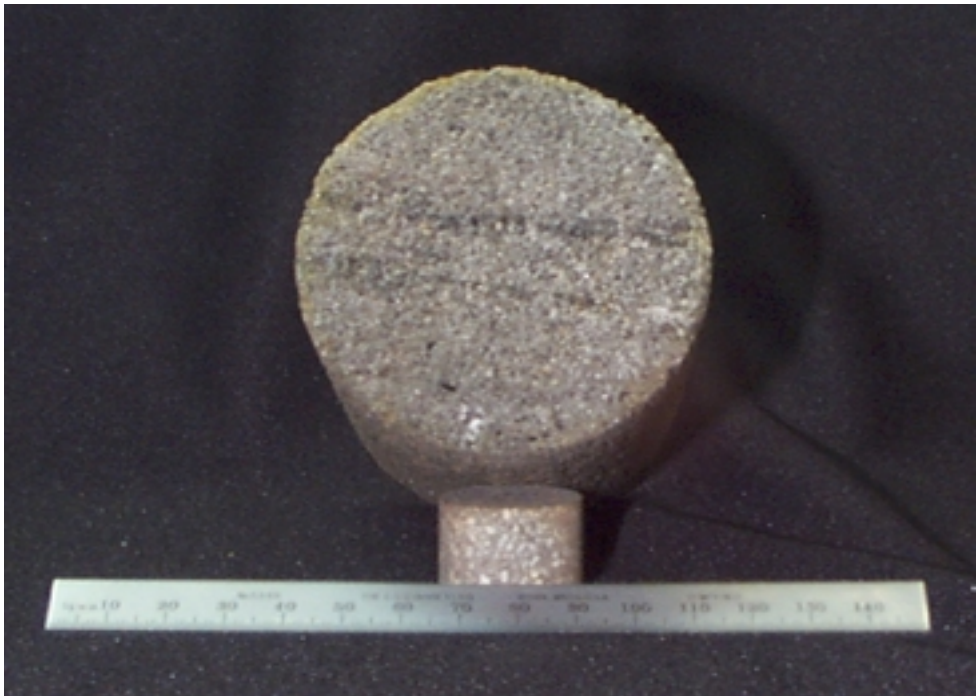

**Core #3/11, cored parallel to flow banding**
2.79" diameter, 4.45" length
porosity-wet = 26%, porosity-dry = 81%
hydraulic conductivity = 2.9E-2 m/day
reactive surface area = 26 $cm^2/g$

**Appendix 2-3. Photomicrographs of cores tested.**

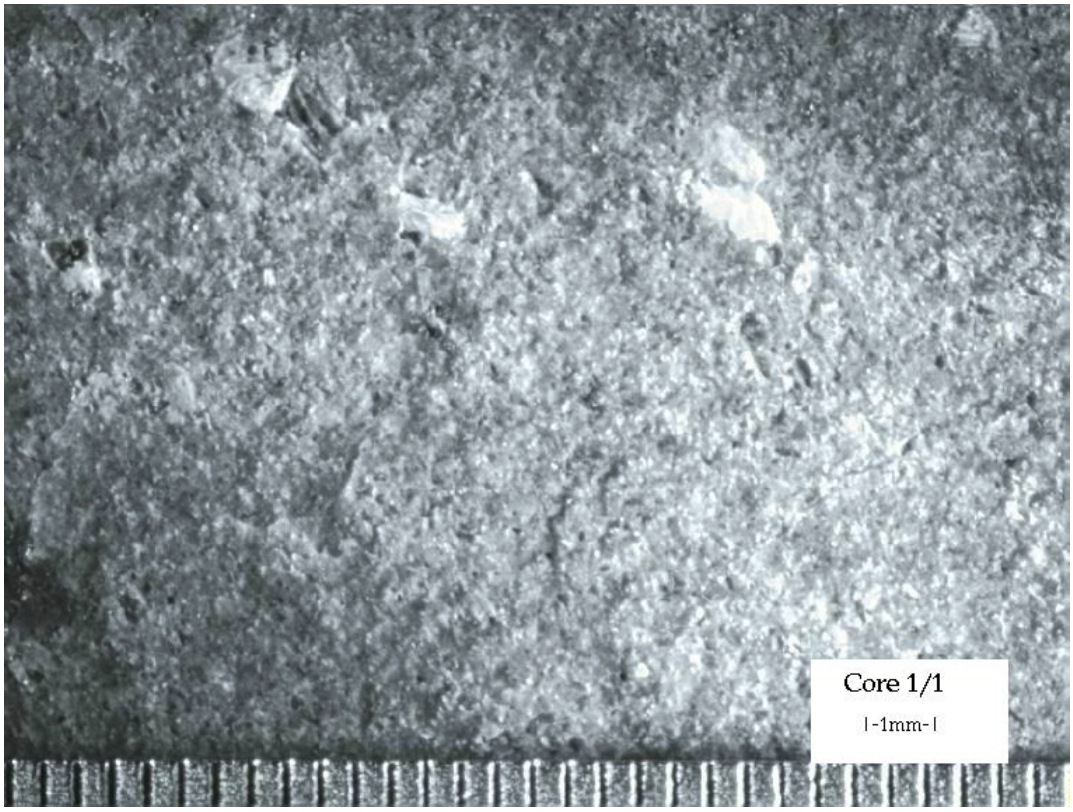


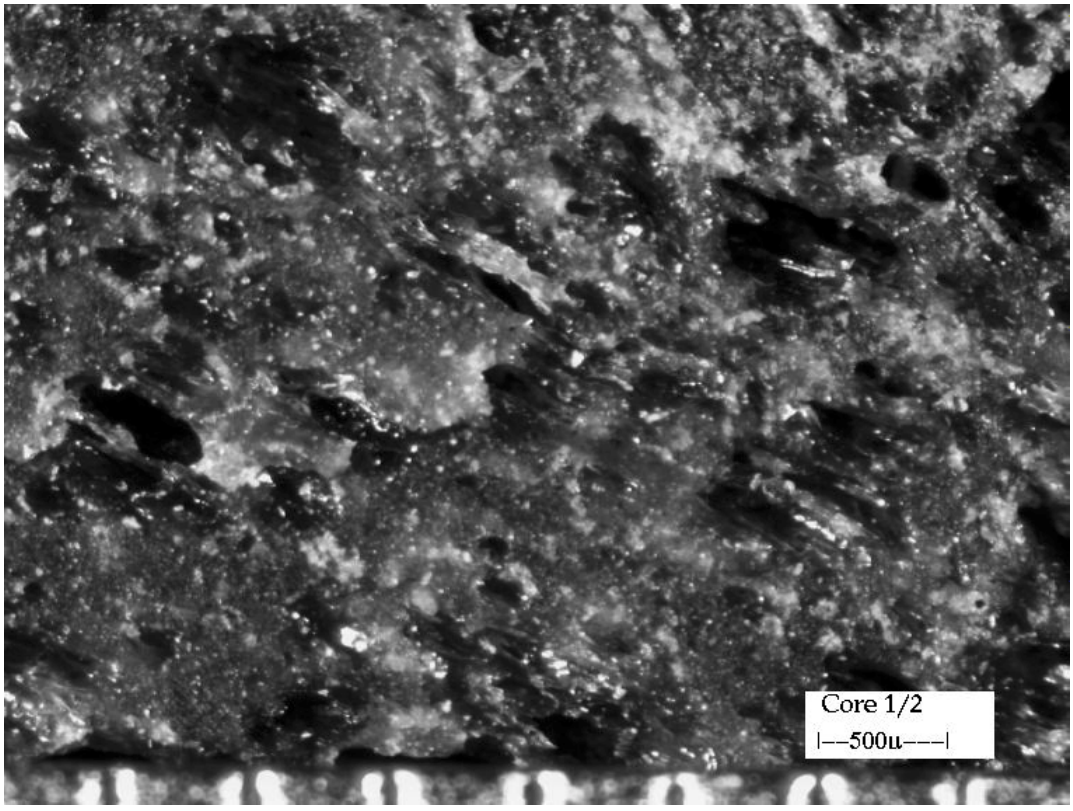

**Appendix 2-3. Photomicrographs of cores tested.**

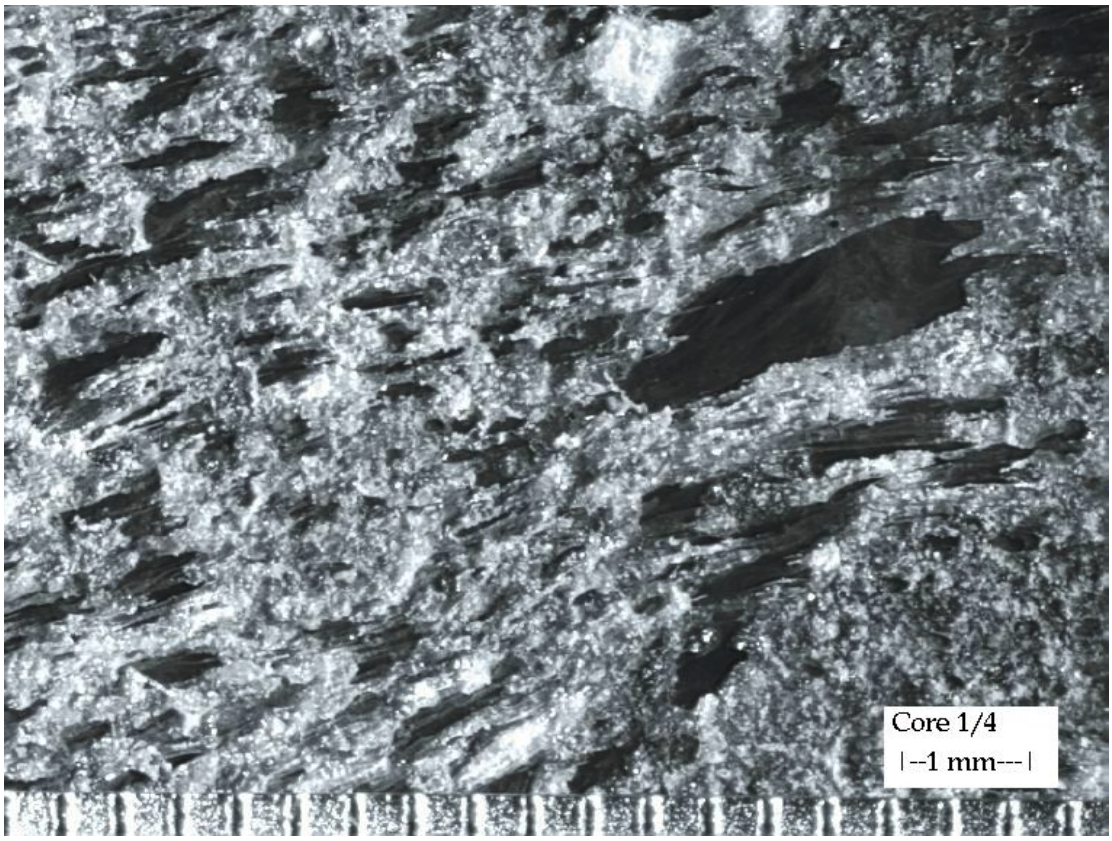


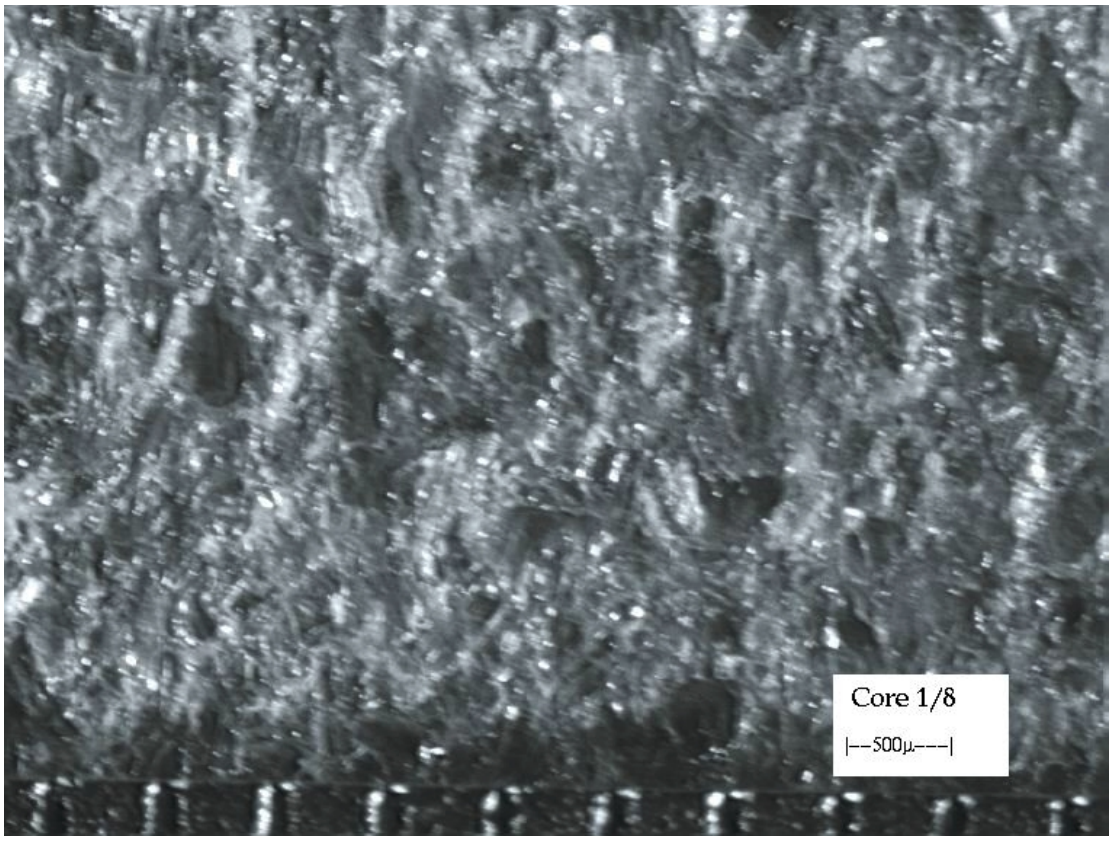

**Appendix 2-3. Photomicrographs of cores tested.**

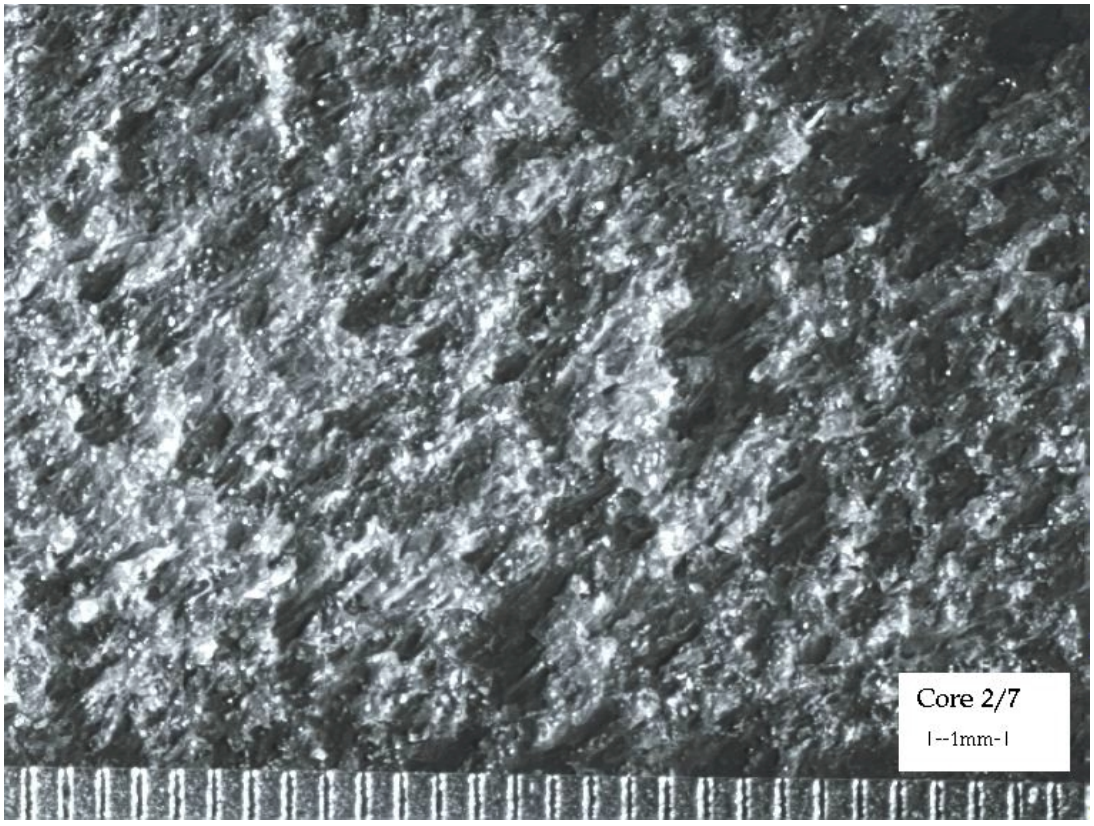


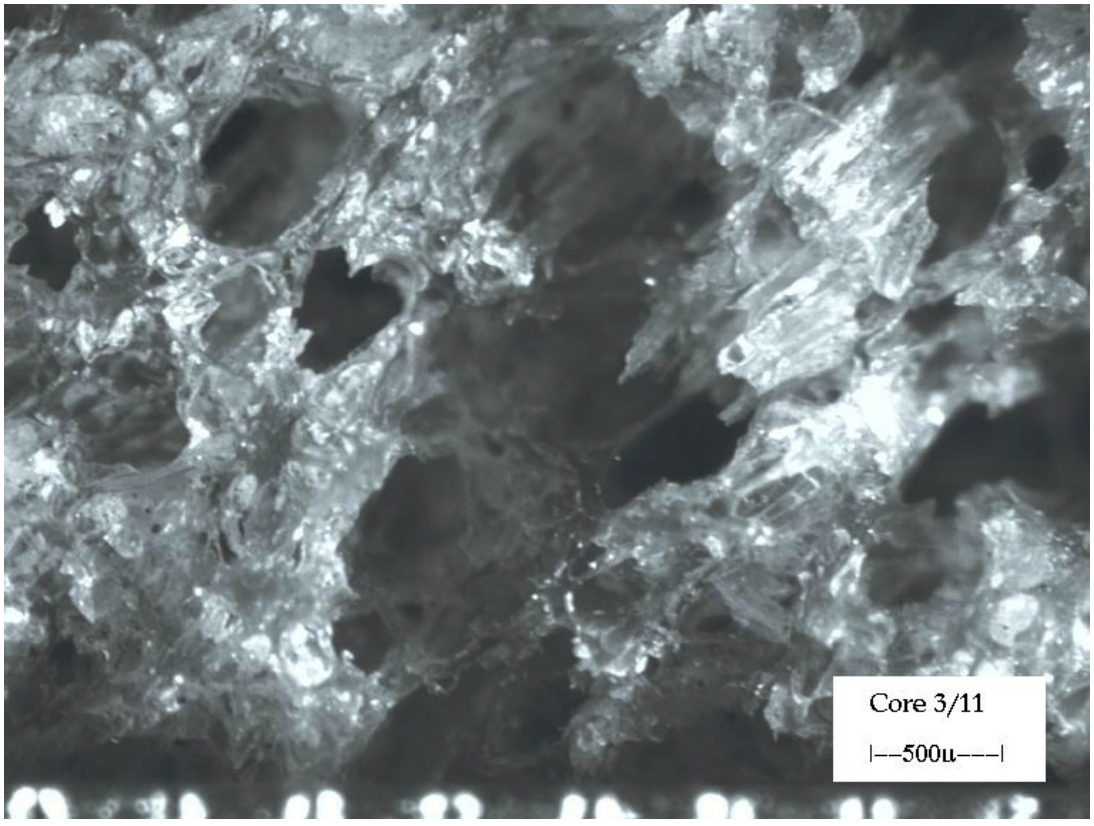

**Appendix 2-3. Photomicrographs of cores tested.**

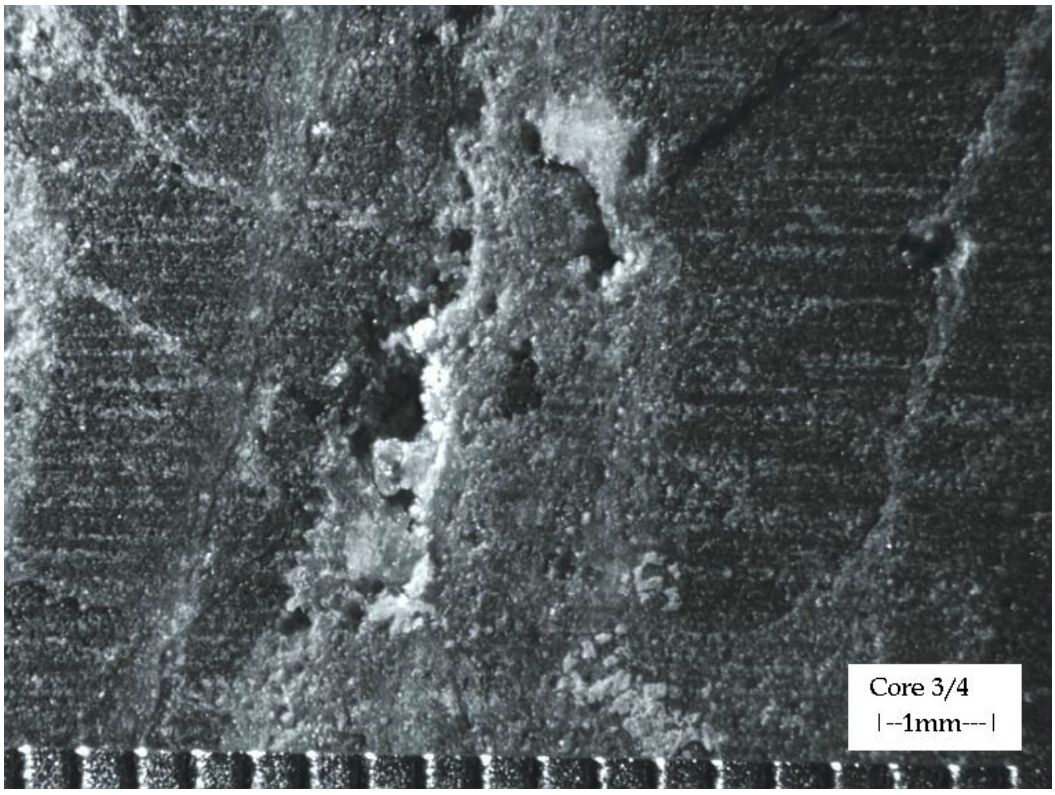


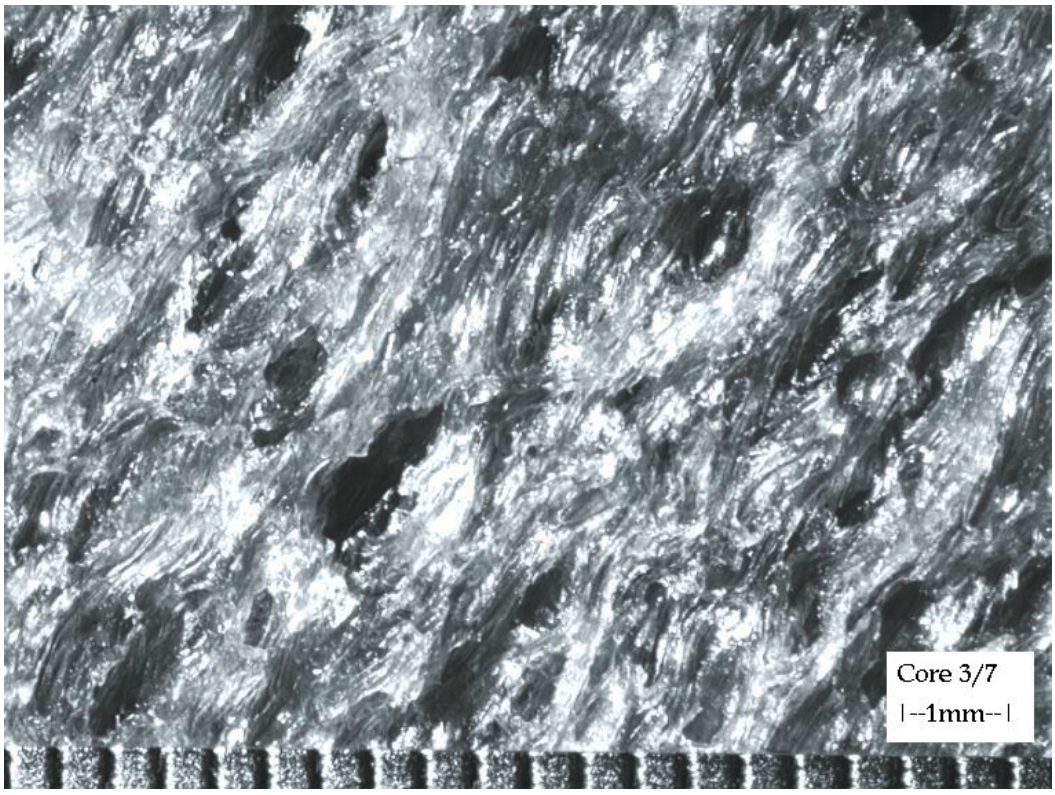

## PART 3. MEASURING THE SPECIFIC SURFACE AREA OF NATURAL AND MAN-MADE GLASSES. EFFECTS OF FORMATION PROCESS, MORPHOLOGY, AND PARTICLE SIZE

*Charalambos Papelis, Wooyong Um, Charles E. Russell, and Jenny B. Chapman*

*Desert Research Institute*

### Introduction

It is widely recognized that processes at mineral-water interfaces play an important role in the distribution and transport of chemical elements in the environment. The transport and concentration of environmental contaminants may be regulated by interfacial processes, such as dissolution, precipitation, adsorption, absorption, surface precipitation, and surface-catalyzed oxidation-reduction processes. Our ability to model the movement of potential contaminants in the environment hinges on the availability of appropriate transport models and the reliability of the model parameters required.

The reliability and accuracy of geochemical models are also directly dependent on the quality of geochemical model parameters. Some parameters are either known *a priori* or can be determined from laboratory experiments. Regardless of the specific type of model used, however, (i.e., equilibrium or kinetic), estimation of the solid surface area is required to model any type of interfacial process. Increased surface area per unit mass of solid material (and therefore increased concentration of reactive sites) is expected to lead to increased reaction rates, increased dissolution of a solid phase, or increased ion sorption at the mineral-water interface.

Determination of interfacial surface areas presents significant challenges. Unlike other parameters, the surface area estimate must be relevant to the scale of the process being modeled, which, for most environmental problems, is the field scale. Determination of surface areas at the laboratory scale requires significant scaling up to derive parameters appropriate for field scale models. A number of different methods have been used over the years to arrive at surface area estimates. The more common methods include estimates based on geometric considerations and estimates based on the physisorption of gas molecules on the surface of interest. By assuming particles of a certain geometry, usually spheres or cubes, the surface area of a solid can be calculated as a function of particle size. The estimates derived based on particle geometry represent, obviously, minimum values, because the roughness of real particles tends to increase the surface area. Surface area estimation based on gas sorption experiments requires an estimate of the gas cross sectional area and the amount of gas necessary to form a monolayer. The more commonly used gas adsorbates are nitrogen and krypton, and the BET model (Brunauer et al., 1938) is typically used to estimate the amount of gas required for the formation of a monolayer. Surface area measurements based on physical sorption of gases (physical surface area) always

result in higher surface area estimates than estimates based on particle geometry (geometric surface area). The discrepancy is typically a function of the nature of the particles. For fresh mineral surfaces, the difference was on the order of 7, while the difference for naturally weathered silicates ranged from 20 to 200 (White and Peterson, 1990). In addition, it has been argued that the physical surface area may not be a good approximation for the reactive surface area, that is, the area relevant to a chemical reaction such as dissolution or sorption.

The compilation of data from different studies reported by White and Peterson (1990) suggests that reactive surface areas are typically 1 to 2 orders of magnitude lower than physical or geometric surface areas, although in some cases the difference was almost 3 orders of magnitude. Finally, in one study the physical and reactive surface areas were essentially identical and in another study the physical surface area was actually larger than the reactive surface area. White and Peterson (1990) suggest that the discrepancy between physical and reactive surface areas is correlated with the residence time in the system.

There are several possible reasons for the reported differences between physical and reactive surface areas. First, different sites may be involved in different types of reactions so that the effective reactive surface area becomes a function of the reaction studied (e.g., precipitation, dissolution, sorption, etc.). In a complex natural system, several reactions may take place simultaneously, thus complicating the estimation of parameters based on existing models. Physical surface areas on the other hand, depend only on the degree of interaction of the adsorbent gas with the surface studied, under specific conditions. Second, reactive surface areas determined either in the field or in the laboratory may be affected by hydraulic conditions. Specifically, accessibility of reaction sites and potential mass transfer limitations may affect parameter estimation. In contrast, physical surface area measurements, based on gas adsorption, are not affected as much by mass transfer limitations and can account for surface areas associated even with angstrom-sized pores.

The potential for groundwater contamination by radionuclides from nuclear tests has been the focus of numerous investigations and continues to be a source of concern to citizens and regulatory agencies in many countries. Much of the radioactivity produced by a nuclear test is concentrated in a solidified glassy rock puddle at the bottom of the nuclear cavity, formed as rock melted by the explosion cools. Transport of radionuclides trapped in nuclear melt glass away from the point of testing, therefore, is controlled by the dissolution rate of the nuclear melt glass; the glass dissolution rate in turn is controlled by the specific surface area of the glass, among other factors (White and Peterson, 1990). Although chemical and morphological studies of nuclear melt glasses have been conducted (Borg, 1975, Smith, 1995, Schwartz et al., 1984), the limited availability of and restricted access to nuclear melt glass, as well as health and safety considerations, are significant limitations in the study of nuclear melt glass specific surface areas.

The only investigation of surface areas of nuclear melt glass as a function of particle size known to us was conducted more than 30 years ago (Essington and Sharp, 1968). As part of that study, the authors measured the specific surface area of glass originating from an underground nuclear test as a function of particle size. Their results indicated that for particles larger than approximately 0.5 mm the specific surface area of nuclear glass was independent of particle size. The limiting surface area for these particles was between 0.01 and 0.1 $m^2/g$. This relatively high, particle size-independent surface area can be explained by internal porosity, significant surface roughness, or the presence of high surface area minerals, such as clays. These early results have been questioned on the basis of the analytical detection limit available to these early investigators. Indeed, if analyses were limited by the detection limit of the method, any variations of surface area as a function of particle size would be impossible to detect. The combination of experimental apparatus and gas used today for low surface area analysis (krypton) provides a much lower detection limit compared to analyses performed more than 30 years ago, thus allowing us to address such concerns.

In addition to the migration of radionuclides incorporated into nuclear melt glass, dissolution of glass is likely to control the release of contaminants from *in situ* vitrified materials. *In situ* vitrification has been proposed as a remediation method to control the migration of radioactive substances and other contaminants in soil. The surface area of the manmade glass would influence the dissolution rate and therefore the release of contaminants to the environment.

To help decrease the uncertainty associated with the rate of contaminant release from glasses, we measured the specific surface area of several different types of natural and manmade glasses as a function of particle size. To obtain a better understanding of the possible range of surface areas, we examined glasses of different composition, different origin, and different morphology. Although these measurements were performed *ex situ* and, therefore, it is impossible to determine *a priori* the suitability of any specific surface area results for transport codes, this work provides significant insights with respect to trends in the specific surface area of glasses. The results reported in this section focus on the physical surface area of natural and manmade glasses, excluding nuclear melt glasses. Results from experiments with nuclear melt glass are reported in Part 4 and results of reactive surface area determination based on dissolution experiments are reported in Part 2.

**Materials and methods**

Several different natural and manmade glass materials were examined, including 1) vitric volcanic ash from the 1980 volcanic eruption of Mount St. Helens, Washington, 2) vitric volcanic tuffs from Nevada, 3) tektites from Southeast Asia, 4) obsidian glass from Inyo County, California, and 5) *in situ* vitrified rock from

Hanford, Washington. Because of the limited information available on nuclear melt glass, our intent was to measure the surface area of natural glass analogs as diverse as possible to allow us to establish a range of surface areas. Brief background information on these materials is given below.

The volcanic ash resulted from the eruption of Mount St. Helens in southwestern Washington, the most active and explosive volcano in the contiguous United States. The volcano erupted on May 18, 1980, sending ash up to 25 km high, bringing darkness at noon to an area 250 km to the east, and depositing ash up to 10 cm deep in much of Washington, northern Idaho, and western Montana. The peak of the mountain was reduced by 350 m in the process (Press and Siever, 1986).

Tuffs are compacted, lithified volcanic ash deposits formed from pyroclastic processes in which the grain size of the pyroclasts is less than 2 mm. The sample analyzed was obtained from the Nevada Test Site (NTS), Nye County, in southern Nevada, located in the Great Basin section of the Basin and Range physiographic province. During the Tertiary, volcanic activity produced layers of volcanic tuff reaching a thickness of up to 4 km.

Tektites are fragments of silica-rich glass that are thought to have formed from the impact of meteorites on silica-rich rocks. It is hypothesized that the material was melted on impact, was thrown in the atmosphere, and landed far from the point of impact. Rapid cooling led to the formation of the glass. This theory is supported by the common shapes of tektites (drops, etc.). The 5 tektite samples used in this study were rather large for tektites, having dimensions of approximately 3-5 cm.

Obsidian glass is volcanic glass of either dacitic or rhyolitic composition. Dacitic rocks are light-colored, fine-grained igneous rocks containing 65-70% silica, feldspars, quartz, biotite, and hornblende. Rhyolites are fine-grained, extrusive igneous rocks, often with a sugary texture, consisting primarily of quartz, alkali feldspar, and, most commonly, biotite. The samples used in this study were obtained from Obsidian Dome, near Mammoth Lakes, Inyo County, California. Obsidian Dome is comprised of flow-banded obsidian and rhyolite extruded as extremely viscous lava. Both black, massive rhyolite and gray, vesiculated blocks can be observed. It is believed that the age of the Dome is no more than a few thousand years. A total of 12 different samples were collected, numbered 1 through 10, A and B representing different textures. Samples A and B were qualitatively different (more massive) from samples 1 through 10.

The *in situ* vitrified material was provided by GeoSafe Corporation, Richland, Washington. Six different samples (A through F) were received, representing both highly massive glass and samples representing transition zones between the melt glass and the original rock. In the latter samples, the transition between the

melt glass and the parent rock material occurs across a distance of a few inches. *In situ* vitrification has been proposed as one method of controlling the migration of radionuclides and other contaminants from contaminated sites by incorporating the contaminants in a highly insoluble glass matrix. The *in situ* vitrified material was the only manmade glass sample examined.

**Characterization by scanning electron microscopy**

Rock samples (tektites, Obsidian Dome glass, and *in situ* vitrified rock) were examined by scanning electron microscopy (SEM) with an energy dispersive x-ray (EDX) attachment. Scanning electron micrographs can provide higher magnification and greater depth of field compared to optical microscopy (Goldstein et al., 1992). The higher magnification can provide additional information regarding sample composition. For example, glass alteration products, such as clays, can frequently be observed. The presence of such minerals may have a significant effect on the overall particle surface area measured. In addition, EDX analysis can provide a fast, at least semiquantitative, estimate of major element composition. Although the determination of minor element composition is difficult and the determination of trace elements is beyond the sensitivity of the instrument, these disadvantages are offset by the relatively low level of operator skill required and the ability to analyze small, micrometer-size areas. The JEOL JSM-840A SEM/EDX instrument used for all measurements was operated at 15.0 kV with beam current varying between 1 and 3 nA. Typical working distance varied between 19 and 39 mm, depending on image magnification. The major element composition was determined based on standards.

**Specific surface area measurements**

All specific surface area measurements were performed with a Micromeritics ASAP 2010 automatic physisorption analyzer with multi-gas option. Because of the low specific surface area of most samples, the majority of analyses were performed with krypton (Kr) as gas adsorbate at liquid nitrogen temperature (approximately 77 K). The detection limit of this instrument, using Kr, is 0.0005 $m^2/g$. To improve analysis accuracy, the ASAP 2010 is equipped with a high vacuum molecular drag pump capable of producing a vacuum of $10^{-5}$ mm Hg or better, 1000 and 10 mm Hg pressure transducers, completely independent vacuum systems for sample outgassing and analysis, and patented isothermal jackets to maintain constant sample temperature throughout the experiment. The instrument was calibrated using high ($214 \pm 6$ $m^2/g$) and low ($0.46 \pm 0.03$ $m^2/g$) alumina surface area standards. During all measurement phases, sample equilibration was determined by monitoring the rate of pressure change in the manifold as a function of time. Complete evacuation of the sample (see discussion below) in combination with a strict tolerance for sample equilibration guarantees measurement of the total specific surface area of the particles, independent of diffusional limitations in fine pores.

All samples were outgassed at 110 ˚C under vacuum. Because of the low porosity and low specific surface area of most samples, higher temperatures were not necessary during sample evacuation. For most samples, complete evacuation was attained within 3 to 4 hours; the higher surface area samples were outgassed overnight or until pressure increase in the manifold, with the vacuum valve shut off, did not exceed 1 μm Hg/min. This procedure assures complete outgassing of the finer pores that may contribute substantially to the total specific surface area of porous materials. To prevent sample contamination during transfer from the outgassing to the analysis station, all sample tubes were capped with self-closing valve assemblies. To further increase the accuracy of the measurements, the free space in the sample tube was minimized by inserting a glass rod, except during measurements of the lowest surface area materials, where the entire sample tube was filled with sample, to increase the total surface area available. For most samples, the specific surface area was measured as a function of particle size. Particle size was limited by the inner diameter of the sample tubes, approximately 10 mm.

The specific surface area of a solid is given by

$$A = \frac{v_m}{22414} a_m L \times 10^{-20} \qquad (3\text{-}1)$$

where $A$ is the specific surface area ($m^2g^{-1}$), $v_m$ is the volumetric monolayer capacity (volume of gas at standard temperature and pressure required to form a complete monolayer), $a_m$ is the average area occupied by a molecule of the adsorbate ($Å^2$) and $L$ is the Avogadro constant (Gregg and Sing, 1982). The average area occupied by Kr and $N_2$ adsorbate gas molecules was assumed to be 21.0 and 16.2 $Å^2$, respectively.

Estimation of the specific surface area, therefore, requires estimation of the monolayer capacity of a solid based on a gas adsorption isotherm (i.e., the amount of gas adsorbed as a function of relative pressure, $P/P_o$, where $P_o$ is the saturation pressure of the adsorbate (either $N_2$ or Kr)). Several models have been proposed to obtain the monolayer capacity from sorption isotherms; the most well known and most successful, however, is the BET model (Brunauer et al., 1938). In its most convenient form it is given by

$$\frac{P/P_o}{n(1-P/P_o)} = \frac{1}{n_m c} + \frac{c-1}{n_m c}(P/P_o) \qquad (3\text{-}2)$$

where $n$ represents the moles of gas adsorbed per gram of adsorbent, $n_m$ the moles of gas necessary to form a complete monolayer, and $c$ the so-called BET c constant, which is related to the net heat of adsorption. From the slope and

intercept of the sorption isotherm represented by Eq. (3-2), the parameters $n_m$ and $c$ can be obtained. The typical accuracy of surface area determinations based on the BET model is considered to be ±10% (Gregg and Sing, 1982).

Despite the criticisms that have been raised over the years, the BET model remains widely accepted. An obvious criticism is that most instruments, in the usual configuration, can only be used to analyze relatively small size samples (up to approximately 1 cm). It is, therefore, often questioned whether the results obtained with ground up particles can be used to estimate surface areas under field conditions. An insight into this question can be gained by conducting surface area measurements as a function of particle size, as was performed for this study. When the rock sample examined contains high–surface–area minerals (such as clay minerals and zeolites), the total surface area will be orders of magnitude higher than the surface area expected for nonporous particles and largely independent of particle size. Under these conditions, the BET surface area measurements are expected to represent a fairly realistic estimate of the rock surface area *in situ*. For nonporous rock materials the surface area is expected to be a function of particle size. Total BET surface areas inversely proportional to particle size, therefore, may indicate nonporous materials and point out to the possibility that the BET surface area measurements may overestimate the rock surface area *in situ*.

**Results and discussion**

The specific surface area results of the volcanic ash from the eruption of Mount St. Helens, the tuff from the NTS, and the tektites from Southeast Asia will be discussed first. The specific surface area of only a single particle size fraction was measured for all these samples, either because the material was already in powder form (Mount St. Helens ash and NTS tuff) or because of the relatively limited quantity of the sample (tektites). In general, these materials had relatively high surface areas ranging from 1.651 $m^2/g$ for tektite sample 5 to 0.2123 $m^2/g$ for tektite sample 2. The surface areas of the volcanic ash and the NTS tuff were 1.422 and 0.9007 $m^2/g$, respectively.

The specific surface areas of the tektite samples are listed in Table 3-1. The samples were ground and sieved. The fraction between 0.124 and 1.18 mm was used in these experiments. This size fraction was broad enough to ensure production of adequate material for analysis and was compatible with the size fractions used with other materials (see discussion below). Although a spread in the measured specific surface areas can be observed, the mean value was 0.7516 $m^2/g$, a relatively high specific surface area. BET estimates of surface areas were based on isotherms with at least 5 points in the linear range and correlation coefficients of at least 0.9999.

To help correlate the measured specific surface area with particle morphology and composition, two of the tektite samples (1 and 5) were examined by SEM/EDX; the electron micrograph of tektite sample 5 is shown in Figure 3-1. EDX analysis gave an average elemental composition (given in parentheses as percentage by weight of the corresponding oxides) of $SiO_2$ (52.40), $Al_2O_3$ (14.30), CaO (5.16), MgO (3.41), $K_2O$ (4.52), $Fe_2O_3$ (14.36), and $TiO_2$ (5.85).

**Table 3-1.** Specific surface area of tektite samples

| Sample | Specific Surface Area ($m^2/g$) |
|---|---|
| 1 | 0.9986 |
| 2 | 0.2123 |
| 3 | 0.2536 |
| 4 | 0.6427 |
| 5 | 1.651 |

Geometric mean diameter: 382.5 μm

The composition of tektite sample 1 was very similar with $SiO_2$ (53.86), $Al_2O_3$ (18.22), $Fe_2O_3$ (12.53), and smaller concentrations of CaO, MgO, $Na_2O$, and $K_2O$. It is evident by inspection of Figure 3-1 that although massive glass exists in this sample, there is also substantial evidence of weathering and porosity. Clay minerals produced by weathering and the resulting porosity could account for the observed relatively high surface area, compared to what would be expected for smooth nonporous spheres or cubes. Naturally weathered silicates were reported to have a surface roughness of almost 200 (White and Peterson, 1990).

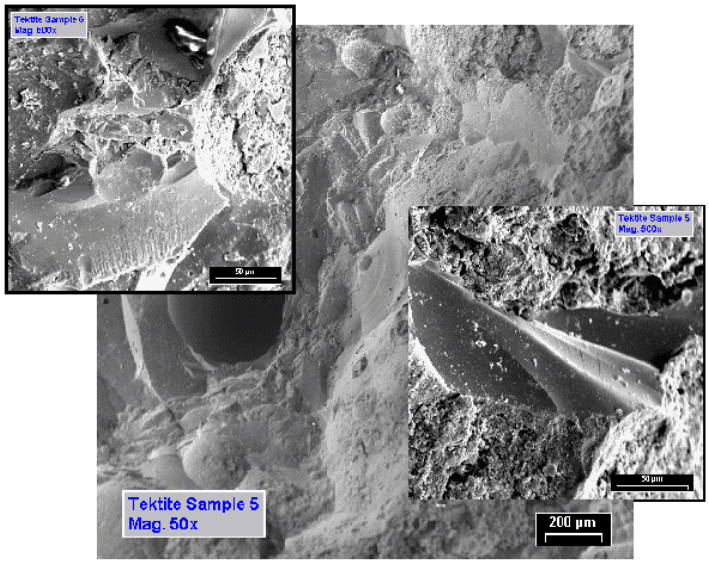


**Figure 3-1**. Scanning electron micrograph of tektite sample 5 (50 and 500x magnification).

The external specific surface area of spheres with diameter $d$ (or cubes with edge length $d$) and density $\rho$ is given by (Gregg and Sing, 1982),

$$A = \frac{6}{\rho d} \qquad (3\text{-}3)$$

where $A$ is the specific surface area ($m^2/g$). If the geometric mean between the cutoff diameters of the sieve sizes used (0.124 and 1.18 mm), 382.5 μm, is used as a single representative diameter describing the particle size distribution (Ball and Roberts, 1991), and assuming a density of 2.65 $g/cm^3$, the expected specific surface area of smooth spheres would be approximately 0.0059 $m^2/g$. This value is approximately 2 orders of magnitude lower than the mean of the measured specific surface areas of the tektite samples. Inspection of the higher magnification (500x) micrographs in Figure 3-1 supports this difference between the tektite specific surface area and the calculated value based on geometric considerations. Comparison of the elemental composition and specific surface area of the two samples does not reveal any obvious trend.

**Specific surface area of volcanic glass**

Several samples were collected from Obsidian Dome, near Mammoth Lakes, Inyo County, California. These samples were labeled either by numbers, 1-10, or by letters, A and B. The distinction between the two groups was based on visual inspection during collection. Samples 1-10 were thought to have at least some porosity, while samples A and B were massive obsidian. All samples were crushed and separated into at least 4 different size fractions. Surface area measurements were conducted as a function of particle size and results are shown in Figure 3-2. Although not all samples are included, the group shown represents all observed trends. The results for all samples are included in Table 3-2.

Inspection of the results for the 6 samples shown in Figure 3-2 reveals three distinct pairs: samples 6 and 10, samples 3 and 9, and samples A and B. Samples 6 and 10 were the highest surface area samples, ranging from 1.242 $m^2/g$ for the smallest size fraction of sample 10, to 0.142 $m^2/g$ for the largest size fraction of sample 6. In addition to the absolute numbers, however, it is important to note the trend of specific surface area dependence on particle size. According to Eq. (3-3), the specific surface area of nonporous particles is expected to be inversely proportional to particle size. Although the measured specific surface area decreases with increasing particle size, a three-order-of-magnitude change in particle dimension resulted in a decrease of specific surface area by a factor of 3 at the most. The difference between the expected surface area of nonporous spheres of diameter $d$ and the measured surface area of the samples can be seen in Figure 3-2, where the dashed line corresponds to the theoretical specific surface area of nonporous spheres with density 2.65 $g/cm^3$.

**Table 3-2.** Specific Surface Area of Volcanic Glass ($m^2/g$)

| | Geometric Mean Particle Dimension (μm) | | | | | | |
|---|---|---|---|---|---|---|---|
| Sample | **4123.1** | **1303.8** | **842.0** | **648.1** | **227.4** | **16.8** | **5.0** |
| 1 | 0.02631 | 0.04872 | | 0.05461 | | 0.2603 | |
| 2 | 0.01903 | 0.01388 | | 0.03283 | | 0.1223 | |
| 3 | 0.03122 | 0.03404 | | 0.03951 | | 0.1678 | |
| 4 | 0.04889 | | 0.05881 | | 0.09228 | | 0.409 |
| 5 | 0.0314 | 0.043 | | 0.04588 | | 0.2145 | |
| 6 | 0.142 | 0.1544 | | 0.1468 | | 0.3475 | |
| 7 | 0.03088 | | 0.03302 | | 0.06887 | | 0.3073 |
| 8 | 0.04424 | | 0.04431 | | 0.0825 | | 0.2546 |
| 9 | 0.0546 | | 0.0511 | | 0.07086 | | 0.346 |
| 10 | 0.3938 | | 0.4896 | | 0.6713 | | 1.242 |
| A | 0.0237 | | 0.03744 | | 0.1035 | | 0.4879 |
| B | 0.009072 | | 0.02248 | | 0.0759 | | 0.3917 |

Although the measured surface areas appear to approach the theoretical limit as the particle size decreases, the difference between measured and nonporous-particle (geometric) surface area exceeds two orders of magnitude for the largest size fraction.

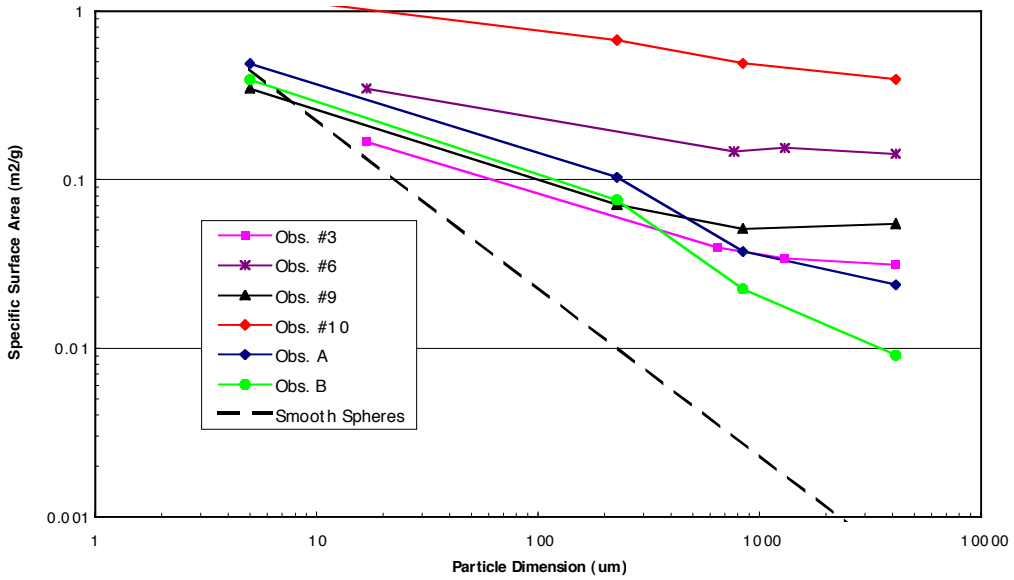


**Figure 3-2**. Specific surface area of volcanic glass as a function of particle size.

These results are consistent with the presence of substantial porosity in these samples. Scanning electron microscopy results confirm this hypothesis. Micrographs of samples 6 and 10 are shown in Figure 3-3 and Figure 3-4, respectively. Inspection of these figures reveals substantial porosity at a relatively small scale. In addition, comparison of the two micrographs shows significant differences between the two materials. Sample 6 was vesicular and pumiceous, with no evidence of clay minerals present, whereas sample 10 had a different structure and SEM examination revealed porosity at a substantially smaller scale compared to sample 6. These results are consistent with the higher specific surface area of sample 10. EDX characterization identified measurable differences in composition between the two samples. Both samples had approximately the same $Al_2O_3$ composition (approx. 16% by weight) but slightly different $SiO_2$ composition (60 and 67% for samples 6 and 10, respectively). Finally, approximately 9% $Fe_2O_3$ was present in sample 6, whereas no $Fe_2O_3$was detectable in sample 10.

The second characteristic group shown in Figure 3-2 includes samples 3 and 9. A steeper slope of the specific surface area curve as a function of particle size, compared to samples 6 and 10, is evident in these samples. In addition, the specific surface area of this group was lower compared to the previous group, for all size fractions. Generally, as the particle size increases, the specific surface area decreases. The two largest size fractions, however, had essentially the same surface area, suggesting that the surface area is controlled by internal porosity. As can be seen in Figure 3-2, the difference between measured surface area and the surface area expected for smooth nonporous spheres was approximately 2 orders of magnitude, consistent with the presence of significant porosity in these samples.

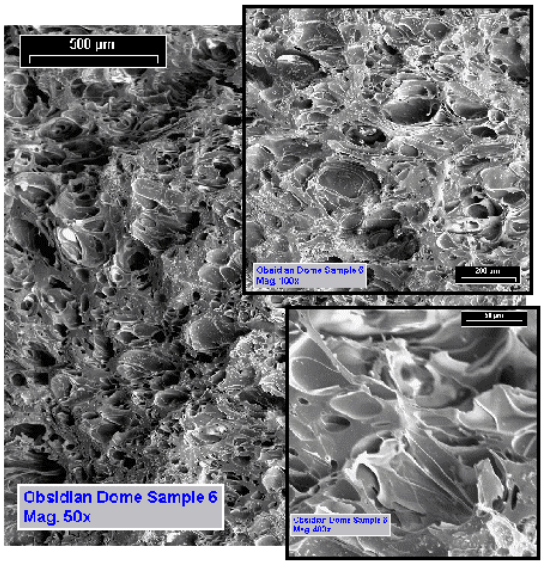


**Figure 3-3**. Scanning electron micrograph of obsidian sample 6 (50, 100, and 400x magnification).

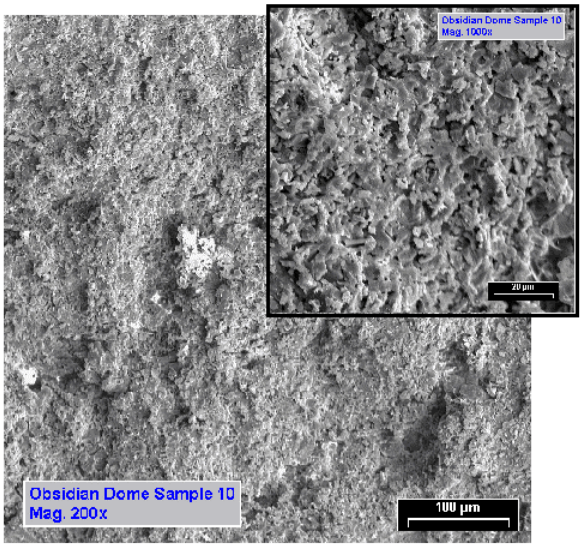


**Figure 3-4**. Scanning electron micrograph of obsidian sample 10 (200 and 1000x magnification).

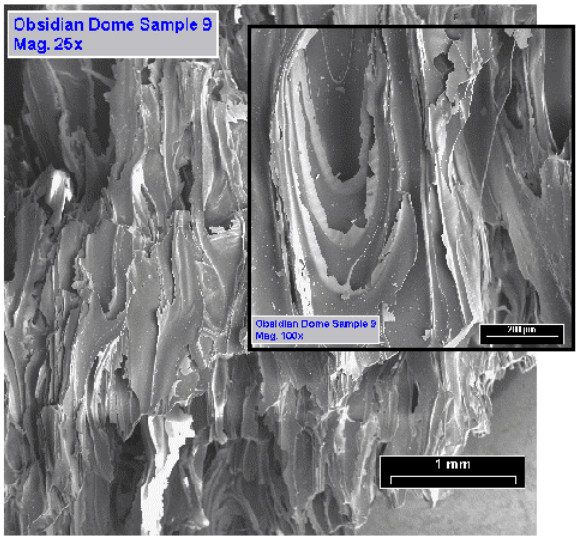


**Figure 3-5**. Scanning electron micrograph of obsidian sample 9 (25 and 100x magnification).

This result can be confirmed by inspection of electron micrographs of sample 9, shown in Figure 3-5. This sample was also vesicular and had larger pores than sample 6 (Figure 3-3), which is consistent with the lower specific surface area of sample 9. The results shown are consistent with a minimum surface area for these types of glass, independent of particle size. In addition, the results are

consistent with earlier specific surface area measurements of nuclear melt glass as a function of particle size, where a plateau of minimum specific surface area was observed between 0.01 and 0.1 $m^2/g$ (Essington and Sharp, 1968). In terms of composition, these samples were very similar to sample 6 ($SiO_2$ (62), $Al_2O_3$ (14), $Fe_2O_3$ (9), and lower concentrations of CaO, $Na_2O$, and $K_2O$. This composition is fairly typical for pumice. It should be noted that the trends in surface area for samples 6 and 9 were substantially different, despite their similar elemental composition.

Samples A and B were examples of the third trend observed. As noted above, samples A and B were intentionally collected because of their massive structure and apparent lack of porosity. The specific surface area measurements confirmed this hypothesis. As can be seen from Figure 3-2, although the smaller particle sizes had similar surface areas to the rest of the samples, the largest particle size fractions had significantly lower surface areas than samples 1-10, up to almost a factor of 10 in some cases. In addition, as opposed to samples 3 and 6, the trend of decreasing surface area with increasing particle size continues even at the larger size fractions and no plateau is observed. This trend is consistent with absence of significant internal porosity and specific surface area being a function of particle size only, as expected based on Eq. (3-3). Finally, the slope of the line of surface area as a function of particle size more closely approaches the slope expected for nonporous spherical particles. The measured surface areas, however, were always higher than the geometric specific surface area by a factor of 5-10. Such differences between geometrically smooth and real particles are common and are typically explained by surface roughness (White and Peterson, 1990).

**Specific surface area of *in situ* vitrified material**

The six *in situ* vitrified samples (A through F) included dark, massive glass (samples A, B, and E) as well as samples representing a transition zone between the pure glass and the native rock (samples C, D, and F). The thickness of the transition zone was typically a few inches. Samples C, D, and F, therefore, included massive glass, native rock, and the true transitional zone. All samples were crushed and divided into four different size fractions. Samples C, D, and F, therefore, were a composite of massive glass and native rock. The specific surface area of all samples as a function of particle size is shown in Figure 3-6 and listed in Table 3-3.

The decrease of specific surface area with increasing particle size is obvious in Figure 3-6. Differences between the two groups of samples (A, B, E and C, D, F, respectively) are also evident. The specific surface area of the massive glass samples decreases monotonically, without any sign of reaching a minimum surface area (plateau). In fact, it appears that as the particle size increases the specific surface area decreases even more dramatically, as evidenced by the steep slope of the surface area vs. particle dimension line. This behavior is expected

for solids with external surface area only (absence of internal porosity). Comparison of the measured surface

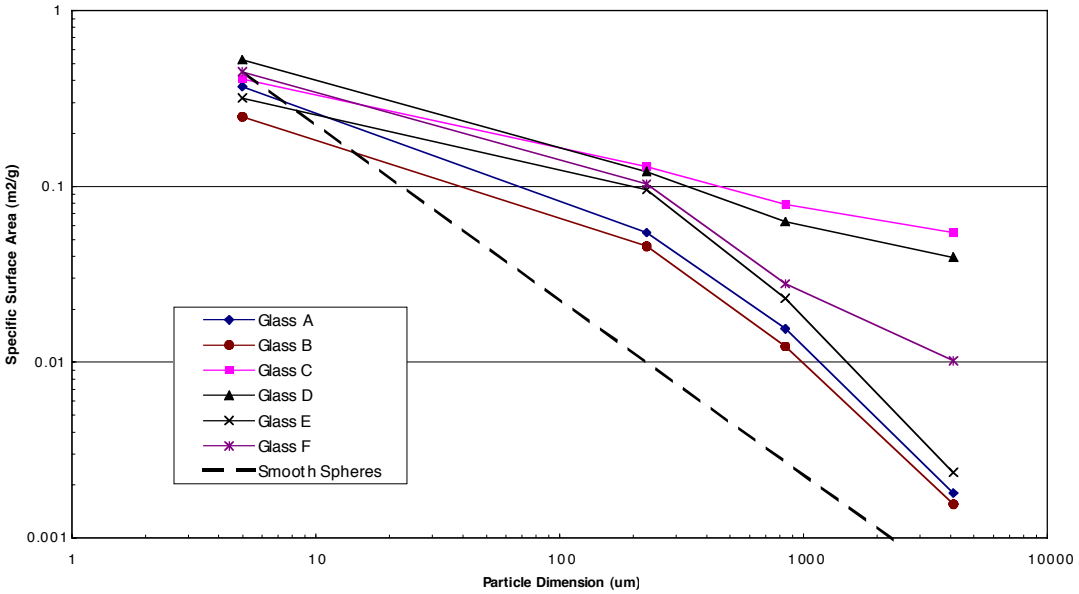


**Figure 3-6**. Specific surface area of *in situ* vitrified material as a function of particle size.

Table 3-3. Specific Surface Area of In Situ Vitrified Material

| | Geometric Mean Particle Dimension (μm) | | | |
|---|---|---|---|---|
| Sample | **4123.1** | **842.0** | **227.4** | **5.0** |
| A | 0.001798 | 0.01542 | 0.05445 | 0.3688 |
| B | 0.001557 | 0.01228 | 0.04552 | 0.248 |
| C | 0.05425 | 0.07898 | 0.1287 | 0.4079 |
| D | 0.03939 | 0.06283 | 0.1213 | 0.5237 |
| E | 0.002357 | 0.02305 | 0.09553 | 0.3177 |
| F | 0.01015 | 0.02784 | 0.1031 | 0.4478 |

area to the theoretical specific surface area of smooth spheres having density 2.65 $cm^3/g$ (represented by the dashed line in Figure 3-6) is consistent with this hypothesis. The slopes of the two lines were similar and the differences between experimentally measured and theoretical values were always smaller than one order of magnitude, and substantially smaller in most cases. These differences could be attributed easily to surface roughness. The lowest surface area of glass measured was 0.001557 $m^2/g$, corresponding to the largest size fraction of sample B. The largest size fractions of samples A and E had similar specific surface areas.

The SEM images were also consistent with this analysis and clearly showed the absence of any porosity in these samples. A characteristic SEM image of *in situ* vitrified material A, demonstrating absence of any significant porosity or other features, is shown in Figure 3-7. The composition of the pure glass samples was very uniform, as determined by EDX analysis. Three different samples gave essentially indistinguishable results, suggesting a process very efficient in producing a uniform melt. Major components included $SiO_2$ (61), $Al_2O_3$ (14), CaO (6), MgO (3), $Na_2O$ (4), $K_2O$ (4), and $Fe_2O_3$ (9).

In comparison to the pure glass samples, the transition zone samples (C, D, and F) had a higher and more variable specific surface area, especially the larger particle size fractions (Figure 3-6). Although a minimum surface area cannot be observed for any of these samples, as the particle size increases the difference between the measured value and the geometric surface area increases. The specific surface area differences between the two groups of *in situ* vitrified glass materials can be justified by comparing Figure 3-7 (pure glass) to Figure 3-8.

As opposed to sample A, which is essentially featureless (Figure 3-7), sample C shows clearly the transition zone (Figure 3-8). The vitrified area can be seen in the right portion of the lower magnification (12x) micrograph and at higher magnification (50x) in the inset at right. This part of the matrix shows relatively few features and would contribute little to the overall specific surface area. The area to the left (shown at higher magnification, 100x, in the

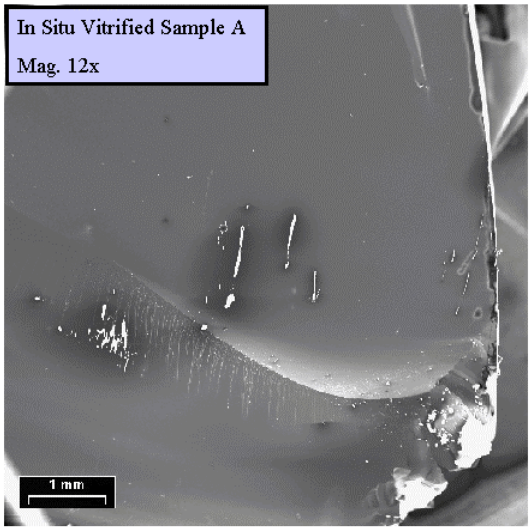


**Figure 3-7**. Scanning electron micrograph of *in situ* vitrified sample A (12x magnification).

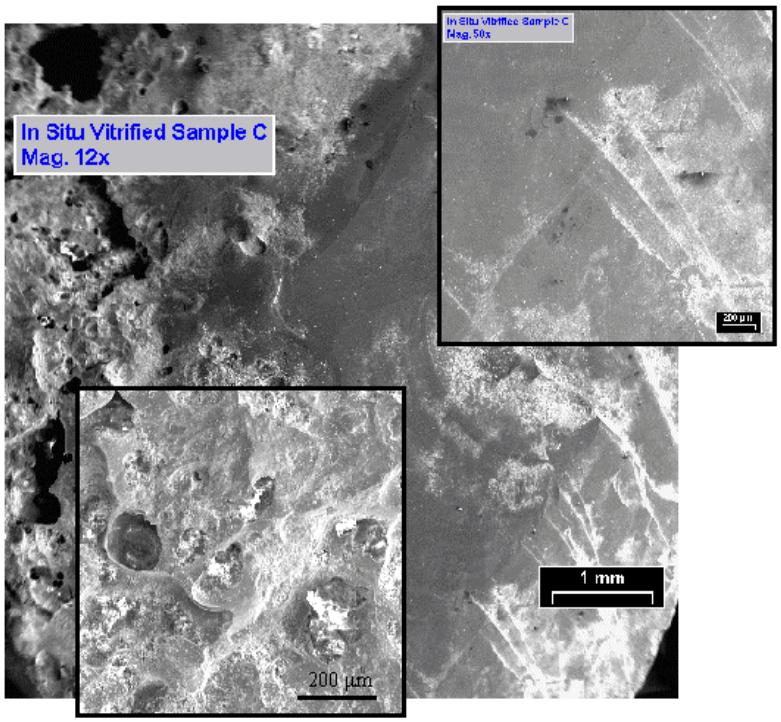


**Figure 3-8**. Scanning electron micrograph of *in situ* vitrified sample C (12, 50, and 100x magnification).

inset at left) is much more similar to the native rock and shows substantial topography and some porosity at this scale. It is expected that this area of the rock would contribute the most to the total surface area.

Major element analysis, based on EDX, was also performed for the transition samples. All areas of analysis of samples C and F gave very similar results, namely, $SiO_2$ (50), $Al_2O_3$ (13), CaO (7), MgO (4), $Na_2O$ (5), $K_2O$ (4), $Fe_2O_3$ (13), and $TiO_2$ (5). Compared to the massive glass samples, the transition and native rock samples had a lower $SiO_2$ concentration (50 vs. 61%) and higher $Fe_2O_3$ concentration (13 vs. 9%). In addition, the native rock appeared to contain 5% $TiO_2$, which was absent from the *in situ* vitrified material. The $Al_2O_3$ content was essentially unchanged. The consistency of the results of the EDX analysis argues against analytical precision as a reason for these differences. It is possible that the vitrification process resulted in compositional changes. Dehydration and volatilization of the parent rock during the vitrification process could explain some of these differences. Similar changes between the parent rock and nuclear melt glass have been observed (Schwartz et al., 1984). In other studies, however, although it was found that the major constituents of the native rock and glass were the same, a decrease in $SiO_2$ content and a reduction of iron from ferric to ferrous were observed following glass formation (Borg, 1975).

**Comparison of specific surface areas based on morphology and particle size**

To compare specific surface areas of natural and manmade glasses as a function of particle size and morphology, characteristic results are shown in Figure 3-9. Several different trends can be observed. The specific surface area of some glasses was relatively high (approx. 0.2 $m^2/g$ or higher), regardless of particle size. Some natural glasses obtained from Obsidian Dome (samples 6 and 10) were included in this category. Although the two samples had different specific surface areas, the results were only slightly dependent on particle size. Based on these results and SEM images, it must be assumed that sample roughness and porosity are the primary reasons for the observed behavior. The dissolution of such materials, therefore, should be relatively unaffected by the size of individual particles. The overall rate of dissolution, however, may be controlled by the rate of diffusion of dissolution products from internal pore surface areas to the bulk solution.

Obsidian Dome sample 9 was representative of materials characterized by a fairly strong specific surface area dependence on particle size, as long as the particle size was smaller than a material-dependent cutoff dimension. Above this size cutoff, however, the specific surface area was essentially particle-size independent. The minimum specific surface area of these materials was relatively low, between 0.04 and 0.1 $m^2/g$. The overall specific surface area appeared to be a combination of external and internal components. For small particle sizes, external surface area appeared to be the largest contributor, consistent with variation as a function of particle size. As the particle size increased, the contribution of the external surface area to the total decreased, until the contribution of surface area due to porosity and surface roughness became more important. Obviously, when the particles are large enough so that the external surface area becomes a minor component of the total, the specific surface area becomes independent of particle size. Under these conditions, even very large particle assemblages are expected to have a relatively high specific surface area, substantially higher than expected based on size alone.

The relative importance of external and internal surface area is a function of the pore structure. Particles with an extensive network of fine pores are expected to have specific surface areas independent of particle size. On the other hand, particles with wider pores, or surface roughness only, are expected to have specific surface areas that depend on particle size. For large particles, roughness and pores with widths substantially smaller than the dimension of the particles result in specific surface area substantially higher than the geometric surface area; when the size of the particles becomes comparable to the scale of roughness or pore dimensions, the specific surface area approaches the geometric surface area.

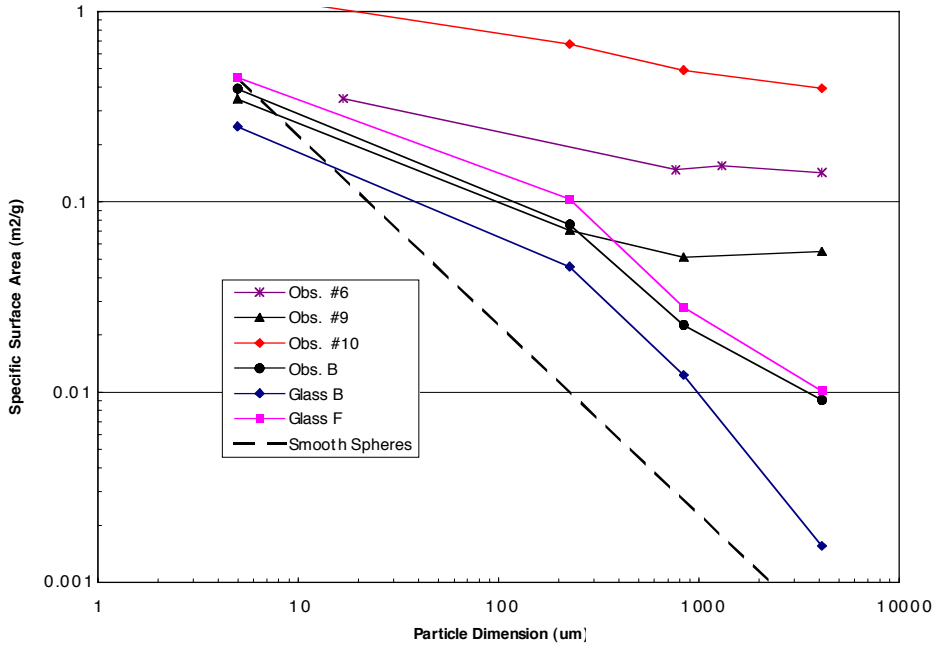


**Figure 3-9**. Comparison of specific surface area of glasses as a function of particle size and morphology.

A third group was represented by Obsidian Dome sample B, a sample representative of the more massive natural glasses, and samples representing the transition zone between native and vitrified rock. In these samples, and for the particle sizes analyzed, the external surface area appeared to be the determining factor. It is possible that a minimum surface area, independent of particle size, would be observed at larger particle dimensions. This minimum surface area would have to be lower than 0.01 $m^2/g$, based on the results shown in Figure 3-9. This hypothesis is based on the fact that as the particle size increases, the slope of the curve describing specific surface area as a function of particle size decreases. This hypothesis, however, cannot be verified without additional experiments using larger size fractions.

The last group of glasses included the manmade, massive, *in situ* vitrified glasses. These glasses had specific surface areas very similar to nonporous smooth spheres, suggesting complete absence of internal porosity and very low surface roughness. These results were consistent with particle morphology based on SEM images. The specific surface area of such materials is therefore expected to become exceedingly small with increasing particle size. It should be noted, however, that the only glass material with such characteristics was the manmade vitrified sample. The specific surface area difference between this material and the most massive natural sample was almost one order of magnitude.

Comparison of the results from all glass samples, including the tektites and volcanic material, in combination with the SEM analysis, clearly shows the effects of weathering on specific surface area. The *in situ* vitrified material (samples A, B, and E) was least weathered and clearly had the lowest surface area, approaching the expected geometric surface area within a factor of 2-3. Inspection of the tektite samples, on the other hand, revealed substantial weathering, consistent with surface areas that exceeded the geometric specific surface area of smooth spheres by 2-3 orders of magnitude. These results are in good agreement with previously published surface area data of common minerals as a function of particle size (White and Peterson, 1990).

**Summary and Conclusions**

The specific surface area of natural and manmade glasses was measured as a function of particle size and morphology. Differences in surface area of more than two orders of magnitude were observed. As expected, the specific surface area decreased with increasing particle size. The dependence of specific surface area on particle size, however, was material dependent, revealing distinct trends.

Tektite samples from Southeast Asia, volcanic ash from the eruption of Mount St. Helens, and tuffs from the Nevada Test Site had the highest surface areas, on the order of 1 $m^2/g$. The trends in surface area of obsidian glass and *in situ* vitrified rock as a function of particle size were more complex. In general, the surface area of most materials with size around 10 μm was similar to the surface area expected for nonporous, smooth spheres, suggesting that at small particle sizes external surface area accounts for most of the total surface area. At larger particle sizes, deviations from the theoretical surface area of nonporous spheres can be interpreted as an indication of increased surface roughness or internal porosity. Three different material types could be identified: 1) materials with high specific surface area, relatively independent of particle size, with minimum surface area approximately 0.2 $m^2/g$ or higher; 2) materials whose specific surface area appears to reach a terminal value of approximately 0.03 $m^2/g$ or higher; and 3) materials whose surface area does not appear to reach a terminal value, even at the largest sizes examined. Even this last group of materials, however, had a surface area of at least 0.01 $m^2/g$, which is more than one order of magnitude higher than the specific surface area of nonporous spheres.

Manmade, *in situ* vitrified rock was the only type of material with specific surface areas approaching values corresponding to flat, nonporous surfaces. The minimum specific surface area of the *in situ* vitrified rock was 0.00156 $m^2/g$. In general, the relative magnitude of specific surface areas of the different samples was qualitatively consistent with the morphology and porosity of the samples, observed in scanning electron micrographs. The correlation of specific surface area with elemental composition was inconclusive. Although substantial differences in the $SiO_2$ content of the *in situ* vitrified rock and the parent material

were observed, the elemental composition of obsidian glass and tektites did not reveal a correlation with specific surface area trends.

These results have significant implications for the surface area of natural glasses and the dissolution of *in situ* vitrified soil. Specifically, the surface area of natural glass is not necessarily a strong function of particle size. A specific surface area range of at least two orders of magnitude is possible, depending on particle morphology and porosity. In most cases, a limiting minimum surface area between 0.01 and 0.1 $m^2/g$ can be expected. Although specific surface areas below 0.01 $m^2/g$ are possible, even the most massive samples are expected to have specific surface areas higher than smooth spheres of equivalent size and the difference between real samples and geometrically smooth spheres is expected to increase with increasing particle size.

Because the specific surface area is a key parameter in many interfacial processes controlling the fate and transport of contaminants in the environment, including dissolution and sorption processes, better estimation of surface areas of natural materials is expected to lead to increased accuracy of transport models. Although the specific surface areas determined *ex situ* by physical adsorption and the BET method may not necessarily represent the actual interfacial surface area *in situ*, physical adsorption and the BET model provide a consistent and fast method for determining trends in surface areas of a variety of materials. Significant insights can be gained by analyzing surface area trends as a function of particle size and morphology. Determining parameters to be used in contaminant transport models from any type of laboratory experiment necessarily involves assumptions; it appears that gas adsorption and the BET model can provide reasonable estimates of the specific surface area of natural and manmade glasses.

**References**


Ball, W.P. and P.V. Roberts (1991) "Long-term sorption of halogenated organic chemicals by aquifer material. 2. Intraparticle diffusion," *Environ. Sci. Technol.* **25,** 1237-1249.

Borg, I.Y. (1975) "Radioactivity trapped in melt produced by a nuclear explosion," *Nuclear Technology.* **26,** 88-100.

Brunauer, S., P.H. Emmett, and E. Teller (1938) "Adsorption of gases in multimolecular layers," *J. Am. Chem. Soc.* **60,** 309-319.

Essington, E.H. and J.V.A. Sharp (1968) "Some aspects of ground-water solution chemistry, underground nuclear explosion zones, Nevada Test Site," *The Geological Society of America.* **Memoir 110,** 263-273.

Goldstein, J.I., D.E. Newbury, P. Echlin, D.C. Joy, A.D. Romig, Jr., C.E. Lymanet al. (1992) *Scanning Electron Microscopy and X-ray Microanalysis*. Plenum Press, New York, 820 pp.

Gregg, S.J. and K.S.W. Sing (1982) *Adsorption, Surface Area and Porosity*. Academic Press Inc., London, 303 pp.

Press, F. and R. Siever (1986) *Earth*. Freeman, New York, 656 pp.

Schwartz, L., A. Piwinskii, F. Ryerson, H. Tewes, and W. Beiriger (1984) "Glass produced by underground nuclear explosions," *J. Non-Crystalline Solids.* **67,** 559-591.

Smith, D.K. (1995) "Characterization of nuclear explosive melt debris," *Radiochimica Acta.* **69,** 157-167.

White, A.F. and M.L. Peterson (1990) "Role of reactive-surface-area characterization in geochemical kinetic models." In *Chemical Modeling of Aqueous Systems II*, (Edited by D.C. Melchior and R.L. Bassett), ACS Symposium Series, No. 416. American Chemical Society, Washington, D.C., 461-475.

## PART 4. BET SURFACE AREA ANALYSIS OF NUCLEAR MELT GLASS

*David K. Smith and Suzanne Hulsey*

*Chemistry and Materials Sciences Directorate*
*Lawrence Livermore National Laboratory*

### Introduction

Models of radionuclide release from sites of underground nuclear tests require accurate estimates of the dissolution of the melt glass that volumetrically incorporates a majority of the long-lived radionuclides including plutonium, other transuranics, and non-volatile fission products (Tompson et al., 1999; Pohll et al., 1998). Predictions of the rate of radionuclide release from the glass rely on a measure on the intrinsic dissolution rate of the glass, the relative solubility of the glass in the reacting fluid, and the reactive surface area of the glass. While the rate coefficients of glass dissolution have been experimentally determined, the range in surface area of the glass strongly influences the modeled release rate but is known with less certainty. Although melt glasses are produced in abundance during an underground nuclear test, with approximately 700 tons of glass produced per kiloton of nuclear yield, nuclear weapons diagnostics prioritized measurements of "bomb-fraction" radionuclides in the glass and did not incorporate systematic examination of variations in glass texture or surface area. Determinations of glass surface area are complicated by the heterogeneous conditions under which the glass is produced. Melt glasses are produced from the condensation of the explosion plasma that forms due to the high temperatures and pressures at the time of explosion, shock melting of rock adjacent to the explosion due to the instantaneous release of energy, and melting of wall rock materials that are outside the molten rind of shocked melted glass that line the first-formed standing detonation cavity. Statements regarding glass texture rely on the limited availability of archived glass samples and select descriptions, mapping, and photographs from mined re-entries into cavities that are situated above the water table. For these reasons, this study used gas adsorption BET to measure the surface area of a variety of melt glass samples.

### Previous Work

In 1998 Lawrence Livermore National Laboratory compiled existing information on the texture of glasses produced by a nuclear explosion to better document the variations in and relative proportions of glass textures (Kersting and Smith, 1999). Data were compiled from examining pieces of archived nuclear explosive melt debris, searching nuclear test program archives for descriptions and photographs of in-situ melt glass and compiling published technical reports on this topic. This review concluded that: (1) individual melt glass fragments have a large range in vesicularity ranging from massive to highly vesicular to pumiceous in texture; (2) although the majority of melt glass occurs in a puddle configuration at the bottom of the test cavity, the puddle is a complex body

consisting of both massive and highly vesicular lenses with lithic fragments; (3) the nature of the melt glass is independent of the original host rock composition or the nature of the nuclear test; and (4) melt glass samples exhibit a range in color from white, to dark black, often within a single specimen. In general, the configuration of the puddle at the bottom of the cavity consists of massive pieces of glass that are vesicular and variably fractured due to the cooling of the cavity environment, melting of wall rock, and incorporation of xenoliths of roof materials as the cavity cools and eventually collapses. Three types of glass were identified: 1) black to red massive glass shows some evidence of flow banding, 2) interlayered black to white glass is irregularly banded on the order of less than a centimeter, and 3) highly pumicious, volatile charged glass is frothy in appearance and light in color. These descriptions were used to guide selection of samples for this study.

The only documented work on melt glass texture was the mined re-entry into the 1957 RAINIER test (U-12b) fired in loosely bedded tuffs of RAINIER Mesa (Johnson et al., 1958; Schwartz et al., 1984). This study is unusual because samples were collected from re-entry tunnels and shafts that were driven into the collapse chimney and through the melt glass at the bottom of the RAINIER cavity. Because the tunnel and shaft walls could be mapped, samples could be specifically referenced to exact locations at the base of the puddle, at the top of the puddle, and in the collapse debris above the puddle. Because these samples were thoroughly documented at the macro and micro-scale, they were ideal candidates for measurements of surface area.

**Related BET Surface Area Measurements**

The BET analyses reported here are important for they represent surface area measurements of actual melt glass samples. Five samples of melt glass were analyzed; the five samples include four from the RAINIER mine back and one from the ROQUEFORT test (U-4as) conducted above the water table in Yucca Flat. These analyses complement BET surface area measurements made by DRI in FY2000 on non-radioactive analog materials which include volcanic glass, tektites, and artificial glass made by the in-situ heating and fusion of soils

Previous surface area measurements of melt glasses include those from Wolfsberg (1978) who reported surface areas ranging from 0.63 to 16.5 $m^2/g$ for nuclear test debris that had been ground to a fine powder with particle sizes less than 150 μm. Failor et al. (1983) used particle sizes less than 150 μm and obtained BET measurements for three nuclear melt glasses ranging from 0.396 to 0.465 $m^2/g$, while they estimated surface areas from geometric considerations of 0.031 to 0.033 $m^2/g$. Essington and Sharp (1968) used glass from the RAINIER test to evaluate the relationship between specific surface area and particle size. They evaluated eight size fractions, up to 16,000 μm. They found relatively constant surface areas for particle sizes greater than 1000 μm, indicating that the measured surfaces were internal rather than external. Their BET values ranged from 0.0168 to 0.831 $m^2/g$, with the stable values for the higher size fractions being approximately 0.05 $m^2/g$ for their pre-equilibration samples and 0.0168 $m^2/g$ for

post-equilibration samples (with the equilibration with groundwater believed to have blocked some internal pores by creation of reaction products).

**Sample Description**

The melt-glass samples were taken from LLNL post-test sample archives. DRI and LLNL investigators together selected samples in January 2000. Samples were picked to be representative of the range in textures in post-test glass and debris samples (Kersting and Smith, 1999). Four of the glass samples were taken from the "T" and "I" boreholes drilled vertically from the tunnel invert (floor) downwards through the RAINIER puddle region. Samples were selected near the top and the bottom of the puddle. The RAINIER samples were supplemented by a massive, vesicular, dark black glass returned from the ROQUEFORT test fired Yucca Flat. A brief petrographic description of each sample is provided in Table 4-1. A comprehensive description of the glass samples returned from the RAINIER boreholes is found in Schwartz et al. (1984). Location of the "T-11" borehole in the RAINIER cavity is plotted in Figure 4-1; samples were taken from this boring at the top and the bottom of the melt glass puddle.

**Table 4-1**. Melt Glass Sample Descriptions

| SAMPLE | TEST | DESCRIPTION |
|---|---|---|
| | | |
| T-11 23.0 – 25.0′ | RAINIER | Poorly sorted, moderately to highly welded, dense, ash and lithic-rich. |
| T-11 #2 27.0 –28.5′ | RAINIER | Red and black mixed dense glass, no ash. Massive with few vesicles. Mixing of red and black glass layers conspicuously defined by flow banding. |
| T-11 28.5 – 30.0′ | RAINIER | Frothy, pumicous, well sorted glassy matrix lacking xenocrysts. |
| I-39.0′ | RAINIER | Well sorted ash-rich sample with fine intact glass shards. Fine vesicles and pore space distributed uniformly throughout matrix |
| Core 1 | ROQUEFORT | Dark dense, black melt glass, vesicular, with no lithic or ash fragments, variably conchoidally fractured |

**Analytical Results**

Prior to analysis, the samples were broken into 2 – 3 mm wide chips within a fume hood in order to fit measuring tubes required by the BET gas adsorption analyzer. The weight of individual samples analyzed ranged from 1.1 grams to 3.9 grams; sample weights were minimized to preserve as much of the original intact sample as possible. Prior to gas adsorption analyses, each sample was heated under vacuum (~ 250 mTorr) at 110°C overnight to remove any adsorbed water or other surface contamination. The surface areas were determined in

triplicate for each sample with the exception of Core 1 which was analyzed four times. The analytical results are provided in Table 4-2.

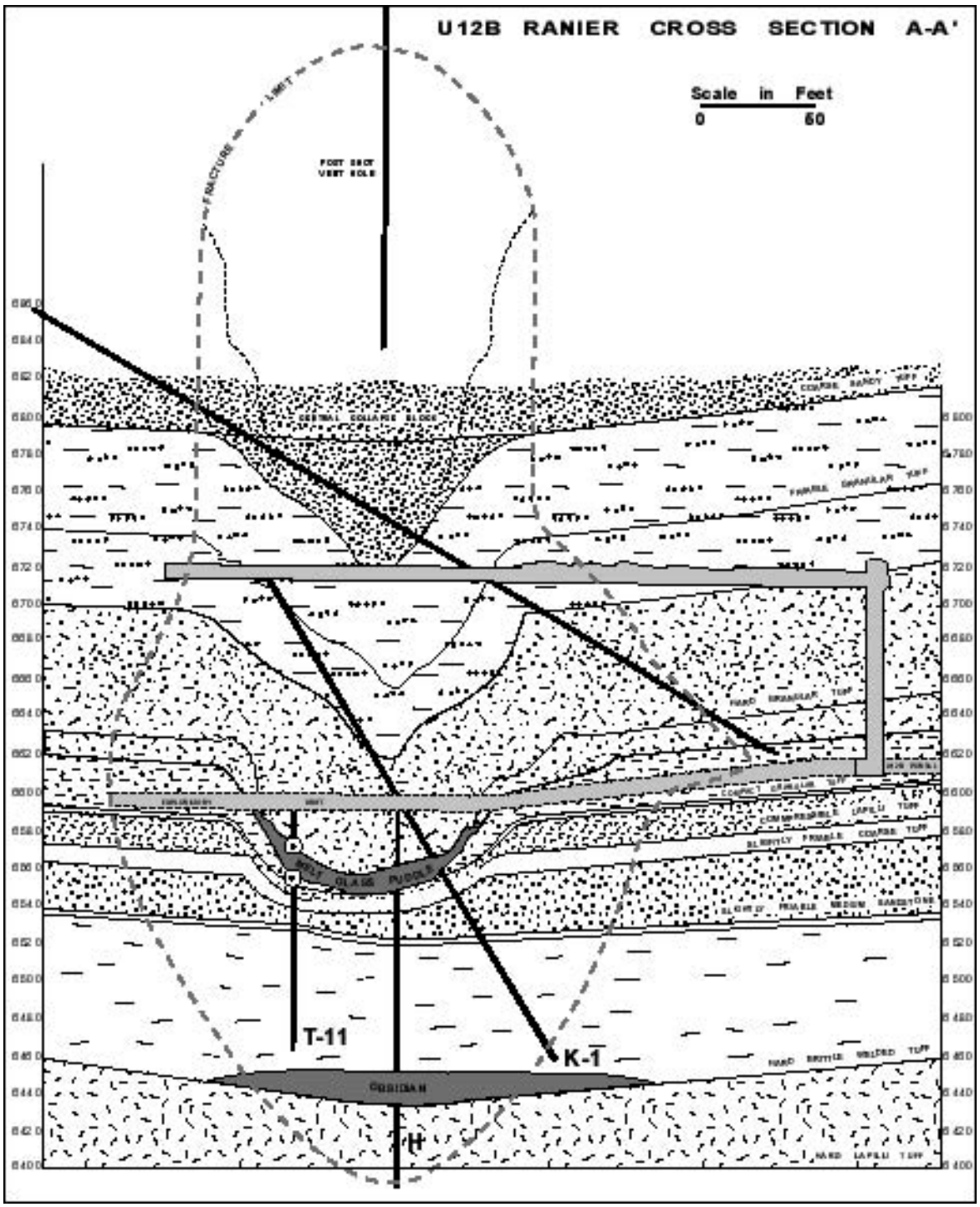


**Figure 4-1.** Schematic cross-section of RAINIER test showing sampling locations. Figure taken from Schwartz et al. (1984).

**Table 4.2.** BET surface area of glass samples, $m^2/g$.

| Sample | Tube | First | Second | Third | Fourth | Average |
|---|---|---|---|---|---|---|
| | | | | | | |
| T-11 23.0 – 25.0′ | O6 | 0.0391 | < 0.025 | < 0.025 | < 0.025 | < 0.025 |
| T-11 #2 27.0 – 28.5′ | F7 | 0.0950 | 0.1527 | 0.1362 | NA | 0.128 |
| T-11 28.5 – 30.0′ | N1 | 0.0573 | 0.1138 | 0.0975 | NA | 0.090 |
| I-39.0′ | C3 | 0.0651 | 0.0555 | 0.0708 | NA | 0.064 |
| Core 1 | S5 | 0.7202 | 0.6886 | 0.9135 | 0.8156 | 0.784 |

NA = not analyzed

In some cases the measurement of the glass sample was near the limit of detection of the surface area analyzer. In particular, the small surface area accounts for the non-detects for three of the four measurements of RAINIER sample T-11 23.0 – 25.0′.

The data indicate that the dark, vesicular melt glass sample from ROQUEFORT has the highest surface area of all the samples measured by an order of magnitude. The samples from RAINIER were more massive and generally more welded in texture. The presence of alteration layers (probably clays) on pore surfaces revealed by electron microscopy may account for the higher measured surface areas. This is consistent with earlier observations on the presence of clay alteration in melt glasses (Eaton and Smith, 2000).

**Imaging Internal Porosity**

An additional question is the extent to which the melt glass posses internal porosity. Internal porosity may account in part for differences between the BET gas adsorption measurements and those determined by reactive flow-through experiments. To address this question, melt glass samples were imaged using scanning electron microscopy. Photomicrographs of the internal surfaces of the glass samples are compiled in Figure 4-2. A 100 μm scale bar is included at the bottom right of each image.

Imaging reveals each of the samples is characterized by internal pores. The sample of the massive dark melt glass from the ROQUEFORT test (Core 1) had the largest pore diameter which is in excess of 200 μm. This sample also had the largest measured BET surface area. RAINIER samples I-39 and T-11 27.0 – 28.5′ have variable pores sizes which are elongated and appear partially interconnected. RAINIER sample T-11 23.0 –25.0′ which had the lowest measured BET surface area is partially welded and has small isolated pores that are not as interconnected as other melt glass samples. In general, the imaging revealed that the internal porosity is extremely variable with large and small pores juxtaposed (e.g., RAINIER sample I-39). This heterogeneity is not unexpected given the extremely volatile and gas charged environment encountered in a cooling explosion cavity.

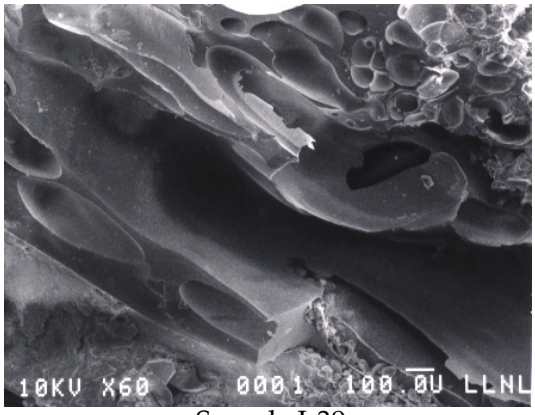

Sample I-39

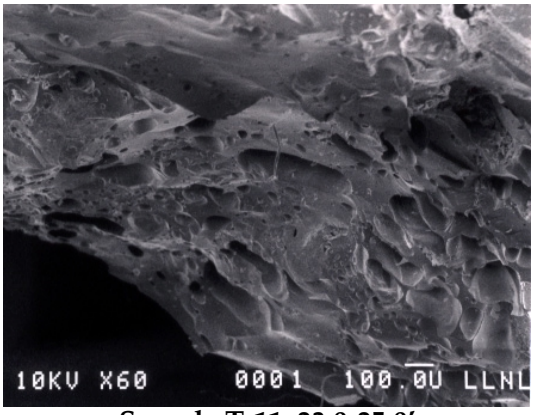

**Sample T-11 23.0-25.0′**

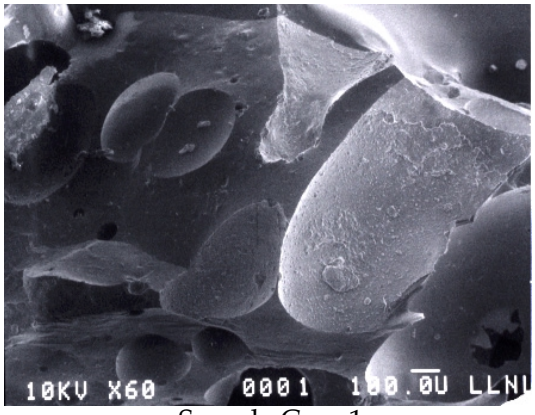

Sample Core 1

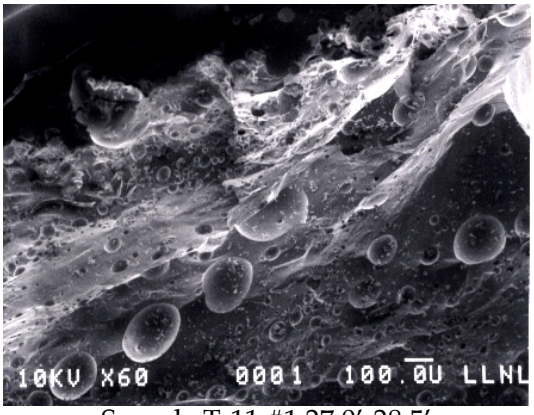

Sample T-11 #1 27.0′-28.5′

**Figure 4-2**. SEM photographs of glass samples.

## Conclusions

The analysis of melt glass indicates that BET surface areas vary widely and in accordance with their textures. BET gas surface areas range from <0.025 to 0.91 $m^2/g$. Based on data from this study, the larger and more through-going the vesicles, the higher the BET surface area. More welded and denser samples had lower measured surface areas. Imaging of the samples revealed that melt glasses possess significant internal porosity that may explain some of the discrepancy between BET and reactive surface area measurements.

## References

Eaton, G. F. and D. K. Smith (2000) Aged nuclear explosion melt glass: Radiography and scanning electron microscope analyses documenting radionuclide distribution and glass alteration. Livermore Lawrence Livermore National Laboratory Report, UCRL-JC-136658, 10 pages.

Johnson, G.W., G.T. Pelsor, R.G. Preston, and C.E. Violet (1958) The Underground Nuclear Detonation of September 19, 1957, RAINIER, Operation Plumbbob, Lawrence Radiation Laboratory, UCRL-5124, 27p.

Kersting, A.B. and D.K. Smith (1999) Observations of Nuclear Explosive Melt Glass Textures and Surface Areas, Lawrence Livermore National Laboratory, unpublished report prepared for the Underground Test Area of the U.S. Department of Energy, Nevada Operations Office, 8p. with illustrations.

Pohll, G., J. Chapman, A. Hassan, C. Papelis, R. Andricevic, and C. Shirley (1998) Evaluation of the Groundwater Flow and Transport at the SHOAL Underground Nuclear Test: An Interim Report, Desert Research Institute, Publication No. 45162, DOE/NV/11508-35, 123p. with appendices.

Schwartz, L.L., A. Piwinskii, F. Ryerson, H. Tewes, W. Beiriger (1984) in L.D. Pye, J.A. O'Keefe, and V.D. Fréchette, eds. Natural Glasses, North Holland, p. 559 – 591.

Tompson, A.F.B., C.J. Bruton, and G.A. Pawloski, eds. (1999) Evaluation of the Hydrologic Source Term from Underground Nuclear Tests in Frenchman Flat at the Nevada Test Site: the CAMBRIC Test, Lawrence Livermore National Laboratory, UCRL-ID-132300, 319p.

## PART 5. RECOMMENDED VALUES FOR REACTIVE SURFACE AREAS FOR MODELING RADIONUCLIDE RELEASE FROM MELT GLASSES

The purpose of this section is to summarize the experimental data collected in this work, reconcile the different values obtained with the different approaches, and recommend values for reactive surface area of melt glass to be used in reactive transport calculations of radionuclide transport.

Three separate studies were conducted. Flow-through dissolution experiments using solid cores of volcanic glass yielded reactive surface areas of 0.0002 to 0.0065 $m^2/g$, with an average value of 0.0026 $m^2/g$. The majority of the data clustered between 0.0015 and 0.0050 $m^2/g$. The use of solid glass cores allowed us to capture (on the scale of our core sizes) the effects of heterogeneity on reactive surface area. It is significant that the reactive surface areas varied by only about a factor of 30, even though the glass cores that were used had widely varying textures.

The hydraulic conductivities of the glass cores were measured as a function of the orientation of flow with respect to banding in the glass cores. The hydraulic conductivity of cores oriented parallel to flow and with no obvious flow orientation ranged from 0.001 to 0.29 m/day, whereas that of cores oriented perpendicular to flow was substantially lower, ranging from 0.0001 to 0.0015 m/day. The hydraulic conductivity values generally clustered between 0.001 and 0.03 m/day.

Krypton-gas based BET measurements on crushed splits of the same volcanic glass samples yielded specific surface areas ranging from 0.0091 to 1.242 $m^2/g$. Though the specific surface area was a function of particle size, tending to decrease with increasing particle size, some samples have a low particle size dependence, or a dependence that decreases with increasing size, that is attributed to internal porosity and surface roughness. Krypton BET measurements of other glasses define a larger range, with a tektite having the highest surface area (1.651 $m^2/g$) and a manmade vitrified sample having the lowest (0.00156 $m^2/g$).

Five samples of crushed nuclear melt glass samples (four from the RAINIER test, one from the ROQUEFORT test) were analyzed for specific surface area using nitrogen-gas based BET measurements. These values ranged from <0.025 to 0.9135 $m^2/g$. Imaging revealed that the samples possess internal porosity (vesicles). Other samples from the RAINIER test were also analyzed by Essington and Sharp (1968) using BET. They measured eight different size fractions under two sets of conditions (16 measurements) and determined a range of specific surface areas of approximately 0.0168 to 0.831 $m^2/g$.

The BET data for both nuclear melt glass and Obsidian Dome samples support a range of physical specific surface area of 0.01 to 1.0 $m^2/g$. The analog volcanic glass work using krypton-gas based BET was able to achieve lower detection limits than the nitrogen-gas based BET. However, krypton-gas based BET did not

find specific surface areas for analog glasses below a value of 0.0091 $m^2/g$, which suggests that the nuclear melt glass values are not strongly limited by the detection limitations of the nitrogen method. The volcanic glass measurements also identified natural glasses that exhibit the same leveling off of specific surface area with increasing particle size as noted in the nuclear melt glass study by Essington and Sharp (1968), which suggests that the values can be extrapolated to larger size fractions than used in the experiments.

A comparison of the flow-through core test reactive surface areas and BET-measured surface areas of the same volcanic glass samples is shown in Table 5-1. The BET surface areas of the largest sample size (4123.1 μm) is consistently about ten times larger than the corresponding reactive surface areas measured with the flow-through test.

In summary, flow-through dissolution experiments yielded reactive surface areas between 0.0002 to 0.007 $m^2/g$, whereas the physical BET surface area measurements were generally in the range of 0.01 to 1.0 $m^2/g$. This suggests the reactive surface areas are about one to two orders of magnitude smaller than the physical surface areas for the volcanic glass samples. Many studies have suggested that reactive surface areas of minerals in the field are one to two orders of magnitude smaller than the BET surface areas of the minerals measured in the laboratory (e.g. White and Brantley, 1995; White and Peterson, 1990). This is in the same range as the differences between our physical and chemical surface areas. A conservative range of 0.001 to 0.01 $m^2/g$ for nuclear melt glass surface area is therefore recommended for hydrologic source term modeling.

**References**


Essington, E. H. and J. V. A. Sharp (1968) Some aspects of ground water solution chemistry, underground nuclear explosion zones, Nevada Test Site. *Geological Society of America Memoir 110: The Nevada Test Site.* E. B. Eckel, ed. Geological Society of America**,** p. 263-273.

White, A. F. and M. L. Peterson (1990) Role of reactive surface area characterization in geochemical kinetic models. in *Chemical Modeling in Aqueous Systems II.*, D. Melchior and R. Bassett eds., American Chemical Society Symposium 416, p**.** 461-475.

White A. F. and Brantley S. L. (1995) Chemical weathering rates of silicate minerals: An overview. In *Chemical Weathering Rates of Silicate Minerals.*, Mineralogical Society of America Reviews in Mineralogy Volume 31, A. F. White and S. L. Brantley eds., p. 1-21.

**Table 5-1.** Comparison of LLNL reactive surface area measurements and DRI BET measurements ($m^2/g$).

| | | Geometric Mean Particle Dimension ( μm) | | | | | | |
|---|---|---|---|---|---|---|---|---|
| Sample | Reactive Surface Area | 4123.1μm | 1303.8μm | 842.0μm | 648.1μm | 227.4μm | 16.8μm | 5.0μm |
| 1 | 0.0038 | 0.0263 | 0.0487 | | 0.0546 | | 0.2603 | |
| 2 | 0.0016 | 0.0190 | 0.0139 | | 0.0328 | | 0.1223 | |
| 3 | | 0.0312 | 0.0340 | | 0.0395 | | 0.1678 | |
| 4 | 0.0017* | 0.0489 | | 0.0588 | | 0.0923 | | 0.409 |
| 5 | | 0.0314 | 0.043 | | 0.0459 | | 0.2145 | |
| 6 | | 0.142 | 0.1544 | | 0.1468 | | 0.3475 | |
| 7 | 0.0011* | 0.0309 | | 0.0330 | | 0.0689 | | 0.3073 |
| 8 | 0.0047 | 0.0442 | | 0.0443 | | 0.0825 | | 0.2546 |
| 9 | | 0.0546 | | 0.0511 | | 0.0709 | | 0.346 |
| 10 | 0.0065 | 0.3938 | | 0.4896 | | 0.6713 | | 1.242 |
| 11 | 0.0030* | | | | | | | |

* Average of all measurements from Table 2-3.